NAL PROPOSAL NO. 144

Correspondent: Samuel C. C. Ting
Department of Physics, M.I.T.
617-864-6900-7586
Deputy: B. Margolis
Department of Physics
McGill University, Montreal

PROPOSAL TO SET UP A TAGGED PHOTON FACILITY AND TO SURVEY PHOTON INDUCED REACTIONS IN 50 - 300 BeV REGION

by

B. Margolis, P. M. Patel, W. Ross, D. G. Stairs
Department of Physics, McGill University, Montreal
and
L. Bird, C. Halliwell, R. Morrison, John Walters
Department of Physics, Carleton University, Ottawa
and
E. Coleman, T. Fesesse, Y. Makdisi
Department of Physics, University of Minnesota
and
U. J. Becker, P. Biggs, W. Busza, M. Chen, T. Nash,
H.F.W. Sadrozinski, Samuel C.C. Ting, Sau Lan Wu, and Tai Tsun Wu
Department of Physics, Massachusetts Institute of Technology

TABLE OF CONTENTS

		PAGE
Chapter One:	Photon physics at high energies	1
	Experiment A: Semi inclusive reactions: $\gamma + p \to \pi^{\pm} + X$	2
	Experiment B: Search for new vector mesons: $\gamma + p \to p + V^{\circ}$	10
	Experiment C: Photoproduction of vector mesons: $\gamma + p \to p + \rho, \omega, \phi$	14
	Experiment D: ϕ-ω Regeneration from nuclei	17
	Experiment E: Search for heavy leptons; $\gamma + Z \to Z + L^{+} + L^{-}$	20
	Experiment F: Compton scattering $\gamma + p \to \gamma + p$	22
	Experiment G: Total cross section	24
Chapter Two:	The forward detector	25
	Section A: Design considerations	26
	Section B: Description of forward spectrometer system.	29
	Section C: Triggering of the system and $e^{+}e^{-}$ rejection	40
Chapter Three:	The Recoil System	48
	Section A: Design considerations	50
	Section B: The apparatus	51
	Section C: Particle identification	52
	Section D: Acceptance and resolution	58
Chapter Four:	The Experiments	60
	Experiment A: Semi inclusive reactions $\gamma + p \to \pi^{\pm} + X$	61
	Experiment B: Two body decays of vector mesons $\gamma + p \to p + V^{\circ}; V^{\circ}(\rho, \omega, \phi)$	67
	Experiment C: Three body decays of vector mesons $\gamma p \to \omega^{*} p; \omega^{*}(\omega, \rho, V^{\circ})$	72
	Experiment D: Multiple body decays of vector mesons $\gamma p \to M_x + p$: Missing mass of x.	80
	Experiment E: ϕ-ω Regeneration from nuclei	85

CONTENTS

		PAGE
	Experiment F: Search for heavy leptons ; $\gamma + Z \rightarrow Z + L^+ + L^-$	87
	Experiment G: Compton scattering $\gamma p \rightarrow \gamma p$	89
	Experiment H: Total γ- nucleon cross sections.	92
	Operations Schedule	100
Acknowledgements.		101
Appendix	I. Cost consideration	102
	II. Non magnetic recoil system	103
	III. Čerenkov Counters	107
	IV. Data acquisition system	113
References		117

Introduction:

We propose to construct a tagged photon facility in the 50-300 BeV region to study the general features of photo-induced reactions. (See attached paper on 'Design of Tagged Photon Beam').

We produce the γ beam from π^0 decays from a Be target, converting the γ rays into electron pairs. With a beam transport system, we collect 10^8 electrons on to a tagging target which produces 4×10^5 tagged photons with a resolution $\delta p/p = \pm 0.5\%$ in the energy band 120-200 BeV.

Comparing this beam with other tagged photon beams, we note that the 4×10^5 γ-rays (or 10^6 total equivalent quanta in the total energy band) are distributed uniformly over one second of spill time, whereas in low energy tagged photon beams from electron accelerators the same amount of beam is distributed over 30 millisecond or less. This feature enables NAL to use large solid angle detectors and to perform accurate experiments with coincidence techniques.

Together with the tagged photon beam we propose the construction of a detection apparatus to perform the following experiments:

A. $\gamma + p \rightarrow \pi^{\pm} + X$

B. $\gamma + p \rightarrow p + V^0$, $V^0 \rightarrow n\pi$, $n \geq 2$ (photoproduction of new vecter mesons)

C. $\gamma + p \rightarrow p + \rho(2\pi)$
$\rightarrow p + \omega(\pi^+\pi^-\pi^0)$
$\rightarrow p + \phi(\pi^+\pi^-\pi^0;\ K^+K^-)$

D. Regeneration experiments for ω and ϕ from nuclei.

E. Search for heavy leptons.

F. Elastic Compton Scattering.

G. Total cross-sections $\sigma_T(\gamma p)$ and $\sigma_T(\gamma n)$.

We now discuss each separately, in the above order.

CHAPTER ONE

Photon Physics at High Energies

Expt. A. $\gamma + p \longrightarrow \pi^{\pm} + X$

Here we measure the $\pi^{\pm}$ accurately, but the rest of the particles X only roughly. We shall refer to such measurements (not necessarily initiated by photons) as semi-inclusive, since Feynman has suggested the term "inclusive" for the extreme case where nothing whatsoever is measured about X.

On the basis of the fireball model (FB)[1], the multiperipheral model (MP)[2], the multi-Regge model (MR)[3], the droplet model of Chou and Yang (CY)[4], the parton model of Feynman (FP)[5], and the field-theoretic model of Cheng and Wu (CW)[4,7], we now have good theoretical descriptions of semi-inclusive reactions. It is extremely important to find out whether these theoretical descriptions are correct or not, particularly for the case of photoproduction processes, where virtually no experimental data exist at all at present.[8]

With a tagged photon beam from a proton accelerator, any experimentally feasible detecting apparatus must give substantial information about X. Since this information, obtained at no cost, contains a great deal of physics, it would be foolish to restrict ourselves to the extreme case of inclusive measurements only.

We discuss in some detail here the present theoretical understanding together with some of the possible experimental tests. We shall however examine only very briefly the possible dependence of various quantities on $\ln E^{inc}$ for two reasons. First, our theoretical understanding on this slow variation, based mostly on considerations from field theory, is achieved only recently. Secondly, experimental determination of such slow variation is quite difficult and may not be possible for first-generation experiments.

i) General Considerations

We choose the z-axis to be in the direction of the incident photon beam. Let $\vec{p}$ be the momentum in the laboratory frame of the π^+ or π^- (to be measured accurately), and p_z and $\vec{p}_\perp$ be the components of $\vec{p}$ in the z and the perpendicular directions. Also p and $p_\perp$ denote the magnitudes of $\vec{p}$ and $\vec{p}_\perp$. If we transform to the center-of-mass system, $\vec{p}_\perp$ remains the same but p_z (CM) is of course quite different. For semi-inclusive measurements, it is convenient to use these variables. For definiteness, we consider here the case of 200 BeV photon beam.

Given $p_\perp \neq 0$, the π cannot come out arbitrarily close to the forward or backward directions. In Fig. 1a, we plot the maximum possible angle θ in the laboratory frame for the produced pion as a function of $p_\perp$. It is seen that for $p_\perp \geq 80$ MeV/c, it is sufficient to detect the pion up to 170°.

We next consider the pions with p_z (CM) = 0, which is the dividing line for forward-moving and backward-moving pions. In Fig. 1b, we plot the values of θ and p for such pions. The interesting point here is that, at 200 BeV, <u>all</u> forward-moving pions come out with θ no more than 5.5°.

ii) Pionization

We first consider the region of pionization where p_z (CM) is small, i.e.,

$$|p_z(\mathrm{CM})| \ll \frac{m_\pi E^{inc}(\mathrm{CM})}{m_p c} = 1.44 \text{ BeV/c},$$

or roughly

$$|p_z(\mathrm{CM})| \lesssim 0.5 \text{ BeV/c}. \qquad (1)$$

We choose X in a way that it is invariant under Lorentz transformations along the z-axis (CW). More precisely, we choose X such that, if any combination of particles is acceptable as X, then the same combination Lorentz transformed along the z-axis must also be acceptable as X. The special case of inclusive measurements satisfies this condition automatically. For reasons to be dis-

cussed below in (iii), the choice of X should not be so stringent that the rate is much lower than, say, 10% of the inclusive case. With such a choice of X, the one-pion distribution function in the CM system is given, for extremely high energies, by (CW) and (FP)

$$E^{-1} d^2\vec{p}_\perp \, dp_z(CM) \, f(p_\perp) \tag{2}$$

when (1) is satisfied, where $E = \left[p_z^2(CM) + p_\perp^2 + m_\pi^2 \right]^{1/2}$ is the energy of the pion in the CM system. This $f(p_\perp) \not\equiv 0$ is independent of p_z and the incident photon energy.

<u>TEST 1</u> Is (2) correct for various choices of X?

The correctness of (2) is crucial to CW. If (2) is not correct, even the general features of quantum field theories fail to hold for the real world at high energies, and hence further study of field-theoretic models has very little relevance to high-energy physics. In the inclusive case, where no measurement whatsoever is performed on X, FP also gives (2) but since in FP $f(p_\perp)$ can be zero, test 1 will not be conclusive for FP. Also in this inclusive case, MP and MR give a weaker form of (2), where $f(p_\perp)$ is independent of p_z but may depend on the incident photon energy. Thus test 1 in this special case is also important for MP and MR, but not for FB and CY. If the charge conjugation quantum number C = +1 an be assigned to the Pomeron (or vacuum trajectory in Regge language), then the functions $f^+(p_\perp)$ for π^+ and $f^-(p_\perp)$ for π^- are equal.

<u>TEST 2:</u> If yes to test 1, are $f^+(p_\perp)$ and $f^-(p_\perp)$ approximately equal for various choices of X?

iii) <u>Further Consideration on Pionization</u>

Suppose we choose X differently from the criteria in (ii). There are numerous possibilities and we shall mention only a few.

α) X contains one and only one charged particle in the region $\theta \leq 5.5^{\circ}$ (for 200 BeV photon beam).

If the pion with low-energy in the CM system is $\pi^{+}(\pi^{-})$, then the major contribution to the cross section comes from the case where the forward charged particle is π^{-} (π^{+}). In this case, either the pions come from the decay of a ρ° or ω , or a pion is exchanged in the cross channel. In either case, (2) does not hold.

<u>TEST 3:</u> Is (2) correct for this choice of X?

β) X contains no charged particle.

This is possible for π^{+}+ X, and X contains one n and in addition $n\bar{n}$ pairs, π°, η , and possibly ω in the decay mode $\pi^{\circ} + \gamma$. This choice is interesting in that the condition of Lorentz invariance in the z direction is satisfied and yet theoretically (2) does not hold (MP, MR, CW).

<u>TEST 4:</u> Is (2) correct for this choice of X?

One purpose of these tests 3 and 4 is to demonstrate that (2) is by no means trivial.

iv) Pion Correlations

We digress momentarily to discuss

$$\gamma + p \longrightarrow \pi^{+} + \pi^{-} + X' \quad ,$$

where X' is chosen in the same way as the X of (ii), and the momenta of both π^{+} and π^{-} satisfy (1). The two particle distribution is (CW)

$$E_{+}^{-1} E_{-}^{-1} \, d^{2}\vec{p}_{\perp +} \, d^{2}\vec{p}_{\perp -} \, dp_{z+}(CM) \, dp_{z-}(CM) \, g \quad , \tag{3}$$

where g is a function of $\vec{p}_{\perp +}$, $\vec{p}_{\perp -}$, and $E_{+}E_{-} - p_{z+}$ (CM) p_{z-} (CM), but not of the incident energy or the values of p_{z+} (CM) and p_{z-} (CM) separately.

TEST 5: Is (3) correct for various choices of X?

This is a generalization of Test 1. A more interesting point is to choose X such that there is no π^0 (this may or may not be essential), and to study the invariant mass of π^+ and π^-.

TEST 6: How strongly does ρ^0 show up in the invariant mass of π^+ and π^-?

Suppose the answer to test 2 is yes, so that we assign C = +1 to the Pomeron. If the π^+ and π^- are the only particles whose momenta satisfy (2), then at extremely high energies the ρ^0 resonance is very prominent according to FP, but suppressed according to CW. This is one of the few points where different theories give opposite predictions.

v) Fireball or Fragmentation

If the answer to test 1 is indeed yes, let us attempt to plot schematically the one-pion distribution in the CM system. Such a plot is shown in Fig. 1c, where A and A' denote the kinematic limits and the value of $p_\perp$ is chosen to be 200 MeV/c. Inclusive measurements give immediately the average pion multiplicity.

If the interest is not in the pionization region, but in the fireball (FB) or fragmentation (CY) region where p_z (CM) is not small, it is more informative to plot $E\, d\sigma / d\vec{p}_\perp dp_z$ (CM), which is Lorentz invariant. The result, again for $p_\perp$ = 200 MeV/c, is shown in Fig. 1d. At B', the pion has the same velocity as the target proton in the CM system, and at B, the pion has half of the energy of the incident photon.

TEST 7: Is the curve of Fig. 1d fairly flat between B' and B?

This is an extension of (2). Whether it holds all the way to B is not clear theoretically, but it is not an unreasonable guess. Also there may or may not be maxima between B' and B, and there may or may not be a maximum or minimum at 0.

<u>TEST 8:</u> Plotted against the variable $p_z(CM)/E^{inc}(CM)$, is this curve of Fig. 1d independent of the energy of the photon beam for each given p and X?

This scaling has been discussed in detail by CY. This variable p_z (CM)/ E^{inc} (CM) has been called β in CW and x in FP. (Recent work on the field-theoretic model[7] indicates that this curve changes slowly at extremely high energies. However, this change may not be visible at 200 BeV/c).

We list some more detailed tests concerning the curve of Fig. 1d.

<u>TEST 9:</u> If yes to test 8, is the <u>left</u> half of the curve, i.e. the part of the curve for p_z (CM) < 0, the same in the case of inclusive measurements (except for an overall factor) as the ones from

$$p + p \longrightarrow \pi^{\pm} + \text{anything},$$

$$\pi^{\pm} + p \longrightarrow \pi^{\pm} + \text{anything},$$

and

$$K^{\pm} + p \longrightarrow \pi^{\pm} + \text{anything?}$$

In each case, the curve is determined by fragmentation of the proton. This relation between the various curves is true for CY, MP, and FP, but only approximately true for CW.

The situation here with <u>semi-inclusive</u> measurements is not clear theoretically. Various comparisons will be interesting. Also the right half of the curve may be compared with the case of deuteron target, since this is the fragmentation of the photon projectile (CY).

When p_z (CM) is close to $\pm\, p_{z\,max}$(CM), the mass of X cannot be large because of energy-momentum conservation. Therefore, Regge phenomenology may apply (FP).

<u>TEST 10:</u> For p_z (CM) close to $\pm p_{z\,max}$ (CM) does the curve of Fig. 1d behave like

$$\left[p_{z\,max}(CM) \mp p_z(CM) \right]^{1-2\alpha}$$

where α is the Regge trajectory function for π and N respectively?

Much of the discussion here for the fireball or fragmentation can be generalized to the case where more than one particle is measured accurately. Finally, we add that almost all of the discussions here for the semi-inclusive reaction $\gamma + p \rightarrow \pi^{\pm} + X$ can be applied directly with different kinematics, to $\gamma + p \rightarrow K^{\pm} + X$, $\gamma + p \rightarrow p + X$, $\gamma + p \rightarrow \bar{p} + X$, $\gamma + p \rightarrow \pi^{0} + X$ etc.

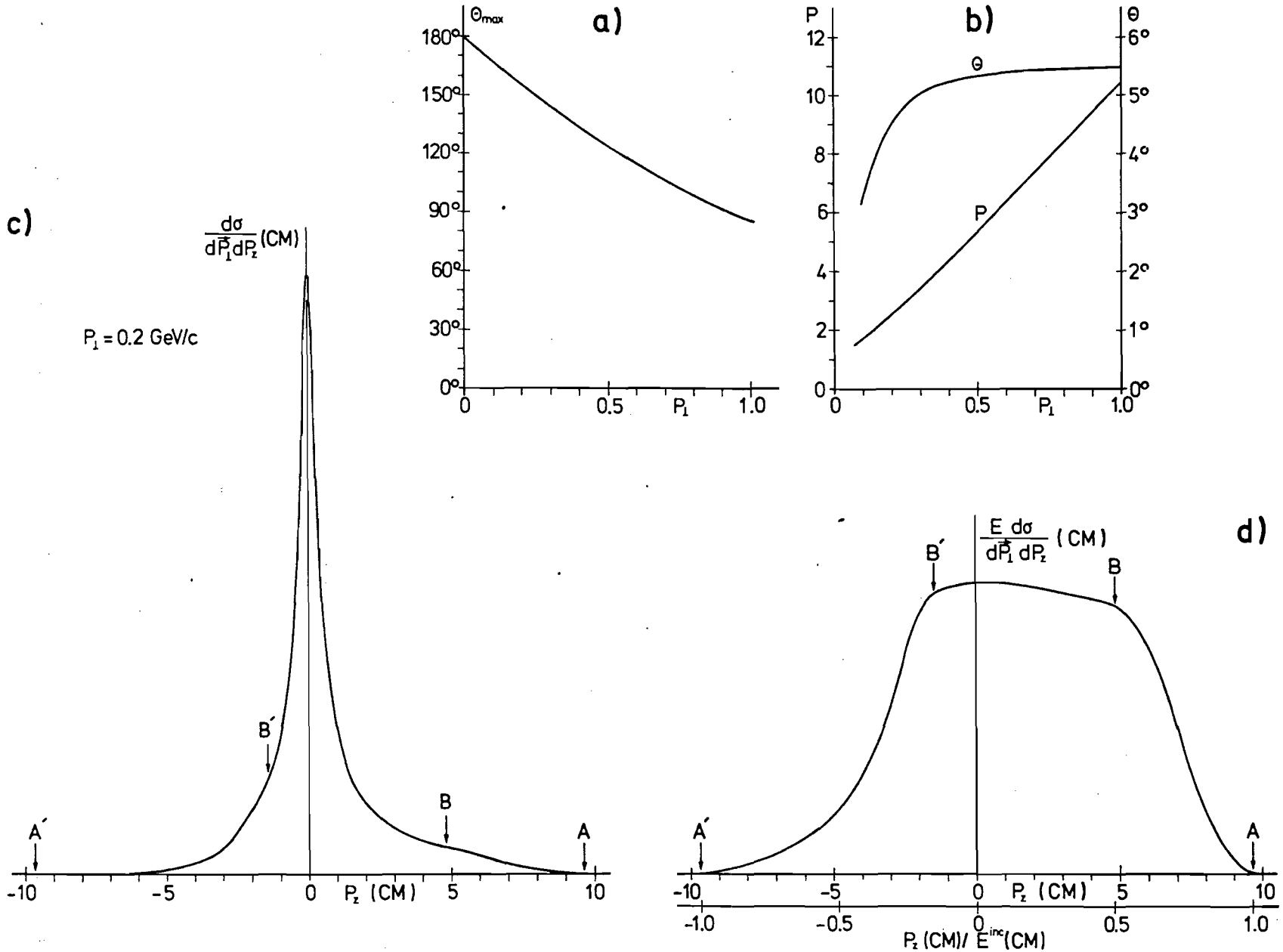
a)
Θ_{max}
180°
150°
120°
90°
60°
30°
0°
0
0.5
$P_\perp$
1.0
b)
P
12
10
8
6
4
2
0
Θ
6°
5°
4°
3°
2°
1°
0°
c)
$\frac{d\sigma}{d\vec{P}_\perp dP_z}$ (CM)
$P_\perp$ = 0.2 GeV/c
A´
B´
B
A
-10
-5
0
P_z (CM)
5
10
d)
$\frac{E\, d\sigma}{d\vec{P}_\perp dP_z}$ (CM)
-1.0
-0.5
0.5
1.0
P_z (CM)/ E^{inc}(CM)

FIG. 1

Expt. B $\quad \gamma + p \rightarrow p + V^0 \rightarrow n\pi \; ; \quad n \geq 2$,

the photoproduction of new vector mesons. Heavy vector mesons are needed[9] as recurrences of the daughter trajectories of ρ, ω and ϕ.

The foundations of the vector dominance model have been described in detail in papers by many physicists.[10] In simple terms, vector dominance means that one relates the electromagnetic current of hadrons to the fields of vector mesons by

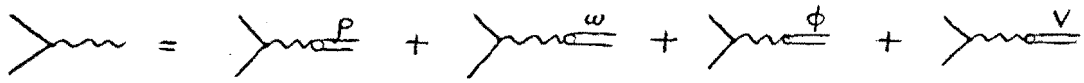

$$j_\mu(q^2) = -\frac{m_\rho^2}{2\gamma_\rho}\rho_\mu(q^2) - \frac{m_\omega^2}{2\gamma_\omega}\omega_\mu(q^2) - \frac{m_\phi^2}{2\gamma_\phi}\phi_\mu(q^2) - \sum_V \frac{m_V^2}{2\gamma_V}V_\mu(q^2) \qquad (6)$$

It follows from (6) that for the interaction of real photons with nucleons

one can write the photon-nucleon amplitude $f_{\gamma N}$ in terms of vector meson nucleon amplitudes f_{VN} by

$$f_{\gamma N} = \frac{m_\rho^2}{2\gamma_\rho}\cdot f_{\rho N} + \frac{m_\omega^2}{2\gamma_\omega} f_{\omega N} + \frac{m_\phi^2}{2\gamma_\phi} f_{\phi N} + \sum_V \frac{m_V^2}{2\gamma_V} f_{VN} \qquad (7)$$

Comparing the total γp cross section[11] with diffraction production of ρ, ω, ϕ mesons one deduced $\gamma_\rho^2/4\pi = 0.3 - 0.4$. Comparison with the storage ring result of $\gamma^2_\rho/4\pi = 0.50 \pm 0.03$ shows that relation (7) is satisfied to the 20% level.

Analysis of photoproduction[11] data from complex nuclei and of the corresponding total cross sections $\sigma_t(\gamma A)$ shows the same amount of discrepancy.

Reactions like $\pi N \rightarrow \rho N$ and $\gamma N \rightarrow \pi N$ can be related to each other by VDM. The comparison fails when linearly polarized photons are used.

The existence of ρ, ω, ϕ alone therefore does not satisfy the VDM when the photon is on the mass shell. The existence of additional vector mesons is the simplest way out.

When the photon is off the mass shell, i.e. in the spacelike region, the VDM with only ρ, ω, ϕ fails completely to describe elastic and inelastic electron-nucleon scattering. It is conceivable that with many new vector mesons one may explain the large discrepancy between VDM and electron scattering data.

The best way to search for heavy vector mesons is through photoproduction, because photons and vector mesons have the same quantum numbers. Photoproduction of vector mesons does not involve changes of quantum numbers and is a diffractive process. This tends to enhance resonance production relative to any background as compared to πp interactions with protons. Typical examples are shown in Fig. 2a, where ρ production from πp and γp are presented together for comparison. As expected, vector meson production by photons shows a much better signal to background ratio. It is a most interesting question whether this applies also to 1^+ mesons including A_1 and B.

Contrary to popular belief, the e^+e^- storage ring is not the best place to look for vector mesons. In the e^+e^- storage ring the energy is well-defined. A systematic search for heavier vector mesons requires a continuous variation and monitoring of the energy of the two colliding beams; a difficult task requiring almost infinite machine time. Storage ring is best suited to perform detailed studies of vector meson parameters once they have been found.

Present experiments[12] at SLAC and DESY searching for vector mesons by photoproduction of pion pairs show an enhancement in the $\pi\pi$ invariant mass region 1400 to 1600 MeV. But since both experiments have been done with spectrometers with limited solid angle, no detailed angular distribution has been measured. In the reaction $p + \bar{p} \rightarrow K_L^0 + K_S^0$ the Reeder group from Wisconsin has found evidence for a 1^{--} particle at 1980 MeV, yet no detailed study of this particle has been made. A systematic search for new vector mesons in photoproduction

by looking for their decay products and recoil proton with a large solid angle detector is one of the experiments needed most in understanding photon physics.

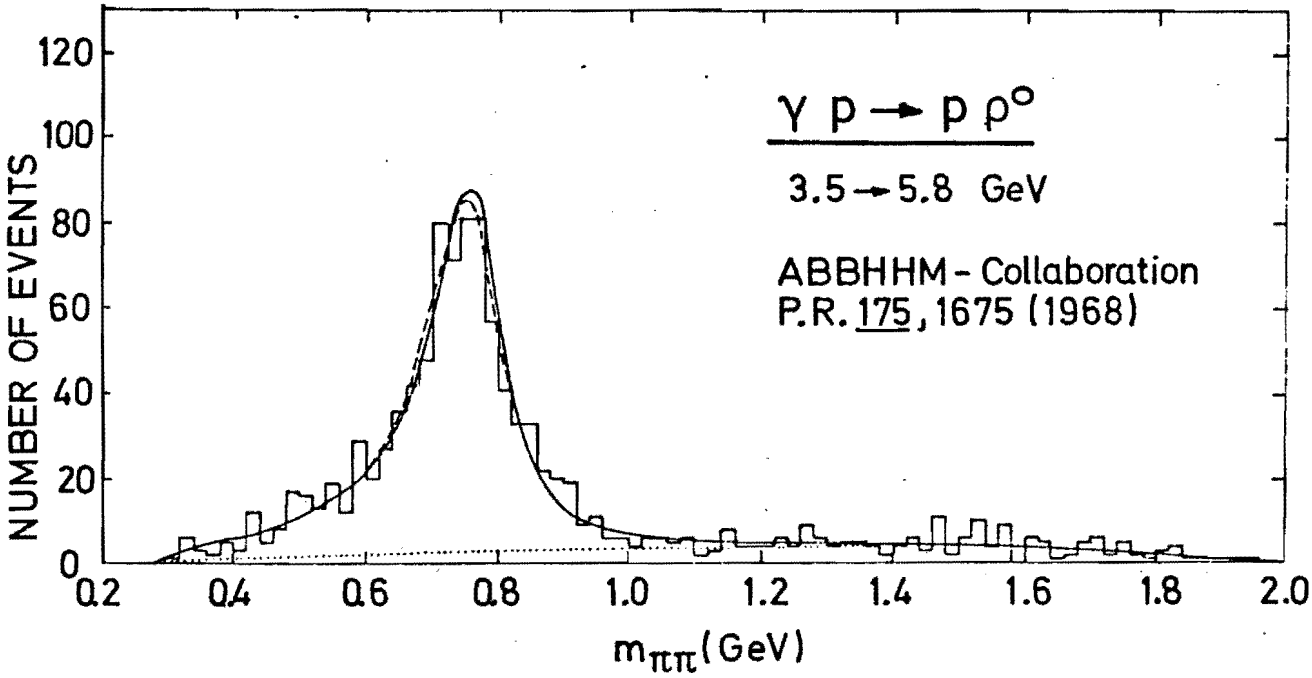
γ p → p ρ°
3.5 → 5.8 GeV
ABBHHM - Collaboration
P.R. 175, 1675 (1968)
NUMBER OF EVENTS
0
20
40
60
80
100
120
0.2
0.4
0.6
0.8
1.0
1.2
1.4
1.6
1.8
2.0
mππ (GeV)

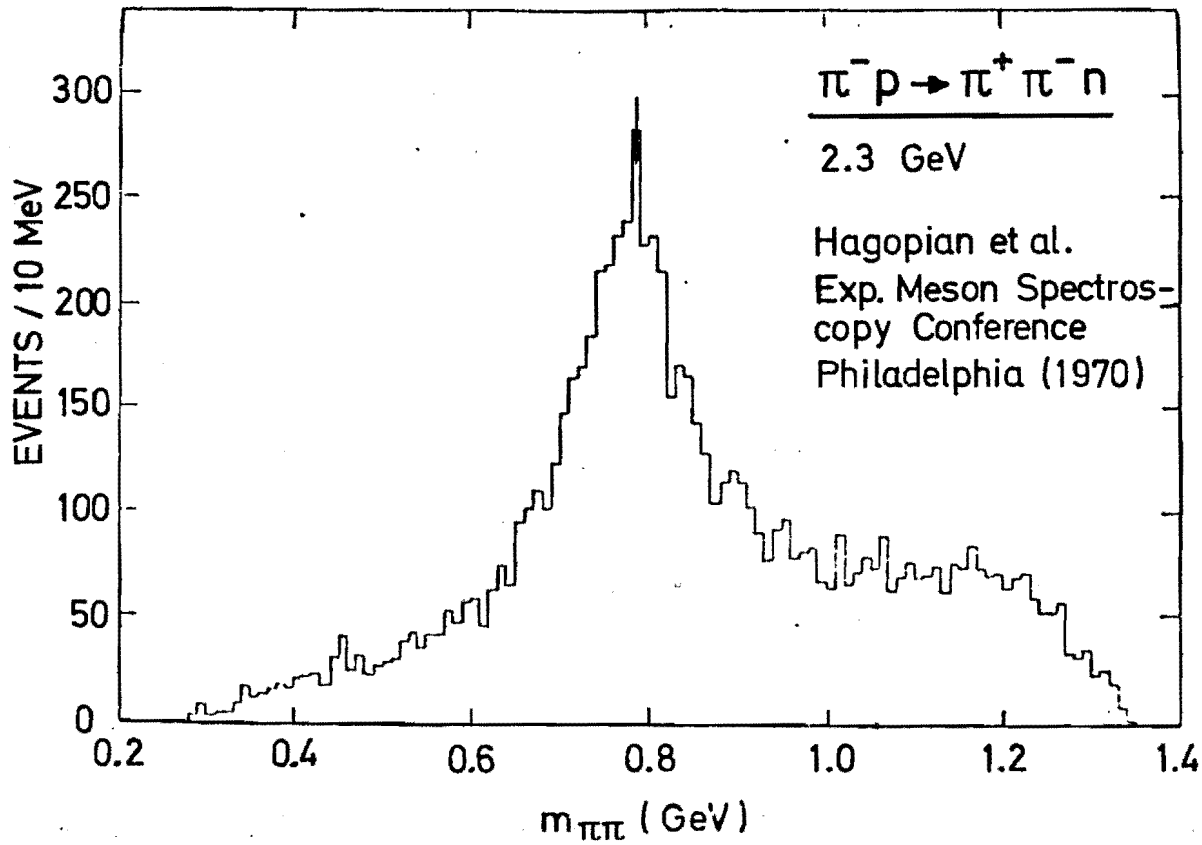
π⁻ p → π⁺ π⁻ n
2.3 GeV
Hagopian et al.
Exp. Meson Spectroscopy Conference
Philadelphia (1970)
EVENTS / 10 MeV
0
50
100
150
200
250
300
0.2
0.4
0.6
0.8
1.0
1.2
1.4
mππ (GeV)

FIG. 2a

Expt. C $\gamma + p \rightarrow p + \rho(2\pi)$

$p + \omega(\pi^+\pi^-\pi^0)$

$p + \phi(\pi^+\pi^-\pi^0, K^+K^-)$

Photoproduction of known vector mesons has been studied extensively in recent years at SLAC, Cornell, CEA and DESY.[13] Experiments show that up to 18 GeV we have a phenomenological understanding of the interaction of these vector mesons with the nucleon. For example:

The ratio of the measured production cross sections of ρ, ϕ, ω are in reasonable agreement with SU3 predictions modified by the quark model.[11]

The cross section of ρ production decreases slowly with increasing s in the same way as πp scattering, the t dependence of ρ production being a = 6 - 8 GeV^{-2}, is very similar to $\pi\rho$ slope of 8 GeV^{-2}. The cross sections are in qualitative agreement with the quark model prediction:

$$\sigma(\gamma p) \rightarrow \rho p) \propto \frac{\sigma(\pi^+ p \rightarrow \pi^+ p) + \sigma(\pi^- p \rightarrow \pi^- p)}{2}$$

However, none of the present results can be used to compare with theories to $\approx$ 20% level, and in particular, there are no s and t dependence studies at all on ϕ and ω productions.

The reason is very simple. The main difficulty is not the counting rate, but rather the duty cycle of the electron machine which makes coincidence experiments extremely difficult. Most of the experiments using counter-spark chamber techniques detect only the decay particles from $\rho \rightarrow \pi\pi$, $\phi \rightarrow KK$

or $\omega \rightarrow \pi^+\pi^-\pi^0$ and not the recoil proton. Thus inelastic contributions of the type $\gamma + p \rightarrow N^* + \rho, \omega, \phi$ (which is $\approx 15\%$), cannot be excluded. Furthermore, in the present energy region, the minimum momentum transfer to the recoil nucleus $m_V^4/4K^2$ is large.

At energies below 10 BeV the K-decay corrections in $\phi \rightarrow K^+K^-$ experiments can be as large as 50%, make it almost impossible to compare accurately the ratio of the results for ρ, ω, ϕ experiments.

At the present energy region, comparison with theories are further complicated by the fact that the production amplitudes are not pure imaginary but contain a sizeable real part. This makes the comparison of ϕ cross section with quark model predictions almost impossible.

A 200 BeV tagged beam with a good duty cycle and a large solid angle detector to measure both the forward particle and the recoil protons will enable us to study systematically, with the same apparatus, both the s and t dependence of vector meson production without the complications of N^* contamination, $K^\pm$ decay correction, etc. This may be done in a large s and t region ; $\sqrt{s}$ = 10 to 20 BeV, t from 0 to 1 BeV^2/c^2. These results will enable us to check accurately the predictions of:

(1) SU (3) and quark model

(2) Quark model : predicts the s and t dependence of ρ and ω to be $\propto \frac{\pi^+p + \pi^-p}{2}$, of ϕ should be $\propto (2\sigma_{K^+p} + \sigma_{\pi^-p} - \sigma_{\pi^+p})$

(3) The vector dominance model: at 200 BeV region the real part of the production amplitude vanishes and vector dominance model allows us a unique prediction of

$$\sigma_{\gamma p}/(4\pi\alpha)^{1/2} = \sum_V \left(\frac{d\sigma}{dt} \Big/ \frac{\gamma_V^2}{4\pi}\right)^{1/2}$$

(4) diffractive scattering.

Theoretically there are many reasons to believe that the inelastic diffraction process $\gamma + p \rightarrow \rho + p$ behaves in a way similar to pp elastic scattering.

In pp elastic scattering, there is a shoulder at

$$\sqrt{|t|} \approx 1 \text{ BeV/c}$$

If the pp differential cross section is divided by the fourth power of the electromagnetic form factor of the proton, this shoulder is seen clearly as a dip,[14] which has the property of becoming deeper for increasing energy. (See Fig 2b)

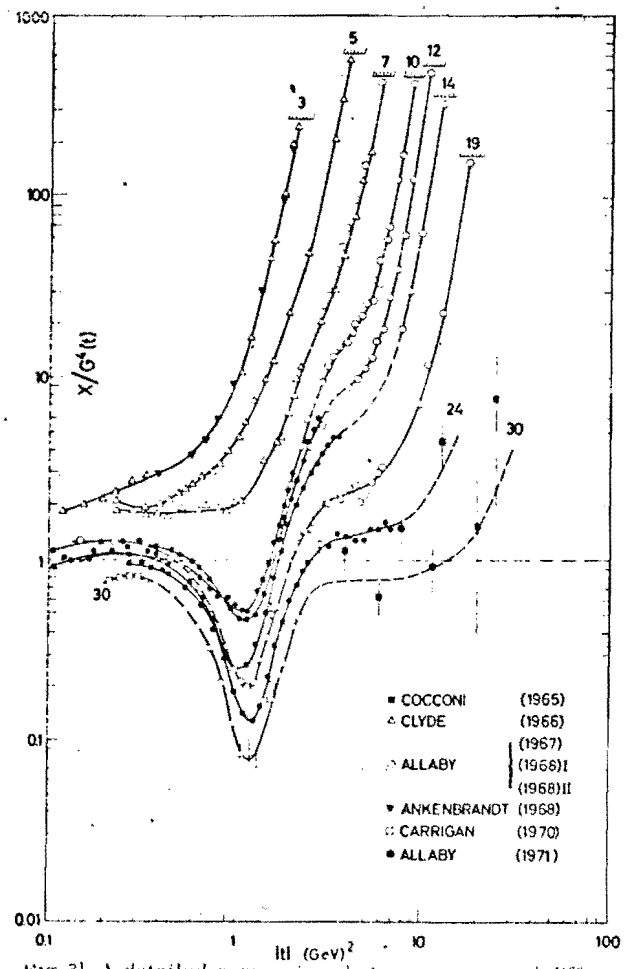

Fig. 2b A detailed comparison between measured differential cross sections and $G^4(t)$. The quantity X is the ratio of the differential cross section, $d\sigma/dt$, to the calculated optical theorem value in the forward direction. The figure shows X divided by $G^4(t)$ as a function of $|t|$.

It is thus very interesting to find out whether a similar dip is present here. The SLAC data is not accurate enough to show a shoulder; if the dip is much more pronounced at higher energies of 100 - 200 GeV, we can perhaps see it at NAL.

Expt. D <u>Regeneration experiments for ω and ϕ from nuclei:</u>

The most interesting physics one may study in photoproduction of ϕ is to use the close similarity between the K_L, K_S system and the ω,ϕ system and to look for possible regeneration of ϕ's from ω's in nuclear matter.

Indeed, the similarity between the K_L, K_S system and the ω , ϕ system are striking;

(1) Both are a coherent mixture of other states:

$$|K_S\rangle = \frac{1}{\sqrt{2}}\left(|K_o\rangle + |\bar{K}_o\rangle\right) ; \qquad |K_L\rangle = \frac{1}{\sqrt{2}}\left(|K_o\rangle - |\bar{K}_o\rangle\right)$$

$$\phi = \cos\theta|\varphi^o\rangle + \sin\theta|\omega^o\rangle ; \qquad \omega = -\sin\theta|\varphi^o\rangle + \cos\theta|\omega^o\rangle$$

Recent measurements from Desy and from Orsay have both shown that the general idea of ω-ϕ mixing is consistent with the data. Both groups yield a mixing angle $\Theta = 35^o$.

(2) For coherent regeneration, K_o, $\bar{K}_o$ must (and they do) have different interaction cross-sections in nuclear matter.

Similarly ω,ϕ also have different cross-sections, i.e.

$$\sigma_{\phi N} \simeq 10 \text{ mb}, \quad \sigma_{\omega N} \simeq 30 \text{mb}$$

(3) The difference of K_L, K_S mass is small so that coherence occurs in slabs of material.

The difference of ω,ϕ mass is not small, but since coherence is relative to phase development of the wave over the scattering system, at 150 GeV, the phase difference between ϕ and ω passing through <u>nucleus</u> is

$$\Delta t\,(W_\phi - W_\omega) = \frac{m_\phi^2 - m_\omega^2}{2k}\,\Delta t = \Delta t \cdot 0.008 \text{ rad/fm}$$

Thus it is possible that the ω, ϕ combination can be coherent over a substantial number of nucleons in a nucleus. This idea was first suggested by Ross and Stodolsky[15] many years ago.

The only possible difference between the K system and the ω, ϕ system is that whereas K_L, K_S, K_o, and $\bar{K}_o$ all exist in nature, there is no evidence for or against the existence of pure SU_3 states, ω^o, ϕ^o inside the nucleus.

If ω^o, ϕ^o really exist inside the nucleus, then measurement of photoproduction as a function of various nuclei (corresponding to varying the thickness of the regenerator) will enable us to look for a kind of regeneration phenomena very similar to that of K_L, K_S.

The experiment itself is very simple. One measures the $\phi \to \pi^+\pi^-\pi^o, (K^+K^-)$ rate off various nuclei. Choosing 14 elements uniformally across the periodic table, then independent of the absolute normalization, the ϕ yield as function of A should exhibit either of the following characteristics:

(1) the yield increases as $A^{1.8}$ (in the same way as coherent ρ production off nuclei)[16] - then there is no regeneration; the idea of Ross and Stodolsky is wrong.

(2) the yield deviates from $A^{1.8}$ law, indicating that ϕ's are regenerated from ω. The exact curve will depend on the value of θ, ω and ϕ nucleon cross section, etc.

A typical example, based on simple hard sphere calculations, is shown in Fig. 3 and indicates clearly various striking possibilities one may expect.

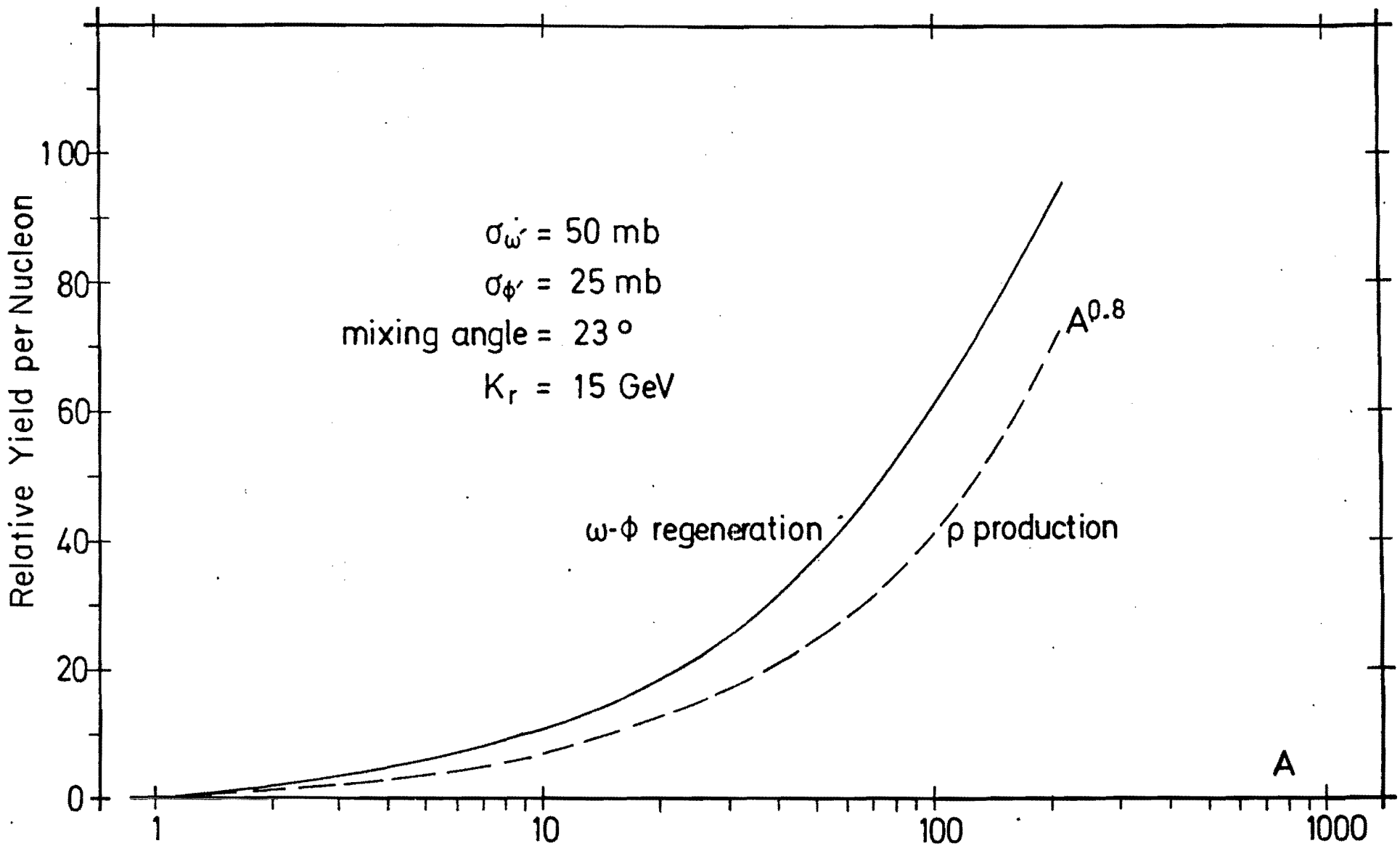

FROM "REGENERATION" EFFECTS IN ω-Φ PRODUCTION
M. ROSS, L. STODOLSKY PRL 17, 563 (1966)

FIG. 3

Expt.E Search for Heavy Leptons

With a tagged photon beam energy known to $\pm 0.5\%$ and an almost 4π detector, the proposed setup offers a unique opportunity to search for electromagnetic production of heavy leptons h^+h^- [17].

(1)The production of heavy leptons.

Assuming that the heavy leptons are coupled to the electromagnetic field in the same way as electrons and muons, the production of h^+h^- by photons in the Coulomb field of a nucleus can be easily calculated. Following Jost, Luttinger and Slotnick,[18] we write the total h^+h^- production cross section as

$$\sigma(E_\gamma) = \alpha Z^2 r_h^2 \left(\frac{28}{9} \ln \frac{2E_\gamma}{m_h} - \frac{218}{27} \right)$$

where r_h is the classical radius of the h . The yields of h^+h^- as a function of M_h for 1 m of H_2 or equivalent radiation length of C and Pb are as follows:

M_h =	0.6	1.0	1.5	3.0
Rate (300 hrs)	2770	847	330	60

(2)The decay of heavy leptons.

If the heavy leptons and their associated neutrinos enter into the lepton current in a symmetric way

$$j_\mu = \bar{\nu}_e \gamma_\mu (1+\gamma_5) e + \bar{\nu}_\mu \gamma_\mu (1+\gamma_5) \mu + \bar{\nu}_h \gamma_\mu (1+\gamma_5) h$$

the interaction of j_μ with the hadronic current gives rise to the semi-leptonic decay processes

$$h^\pm \to \pi^\pm + \nu_h$$
$$h^\pm \to \pi^\pm + \pi^0 + \nu_h$$
$$h^\pm \to \rho^\pm + \nu_h$$

The decay rate into $\pi \nu_h$ is (ignoring the Cabibbo angle)

$$\Gamma = G^2 c_\pi^2 m_h^3 / 8\pi \left(1 - m_\pi^2/m_h^2\right)^2 \; ; \; G^2 \simeq 10^{-5}/m_p^2$$

with c_π the usual charged pion decay constant $\approx$ 94 MeV. Compare this with the usual pure leptonic decay mode into $e^- \nu_e \nu_h$

$$\Gamma = G^2 m_h^5 / 192\pi^3$$

One concludes that:

(a) $M_h < 1$ BeV, the dominant decay mode is $\pi\nu_h$ which by far outnumbers the pure leptonic channels. For example, if $M_h = 0.6$ BeV, the $\pi\nu$ mode outnumbers the leptonic channel by a factor of five. This could explain, as first pointed out by Sakurai,[19] why the Frascati storage ring, looking for $e^+e^- \to \mu^+e^-$ for $M_h < 1$ BeV, fail to see any h^+h^-.

(b) $M_h > 1$ BeV, the dominant decay modes are the pure leptonic ones, as the pure leptonic modes increase as M_h^5 while the semi-leptonic mode increases as M_h^3.

(3) The detection of heavy leptons.

Following the above discussion, the best way to detect the heavy leptons is to use a tagged photon beam with a nearly 4π detector and look for events of the type

$$\begin{aligned} \gamma + Z &\to Z + h^+ + h^- \\ &\to Z + \mu^\pm e^\mp + 4\nu \qquad (8a) \\ \text{or} \quad &\to Z + \pi^\pm \pi^\mp + 2\nu \\ &\to Z + \pi^\pm \mu(e) + 3\nu \end{aligned}$$

The above calculations are for ordinary leptons. If leptons with strangeness $S = \pm 1$ are produced, they may decay predominately into $K^\pm \nu$

$$\gamma + Z \to Z + h^+ + h^- \to Z + K^+ + K^- + \nu + \nu \qquad (8b)$$

In that case we will look for a K^+K^- pair with a total energy far below that of the photon.

Reactions (8a) and (8b) give the following distinct signals:

(a) The total energy of the μe or $\pi^\pm(K^\pm)$ pair is far below the incident photon energy.

(b) The rate goes as $Z^2 G_E(q^2)$.

With a nearly 4π detector contamination of the following types will be rejected easily:

$$\gamma + A \to A + \mu^+ e^- + \mu^- e^+$$
$$\gamma + A \to A + \rho \to A + \pi^+ + \pi^-$$
or
$$\gamma + A \to A'' + K^+ + K^-$$

Expt. F. Elastic Compton scattering

With the proposed beam, we can study this fundamental reaction up to 200 GeV and momentum transfers up to ≈ 0.5 $(\mathrm{GeV/c})^2$. This enables us to learn the following:

(i) At existing electron accelerator energies, the differential cross-section behaves as A exp (bt),[20] where the slope b (related to shrinkage) and A still show considerable energy variation. At NAL energies, do we still have shrinkage? Has A approached some asymptotic value? These questions are important for the Regge Theory and are intimately connected with the nature of the Pomeron.

(ii) Following the paper by Gell-mann, Goldberger and Thirring[21] which extends the Kramers-Koenig dispersion relation to high energy physics, the forward Compton amplitude and cross-section can be written as follows:[22]

$$\left.\frac{d\sigma}{dt}\right|_{t=0} = \frac{\pi}{\nu^2}\left|f(\nu)\right|^2$$

$$f(\nu) = f_1(\nu)\,\vec{\varepsilon}_2\cdot\vec{\varepsilon}_1 + i\,f_2(\nu)\,\vec{\sigma}\cdot\vec{\varepsilon}_2\times\vec{\varepsilon}_1$$

$$\mathrm{Re}\,f_1(\nu) = -\frac{\alpha}{M} + \frac{\nu^2}{2\pi^2}\,\mathbb{P}\int_{\nu_0}^{\infty}\frac{d\nu'}{\nu'^2-\nu^2}\,\sigma_T(\nu')$$

$$\left.\frac{d\sigma}{dt}\right|_{t=0} = \frac{\sigma_T^2(\nu)}{16\pi} + \frac{\pi}{\nu^2}\left|\mathrm{Re}\,f_1(\nu)\right|^2 + \frac{\pi}{\nu^2}\left|f_2(\nu)\right|^2$$

Our total cross-section measurement will establish the energy dependence of Re $f_1(\nu)$. Almost all theoretical models at present, and experimental data in hadron induced reactions lead us to expect that Re f_1 will become very small at NAL. It then follows that we shall be able to study the functional dependence of f_1 in a very clean way to confront, for example, the predictions of the VDM:

$$f_{\gamma\gamma} = f_{\gamma\rho}\,g_{\gamma\rho}^{+} \quad f_{\gamma\omega}\,g_{\gamma\omega}^{+} \quad f_{\gamma\phi}\,g_{\gamma\phi}^{+} \quad f_{\gamma V}\,g_{\gamma V}^{+} \quad \ldots$$

$$\frac{d\sigma}{dt}(\gamma p\to\gamma p) = \sum_{V'}\frac{d\sigma}{dt}(\gamma p\to V' p)\,g_{\gamma V}^{2}$$

At existing energies, the comparison is limited to $\pm$ 20% because of the large real parts of $f_{\gamma\gamma}$ and $f_{\gamma V}$, and because of the difficulty of performing large solid angle detector experiments with coincidence techniques. We propose to measure both sides of the above equation with the same apparatus, thus reducing systematic errors. A clear-cut comparison of the s and t dependence of the Compton cross-section and vector photoproduction cross-section is one of the best ways to check vector dominance model.

(iii) If one assumes the Quark Model in addition to the VDM, then the Compton cross section should show the same energy dependence as

$$\left(\frac{\sigma_{\pi^+p} + \sigma_{\pi^-p}}{2}\right)\left(g^2_{\gamma\omega} + g^2_{\gamma\rho}\right) + g^2_{\gamma\phi}\left(2\sigma_{K^+p} + \sigma_{\pi^-p} - \sigma_{\pi^+p}\right)$$

Is this true at NAL energies?

Expt. G. Total Cross-Sections $\sigma_T(\gamma p)$ and $\sigma_T(\gamma n)$.

The fundamental quantity, the total cross-section[23] for photon-hadron collisions can be measured simultaneously in our detector as the sum of the experiments A, B, C, & D and all other non-electromagnetic interactions. This will allow us to study the following questions:

(i) Regge theory (poles, poles and cuts, etc.) and the simple Quark Model would lead us to expect that the photon hadron cross-section has the same features at NAL energies as the hadron-hadron cross-sections. Is this true? The present parametrization,

$$\sigma_T = c_1 + c_2/\nu^{1/2}$$

gives a good fit for data away from the resonance region and up to 20 GeV. It supports the picture of ρ, ρ' and A_2 exchange. Since this form plays an essential role in dispersion calculations, it is important to ascertain whether this parametrization holds for NAL energies.

(ii) The knowledge of $\sigma_T(\nu)$ enables us to compute $\mathrm{Re}\, f_1(\nu)$ from the Kramers-Koenig relation. We will thus be able to have a direct comparison with the direct measurement of the phase of the Compton amplitude done by measurement of the interference between the Compton amplitude and Bethe-Heitler amplitude in electron pair photoproduction at DESY. This will constitute a test of the dispersion relation.

CHAPTER TWO

THE FORWARD DETECTOR

INTRODUCTION

The design of the forward detector is greatly influenced by the experience with the large solid angle focusing spectrometers developed and used at DESY during the last 5 years. (Similar spectrometers were also used successfully at Cornell and SLAC for coincidence experiments). Basically, it is a simple spectrometer with two dipole magnets which recombines rays of constant ϕ and therefore has a large acceptance and, at the same time, a good t and m resolution. Furthermore, the spectrometer transports all the $0^{o}(e^{-}e^{+})$ background pairs on to a fixed image point to be rejected easily.

The spectrometer consists of two bending magnets, proportional chambers, scintillation counter hodoscopes and shower counters. The detector can be separated into two independent systems; a low momentum resolution large solid angle system and a high momentum resolution small solid angle system. The former is specifically designed to study the lower momentum particles produced at angles up to $\approx$ 120 milliradians (7°) and the latter for particles up to 200 GeV and angles $\approx$ 30 milliradians. In both systems photons are also detected.

The rejection of $e^{-}e^{+}$ pairs enables us to record all non-electro-magnetic events. The large solid angle and good mass resolution enable us to search for rare events.

A. DESIGN CONSIDERATIONS

i) Kinematics and Counting Rates

The total hadronic γp cross-section is $120\,\mu b$. Thus with $4 \times 10^5 \gamma$/ burst and a 1 m hydrogen target a counting rate of 200 events/burst will be obtained. This implies that throughout the detector system scintillation counters together with proportional chambers must be used.

The **purpose of the detector is** to survey multiparticle photoproduction at energies up to 200 GeV, and in particular study the following class of events:

1) $\gamma + p \longrightarrow p + V^\circ$, $V^\circ \longrightarrow \pi^+\pi^-, \pi^+\pi^-\pi^\circ, K^+K^-, n\pi$

Where V may be a heavy vector meson up to about 10 GeV.

2) $\gamma + p \longrightarrow \gamma + p$

3) $\gamma + p \rightarrow \pi$ or K or P + anything.

By noting that in multiparticle production the average transverse momentum of any particle is ≤ 350 MeV/c and studying the production and decay kinematics of the above reactions, it is immediately apparent that, at the energies considered, the high momentum particles tend to go into a very small forward cone, whilst particles at larger angles have low momenta. To illustrate this point, in Fig. 4 we plot the decay kinematics of a few vector mesons with different mass at 150 GeV momentum.

From the above we conclude that the forward cone has to be covered by essentially two distinct spectrometer systems.

a) for small angles, say $\lesssim 30$ milliradians, most particles are very energetic, therefore it is necessary to use strong bending magnets and long lever arms to obtain the necessary precision in angle and momentum measurements.

b) for angles $\gtrsim 30$ milliradians it is sufficient to use weaker magnets and smaller lever arms, but it is necessary to cover a large solid angle.

ii) e^+e^- Background:

The electromagnetic pair production cross-section in H_2 is 200 times greater than the total hadronic cross-section. For heavy elements it is even worse; in lead, for example, the ratio is 3000 . Thus a necessary requirement on the detection system is that it has a very high rejection efficiency of e^+e^- pairs without a significant loss of hadronic events.

iii) Economic Considerations:

1) With the number of experiments planned for NAL, the machine time will be at a premium and it is important to study as many reactions as possible simultaneously

2) The system has to be sufficiently simple to be economically feasible and not to use too much power. In fact the maximum permissible power level for the forward spectrometer was fixed to be $\leq$ 1.0 MW. This implies, for example, that high resolutions in momentum measurements should be aimed at only where absolutely necessary.

3) It was considered that for practical and economic reasons the maximum number of wires that could be used in the forward detector w[illegible] $\leq$ 10K.

The "Jolly Green Giant" magnet from CEA may be available to us and it should be used rather than building a new magnet.

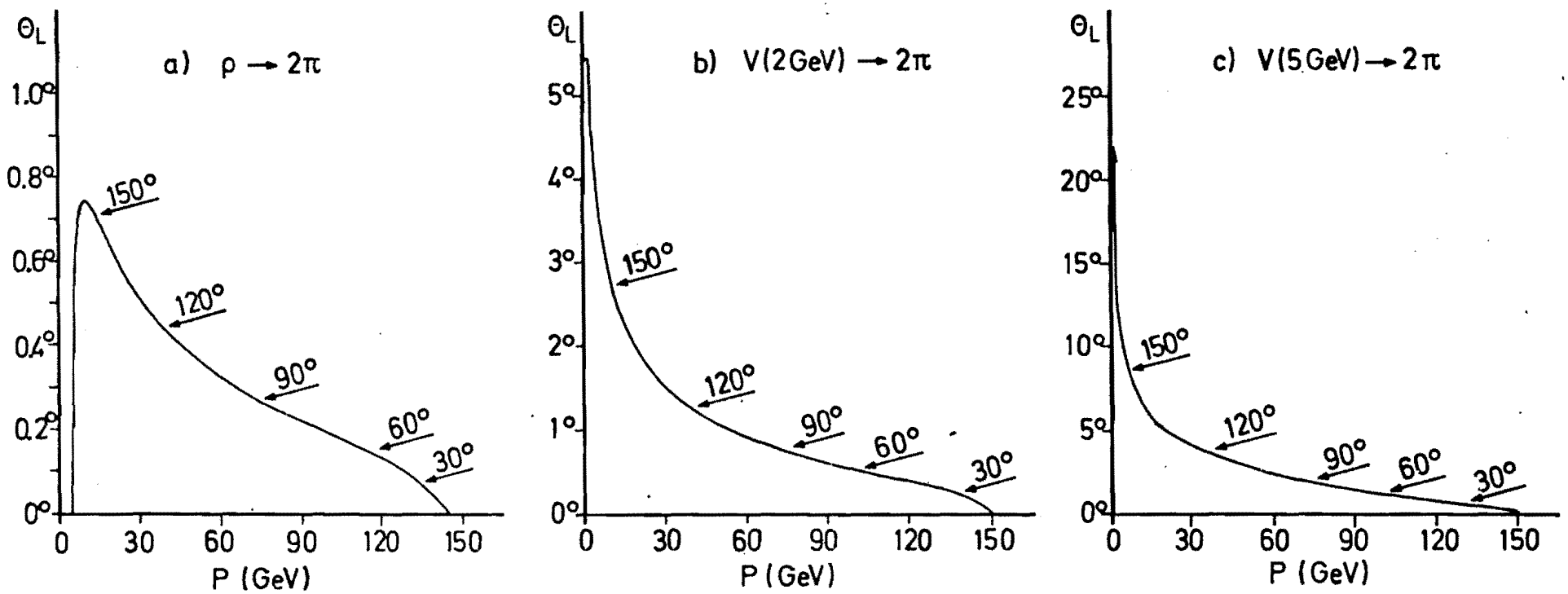

DECAY KINEMATICS FOR $V \rightarrow 2\pi$ AT $P_{TOTAL} = 150$ GeV

PION LAB ANGLE VS PION MOMENTUM

ALSO INDICATED IS THE C.M. DECAY ANGLE

FIG.4

B. DESCRIPTION OF FORWARD SPECTROMETER SYSTEM

Fig. 5 illustrates the complete detection system. The same scale is used in both the x and y directions to give a clear indication of sizes and angles involved. For clarity the same system is shown in Fig. 6, with different scales in both directions. (1) through (5) are planes containing proportional chambers, scintillation counter hodoscopes and shower counters. Details of these detector planes are given in Figs. 7 and 8. Planes (1), (2), and (3) together with magnet M1 measure the direction and momentum of particles produced up to 7°. Planes (1), (4), and (5) together with magnets M1 and M2 measure with high resolution the direction and momentum of particles produced up to 30 milliradians. M1 and M2 are operated with fields in the opposite directions and the distances between M1, M2 and plane (5) are such that there is a $\emptyset$ focus at the end of the detector. This property is extremely valuable in the rejection of e^+e^- pairs, and in the determination of the invariant mass of the final state particles.

At planes (2), (3) and (5) there are scintillation counter hodoscopes for rejecting e^+e^- pairs and for triggering the system. At (3) and (5) there are shower counters to measure the energy of γ's and electrons.

Behind the shower counters, not shown on the diagrams, there are muon detectors consisting of absorbers and scintillation counters. For separating π's from K's at lower momenta ($\leq$ 105 GeV) we are considering the placing of gas threshold Čerenkov counters between planes (3) and (4) and between (4) and (5). (See Appendix III).

I. Large solid angle part of the detection system:

M1 is the Jolly Green Giant Magnet from CEA. It is operated with an aperture of 150 x 50 cms^2 (60"x20") and a field of 15 kGauss. The total integral field is 18 Kgauss-meters.

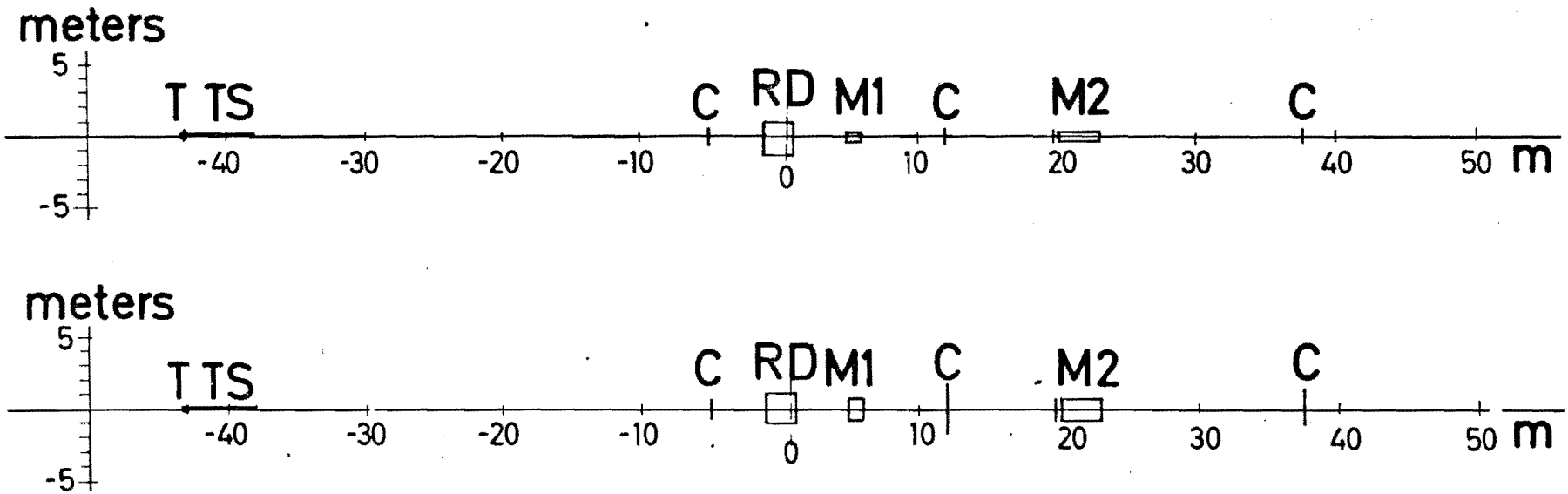

T = Tagging Target
TS = Tagging System
C = Counters or Charpak Chambers
RD = Recoil Detector

The Detector System

FIG. 5

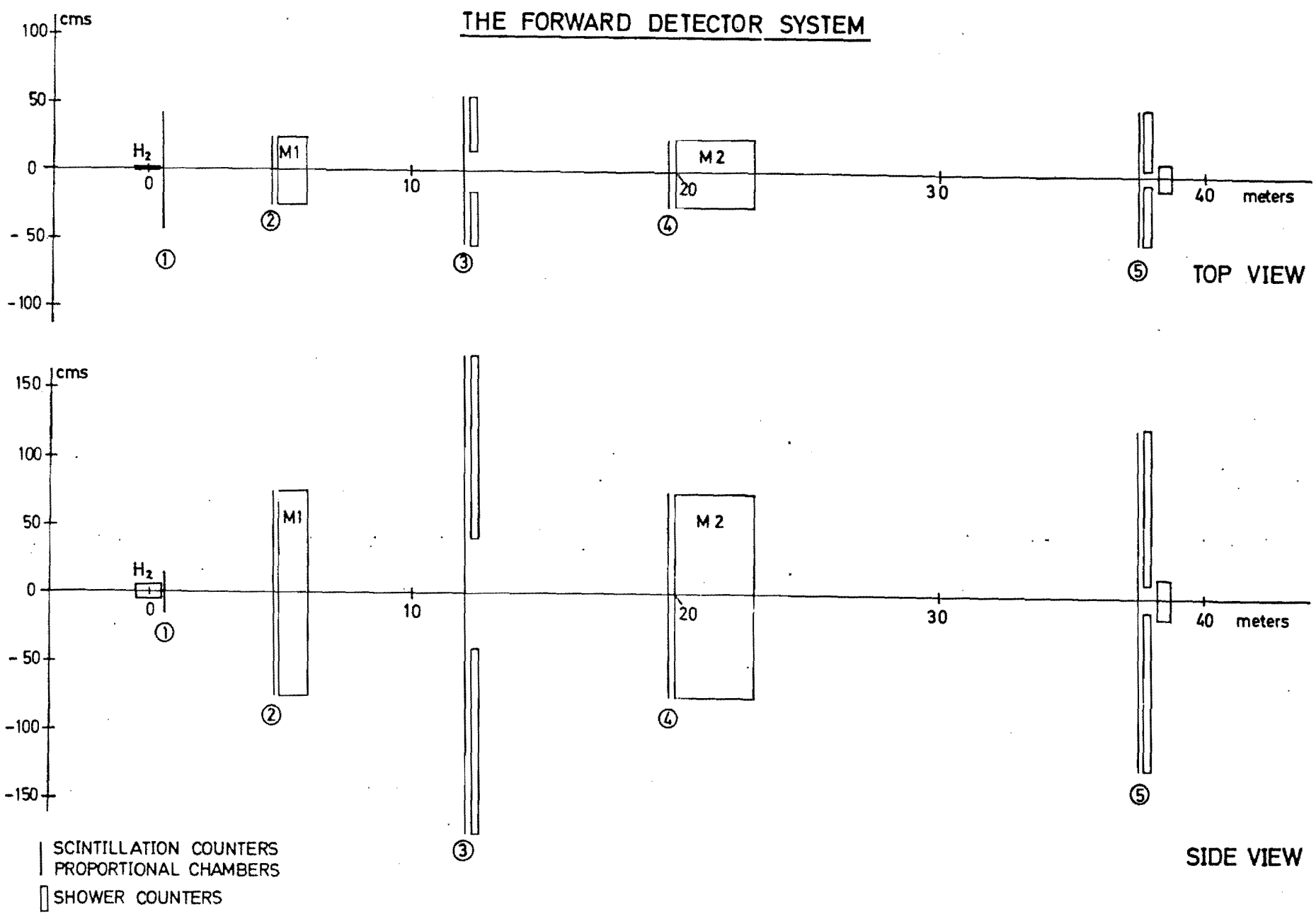
THE FORWARD DETECTOR SYSTEM
cms
100
50
0
- 50
-100
H2
0
M1
10
M2
20
30
40
meters
①
②
③
④
⑤
TOP VIEW
cms
150
100
50
0
-50
-100
-150
H2
0
M1
10
M2
20
30
40
meters
①
②
③
④
⑤
SIDE VIEW
SCINTILLATION COUNTERS
PROPORTIONAL CHAMBERS
SHOWER COUNTERS

FIG. 6

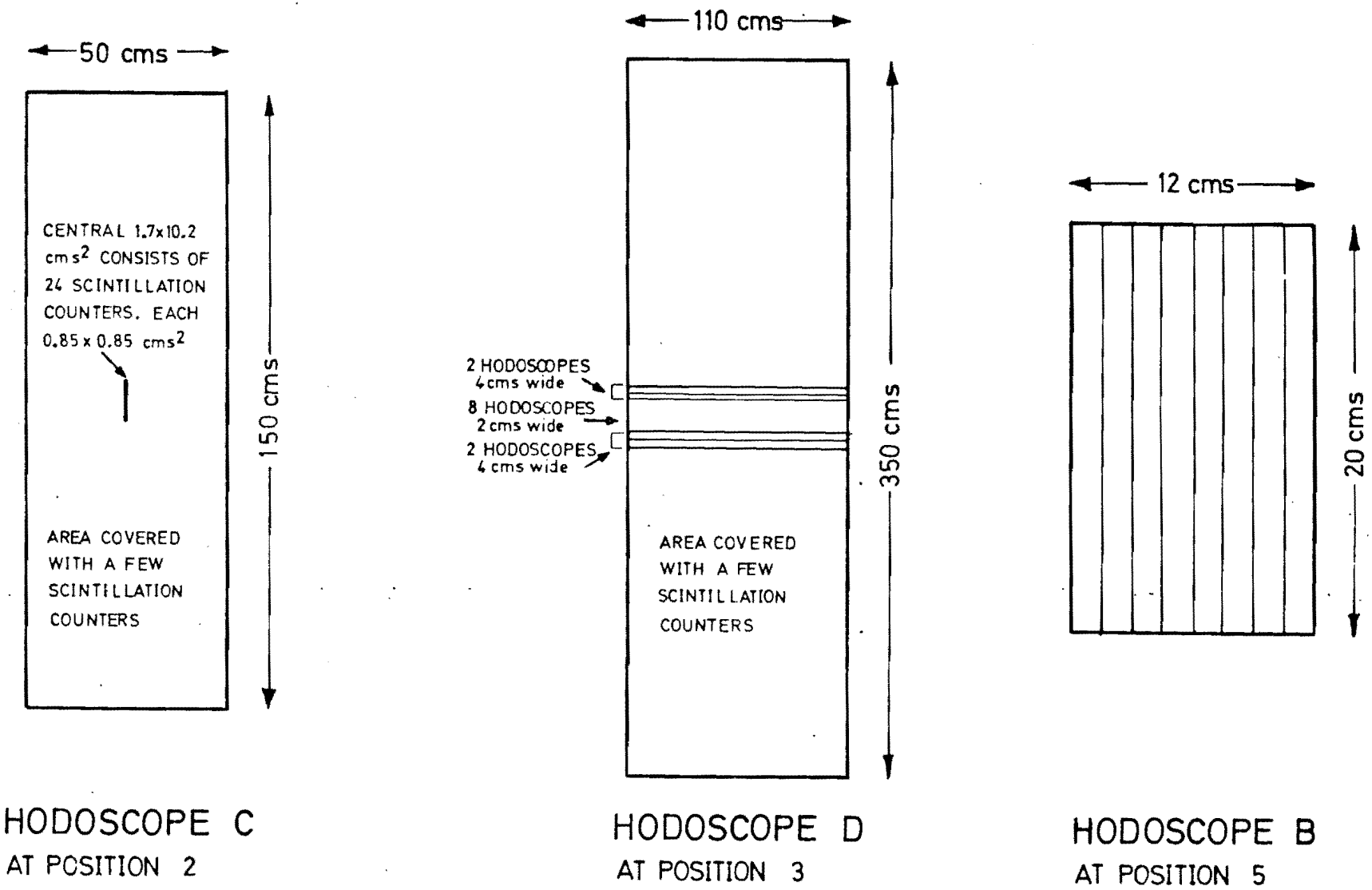

HODOSCOPES B, C, D

FIG. 7

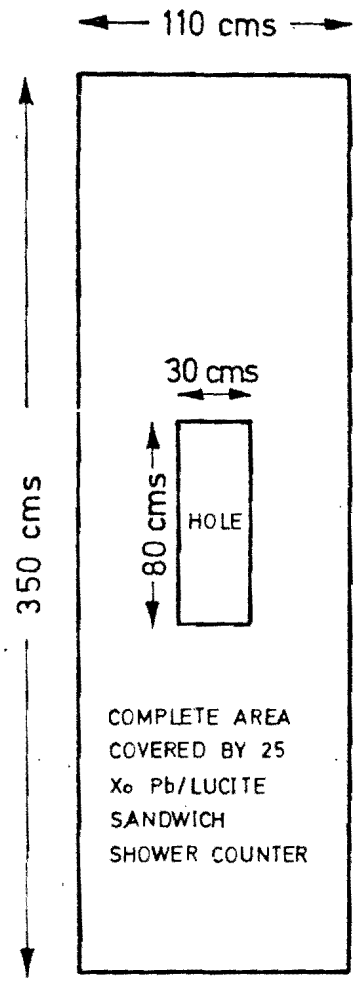

SHOWER 4
AT POSITION 3

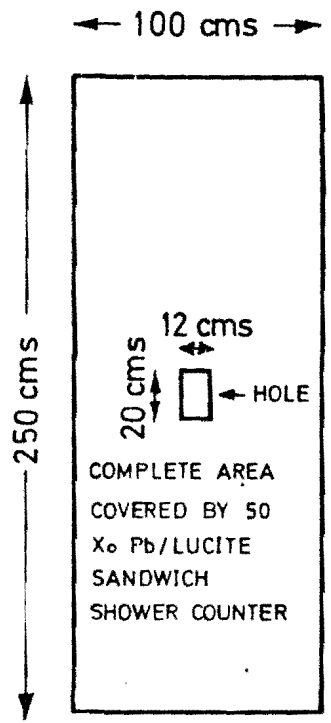

CAN BE EITHER A
SOLID Pb-LUCITE
SHOWER COUNTER
$20 \times 30\ cms^2 \times 50 X_o$
OR
MADE OF TWO
PIECES OF THE
Pb/GLASS SHOWER
COUNTERS ON LOAN
FROM L.R.L.
(TOTAL: $25 \times 50 \times 100\ cms^3$)

SHOWER 3 SHOWER 2
AT POSITION 5

SHOWER COUNTERS

FIG. 8

With this field strength and aperture the power requirement of the magnet is 0.4 MW.

Proportional chambers at planes (1), (2) and (3) measure the momentum and direction of charged particles passing through the magnet. The acceptance of this spectrometer is shown in Figure 6 and the resolution in Table 3. The chamber at position (3) consists of 3 planes of wires at different angles with a $3X_0$ Pb sheet between the first and second plane as shown in Fig. 9. This last chamber measures the direction of γ's (e.g. from π^0 decay) in addition to that of charged particles.

II. Small angle, high momentum resolution spectrometer system:

Magnets M1 and M2 form the high momentum part of the detection system. M1 has been described above. M2 is a magnet with an aperture 150 x 50 cms and a 300 cms pole piece. It is operated at 12 Kgauss, i.e. the total integrated field is 36 Kgauss-meters. At this field strength it will use 0.6 MW of power.

The optical properties of the combination of M1 and M2 are illustrated in Fig 10 . The large lever arms on either side of M2 allow an accurate determination of momentum of particles passing through the magnet. As in System I the last proportional chamber, (5) consists of a sandwich of a lead sheet between proportional wire planes, allowing a determination of the direction of π^0's. The acceptance of this system is shown in Fig. 11 and the resolution in Table 1.

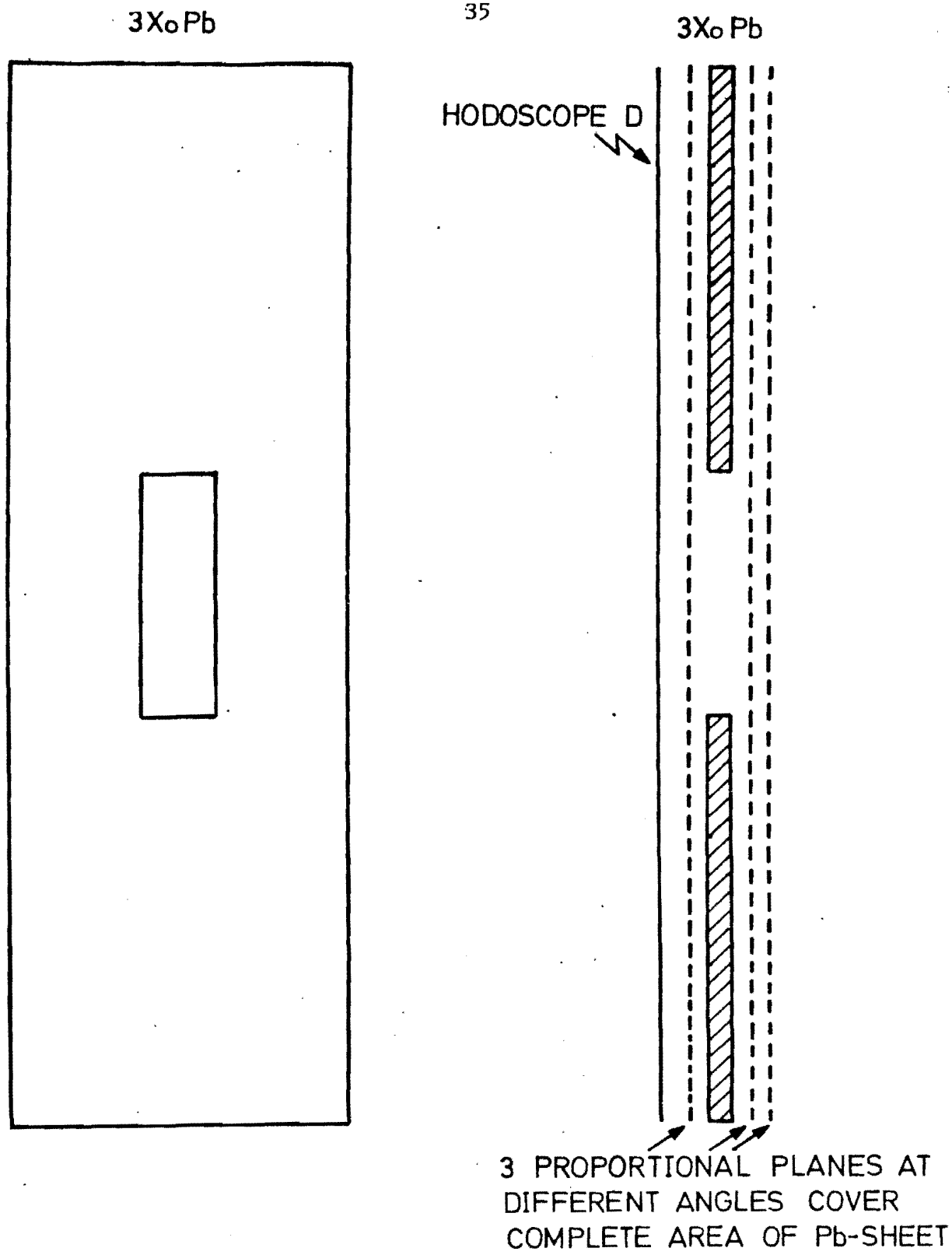

PROPORTIONAL CHAMBER AND Pb SHEET FOR γ DETECTION AT POSITION 3 (12m from target)

FIG. 9

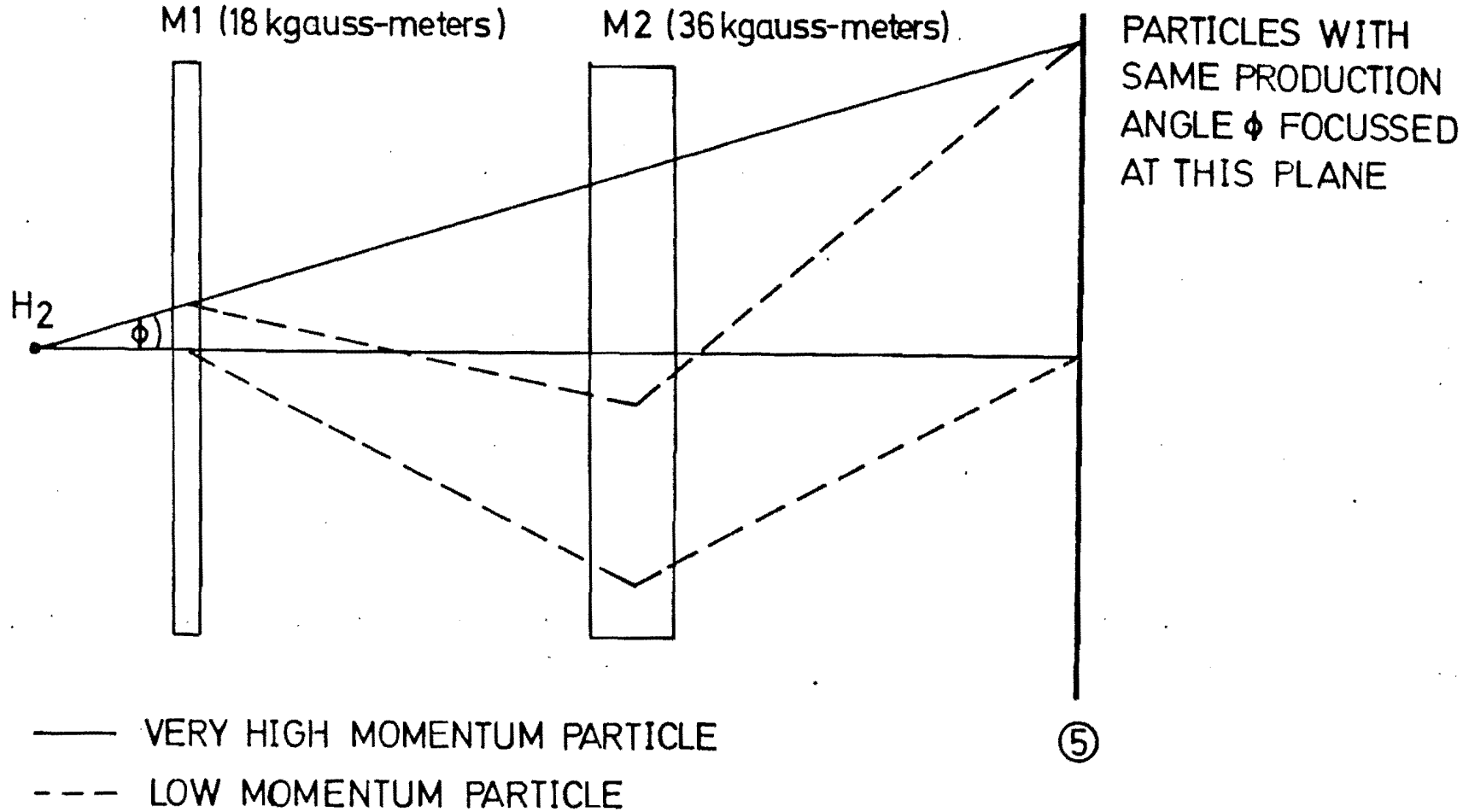

ILLUSTRATION OF OPTICAL PROPERTIES OF M1, M2 SYSTEM

FIG.10

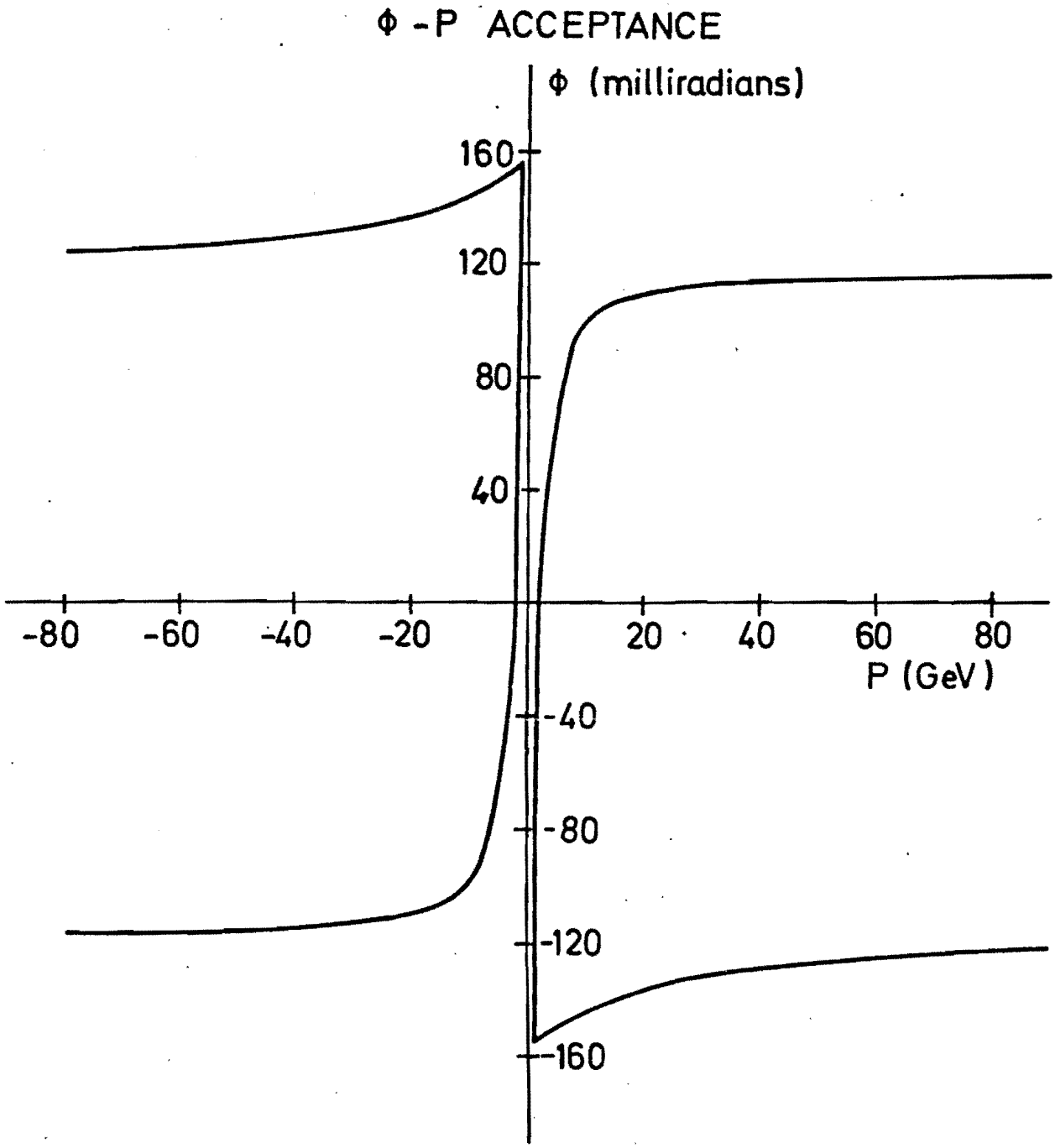

Θ ACCEPTANCE = ±40 milliradians

ACCEPTANCE WINDOW FOR LARGE ANGLE REGION (I)

FIG. 11a

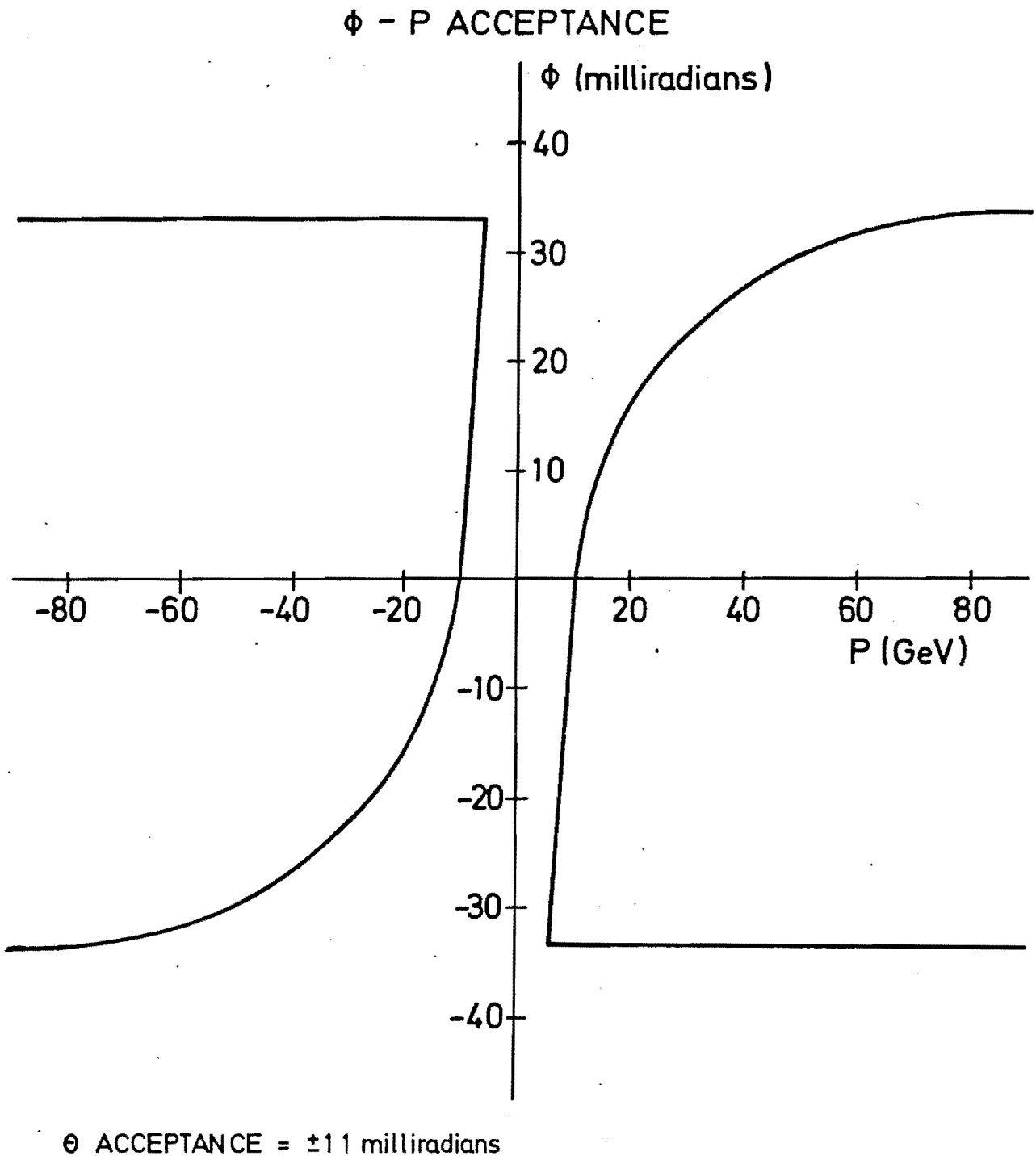

ACCEPTANCE WINDOW FOR SMALL ANGLE REGION (II)

FIG. 11b

TABLE 1 -- RESOLUTION OF SPECTROMETER

I. LARGE ANGLE SYSTEM:

For charged particles:

$\Delta\Theta = \pm 0.12$ milliradians

$\Delta\phi = \pm 0.16$ milliradians

$\frac{\Delta P}{P} = \pm 0.075\ P\ \%$

For neutral particles with energy $E \sim 50$ GeV:

$\frac{\Delta E}{E} = \pm 3\ \%$

$\Delta\theta = \Delta\phi = \pm 0.25$ mr

II. SMALL ANGLE SYSTEM:

For charged particles:

$\Delta\Theta = \pm 0.04$ milliradians

$\Delta\phi = \pm 0.04$ milliradians

$\frac{\Delta P}{P} \leq \pm 0.014\ P\ \%$ for $P \gtrsim 50$ GeV/c

For neutral particles with energy ~ 50 GeV:

$\frac{\Delta E}{E} = \pm 3\ \%$

$\Delta\theta = \Delta\phi = \pm 0.08$ mr if the vertex is determined.

P, E in GeV

C. TRIGGERING OF THE SYSTEM AND e^+e^- REJECTION

The philosophy of the triggering system is that whenever, in coincidence with a tagged photon, an interaction occurs which is not just an e^+e^- pair, the information about the interaction is stored.

I. The characteristic features of the e^+e^- pairs are that:

a) the pair is produced in the same direction as the incident γ.

b) the electrons are produced with an extremely small opening angle ($\sim \frac{m_e}{E_\gamma} \log \frac{E_\gamma}{m_e}$).

c) in a shower counter the two electrons deposit an energy equal to that of the original photon.

d) since the e^+e^- carries the total energy of the beam, the minimum e^-e^+ opening angle after bending magnets is fixed.

Corresponding to the above four features, three sets of veto signals can be generated to reject e^+e^- pairs. A sketch of all the trigger counters is shown in Figure 12.

II. The triggering counters:

a) Hodoscope A, lead glass counter SH_1 and veto counter V:

The coincidence between one of the counters A_i and SH_1 signifies that a tagged photon has been produced. The energy of the photon is approximately equal to the energy of the primary electron less the energy corresponding to the pulse height in SH_1.

The origin of the photon in the horizontal direction is given by A_i. The vertical position is defined by the size of the tagging target, which is 0.4" high.

A lead collimator is placed between the hydrogen target and the tagging target. Immediately behind the aperture of the collimator a thin veto counter V is situated. Any photon interacting in the collimator or any random background particle, e.g. electron or muon, is vetoed by this counter.

An incident photon signal is thus given by $A_i \cdot SH_1 \cdot \overline{V}$.

The time the photon is emitted is defined by hodoscope A.

b) Lead glass shower counter SH_2 and hodoscope B:

SH_2 is a lead glass total absorption shower counter situated at the back of the detector. All the non-interacting photons are counted by SH_2. which serves as a monitor of the beam. The focusing property of the forward detector is such that all charged particles with momentum >12 GeV and production angle <2.5 milliradians pass through SH_2. Thus SH_2 also measures the energy of the e^+e^- pairs

Hodoscope B, situated in front of SH_2 determines whether the shower in SH_2 is due to charged particles ($e^{\pm}$) or photons.

Because the e^- beam has a sharp focus in the horizontal plane at the hydrogen target, hodoscopes B_i and A_i identify particles produced in the forward direction, i.e. with angles < 0.4 milliradians. Since e^+e^- pairs are produced predominantly in the very forward direction, this property enables us to reject e^+e^-.

3) Hodoscopes C and D:

These hodoscopes serve two functions: They identify forward going charged particles, and they identify pairs of charged particles with close to zero opening angle.

The central elements of C are 24 scintillation counters of 0.85x0.85 cms^2 each, covering a total area of 1.7 x 10.2 cms^2. The size of the counters is chosen such that essentially all hadronic events (including, for example, 200 GeV $\phi \rightarrow KK$) will trigger at least two counters in C, while most of e^+e^- pairs will trigger only one counter. Hodoscope C covers the complete aperture of the forward detector for triggering purposes.

Hodoscope D consists of 12 counters. After the magnet M1, e^+e^- pairs are separated and trigger two counters in D. The size of the D hodoscopes is such that the knowledge of which hodoscope fired in C and D can be used to obtain the energy of the e^+e^- pair to $\leq$ 0.5 P%. This information helps in distinguishing hadronic and e^+e^- events.

4) Shower counters SH_3 and SH_4:

The purpose of these counters is

a) to measure the energy of electrons in the energy range 2 to 12 GeV which did not reach SH_2; adding pulses from SH_2, SH_3 and SH_4 gives to within a few per cent, the energy of the photon which produced the e^+e^- pair.

b) to identify π^o's and γ's produced at large angles.

5) Counter P:

In Figure 13 counter P is just a symbol for the detection of a particle, charged or neutral, produced in directions other than into the forward detector.

III. e^+e^- Signal:

It follows from (I) and (II) that an e^+e^- pair is identified by any of the following combinations:

a). charged particles produced in the forward direction with $SH_2 \geq 50$ GeV. The coincidence of the corresponding counters A_i and B_i defines a forward charged particle.

b) A pair of charged particles with 0° opening angle, i.e. $C = 1$ and $D = 2$ and $SH_2 \geq 50$ GeV.

c) At least one counter each in C, D & B are triggered and the sum of the pulses from $SH_1 + SH_2 + SH_3 + SH_4$ is within a few percent of the energy of the primary e^- beam.

If any of the above three is satisfied, the event is classified as an e^+e^- pair and rejected. Conditions a), b), and c) yield an estimated e^+e^- rejection of $10^{-3} - 10^{-4}$. Together with analysis of wire chamber signals we will definitely distinguish any e^-e^+ contamination from hadronic events.

IV. Trigger of System:

We are now in a position to describe the trigger of the system. An event is recorded if the following conditions are satisfied

1) there is an incident photon, i.e. $A_i \cdot SH_1 \cdot \overline{V}$
and
2) there was no e^+e^- pair detected
and
3) at least one of the shower counters SH_3 or SH_4 gave a large signal, say ≥ 10 GeV,

or

there was a recoil proton signal P

or

there was at least one coincidence between C and D.

A logic diagram of the trigger system is shown in Figure 13.

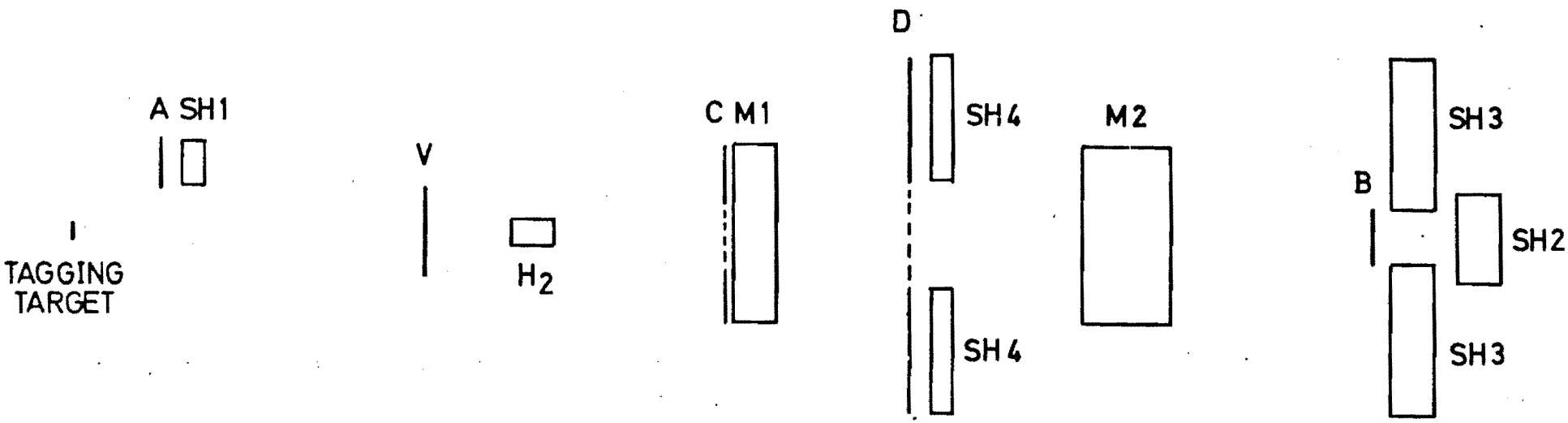

SKETCH OF ALL TRIGGER COUNTERS

FIG. 12

LOGIC DIAGRAM FOR TRIGGER SYSTEM FOR

$\gamma p \rightarrow V p$, $V \rightarrow n \pi^{\pm}_{0}$

$\gamma p \rightarrow \gamma p$

$\gamma p \rightarrow \pi + X$

$\gamma p \rightarrow p + X$

$\gamma p \rightarrow$ all hadrons

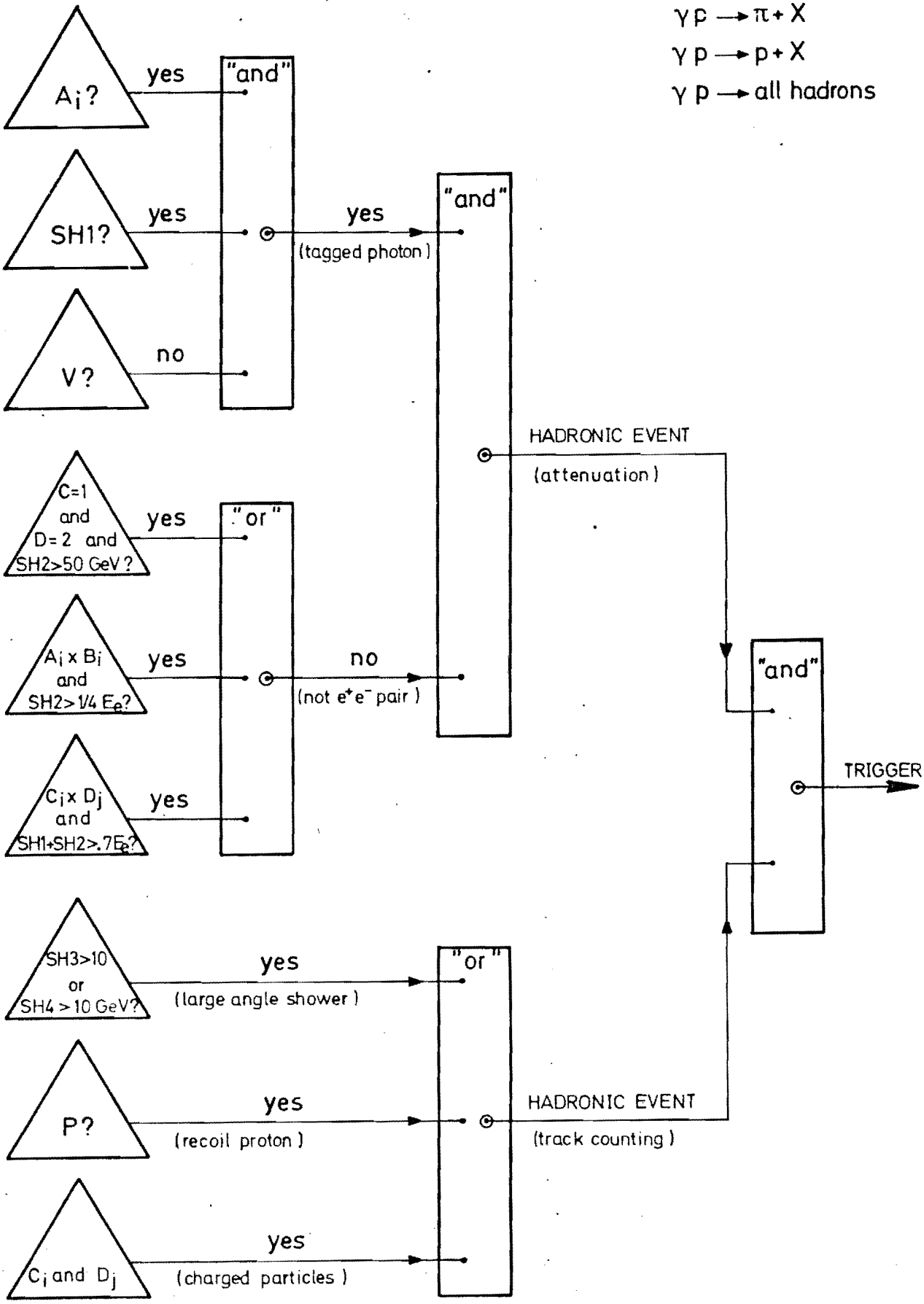

FIG. 13

D. MONITORING OF BEAM AND CHECKS OF THE COMPLETE FORWARD DETECTION SYSTEM:

One of the important features of the design of the forward detector is that there are two built-in independent beam monitoring systems. One of these in addition checks the acceptance and operation of the counters and proportional chambers and the pulse height of the shower counters.

I) Lead glass shower counter, SH_2:

SH_2 is a direct monitor of the beam; the attenuation of the beam between it and the tagging target can be calculated exactly and the background in SH_2 can be essentially eliminated by requiring that :

a) the signal be in coincidence with A_i

b) $SH_2 + SH_1$ = energy of incident electron.

II) e^+e^- pair spectrometer:

The pair production rate and spectrum can be calculated exactly according to Q.E.D. Thus using the complete detection system as an e^+e^- pair spectrometer it is possible to check the acceptance, operation, efficiency and calibration of the system.

This kind of monitoring can be carried out not only during special calibration runs, but also by storing on tape one out of every 1000 e^+e^- pairs. In this way we maintain a continuous check on the operation of the system.

During the actual data collection runs, events with C = 1, D = 2 can be used as a completely independent beam monitor.

E. Gamma Detectors

There are many possible choices of gamma detectors for both the tagging system counters SH_1 and the downstream counters SH_2, SH_3 and SH_4. We prefer to use lead glass counters which are available to us for SH_1 and SH_2 . For SH_3 and SH_4, we intend to use Pb-Lucite sandwiches. The design of the photon detectors will be finalised after extensive tests have been made by us and by other interested groups.

We shall construct all the detectors for the experiments described here.

CHAPTER THREE

The Recoil System

The forward detector covers particle production angles up to about 7°. Wider angles will be handled by a large solid angle detector surrounding the hydrogen target. This system, which we call the recoil detector, is required for the following reasons:

1. The measurement of the recoil proton momentum and angle allows a determination of the missing mass, m_x, in $\gamma p \longrightarrow px$.

2. In two body reactions like

$$\gamma p \rightarrow \gamma p$$
$$\gamma p \rightarrow V^{\circ} p$$

experience at SLAC, DESY, and Cornell has shown that the best way to reject backgrounds like

$$\gamma p \rightarrow \begin{matrix}\gamma \\ V^{\circ}\end{matrix} N^{*}$$

$$\gamma p \rightarrow \begin{matrix}\gamma \\ V^{\circ}\end{matrix} p n \bar{n}$$

is to check the coplanarity and the other kinematic constraints of the particles in the final state.

3. In experimental studies of inclusive reactions like

$$\gamma p \rightarrow \pi^{\pm} + \text{anything}$$

the recoil detector extends the $\pi^{\pm}$ angular range to the backward region and simultaneously measures the "anything".

4. In the search for heavy leptons through the process

$$\gamma + Z \longrightarrow Z + \underbrace{h^+ + h^-}_{\hookrightarrow\ \pi^+\pi^-(2\nu)\ \text{or}\ \mu^-e^+(4\nu)}$$

the recoil system ensures that there is a nearly 4π anti against other possible charged background. It also extends the solid angle for detecting $\pi^+\pi^-$ or μ^-e^+.

A. Design Considerations:

1. As discussed earlier, the trigger rejects the electromagnetic background from e^+e^- pairs (which dominates the desired events by a factor of 200). The forward detector veto of this background is based on two properties of these events: the electron pairs are produced nearly forward, and with nearly 0° opening angle. It is essential that the recoil system not disturb either property. As a result the recoil detector must either use no magnetic field (See Appendix II) or a magnetic field that is parallel to the beam direction.

2. The system must be able to handle a high event rate with sufficient spatial accuracy to do missing mass determinations and to measure the proton angles accurately enough for coplanarity and other kinematic checks. Wire proportional chambers are the only way to satisfy these requirements simultaneously.

3. In order to be able to further reject background from events where an N* instead of a proton is recoiling, the system should be able to distinguish π^+ and p and to detect photons from π^o decays. Since most of the recoil protons have momentum less than 800 MeV/c, a measurement of the rate of energy loss in thick scintillator counters (dE/dx) will provide a good $\pi^\pm p$ discrimination. Large area shower counters will detect photons.

4. The system should have as large a solid angle as possible so that the recoil proton is detected with high efficiency.

B. The Apparatus

Three views of the recoil detector we propose to meet these design requirements are shown in Fig. 14a,b,c.

1. The Magnet

The magnet that we expect to use is the 36" Princeton Spark Chamber magnet which is presently at the PPA. This magnet is ideal for our purpose. A small, 13 cm diameter hole in one pole of the magnet allows the beam to enter and interact with the target located along the center axis of the magnet. At the other pole there is a very large (89 cm diameter) opening through the yoke. This hole is the size of the opening in the center of the donut shaped coils. It allows wide angle but forward going particles (up to about 25°) to pass through without interference. The beam travels along the symmetry axis of the magnet, where the field is in the direction of the beam. Forward going particles will be unaffected by the field. In particular, electron pairs produced near zero degrees by the Bethe-Heitler process will not be opened up by this magnet. This feature is essential to the electron pair veto discussed

in the forward detector section. The height of the magnet (over 6 feet) gives us over 50% ϕ acceptance.

We have given much consideration to running this magnet at as low a field as possible so that its power consumption will not strain the electric and water distribution systems at NAL. The magnet is capable of more than twice the field that we plan to use. 8 kg is a compromise setting that consumes a minimum of power without cutting severely into the physics capabilities of the experiment. Because of this low setting the outer chambers have been located at 75 cm from the target. This long lever arm compensates for the low field to maintain momentum resolution. We will return to this question later on when we describe the missing mass experiment in detail.

In normal use the magnet will be operated at a current of 2100 amperes (about 500 kw). With this current the field in the center of the magnet is 8 kg, and ~9.5 kg near the coils.

2. The detectors

There will be three sets of wire proportional chambers on each side of the target. These will measure the momentum of particles coming off at angles greater than about 35^0. The locations of these chambers within the magnet is shown in a top view in Fig. 14a and in an end view in Fig. 14b. In order to obtain good momentum and angle resolution these chambers must have both good spatial resolution and a small material thickness. The latter is required to keep down the multiple scattering of protons in the 200-800 MeV/c range. The wire spacing will be 2 mm in both directions so that the spatial resolution will be $\pm$ 1 mm or better. In the two inner chambers on each side the material is reduced to a minimum (about

4×10^{-4} radiation lengths). The total active area of the chambers inside the magnet is 6.5 m^2 with about 6000 wires.

Two planes of chambers perpendicular to the beam are placed in and after the downstream aperture of the recoil magnet. These chambers detect decay products at very wide angles, as well as protons recoiling from very high mass particles in the final state. This system measures the number, charge and angle of particles from about 5° to 25°. It is not possible to obtain accurate momentum resolution for particles in this angular range using the recoil magnet alone, because the momentum component transverse to the field is too small. (We are considering the possibility of adding a simple system at some future time to measure the range of particles that have passed through the forward recoil chambers). The forward recoil chambers cover an active area of 2.8 m^2 with about 2700 wires.

The first forward chamber will carry a heavy load of particles as it is used both in this system and in the forward detector. The special requirements (such as time resolution, etc.) for this chamber and the means of satisfying them are discussed in detail in Appendix IV.

3. The Target

The hydrogen target dimensions (10 cm high by 2 cm. wide) allow at least 1/2 cm on each side of the beam spot. This size is minimized so that the energy loss in the hydrogen will be small. With a target of this cross section protons must have at least $\sim$200 MeV/c to get out of the hydrogen target with greater than 50% probability. The target will be 115 cm long. It will extend 30 cm. into the hole in the upstream pole. The pole tip at this end will be cut away as shown in Fig. 14a. The angular acceptance of the system will thus go down to about 35° which increases the missing mass range somewhat.

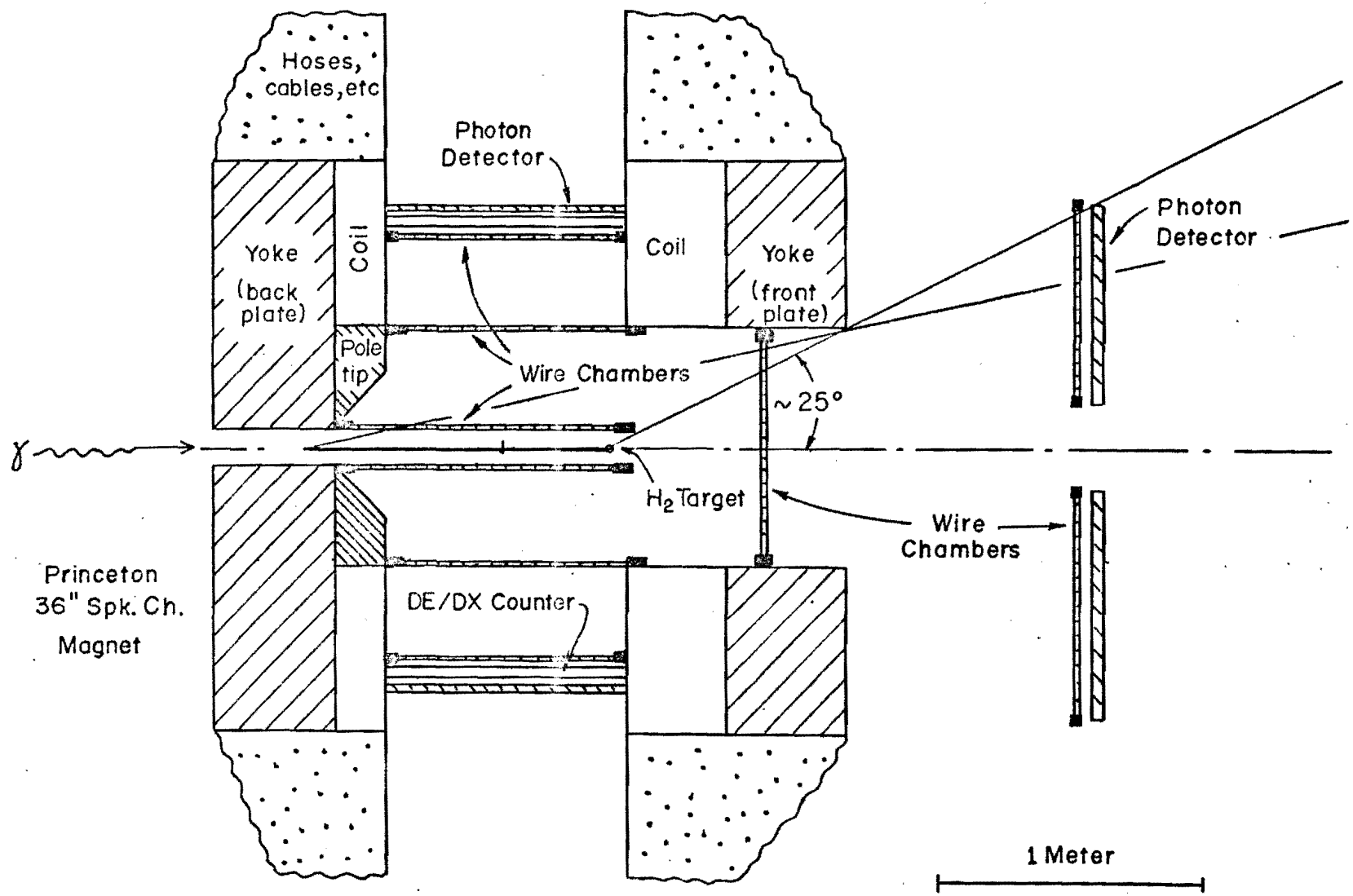

FIG. 14a TOP VIEW OF RECOIL DETECTION SYSTEM (at mid-plane)

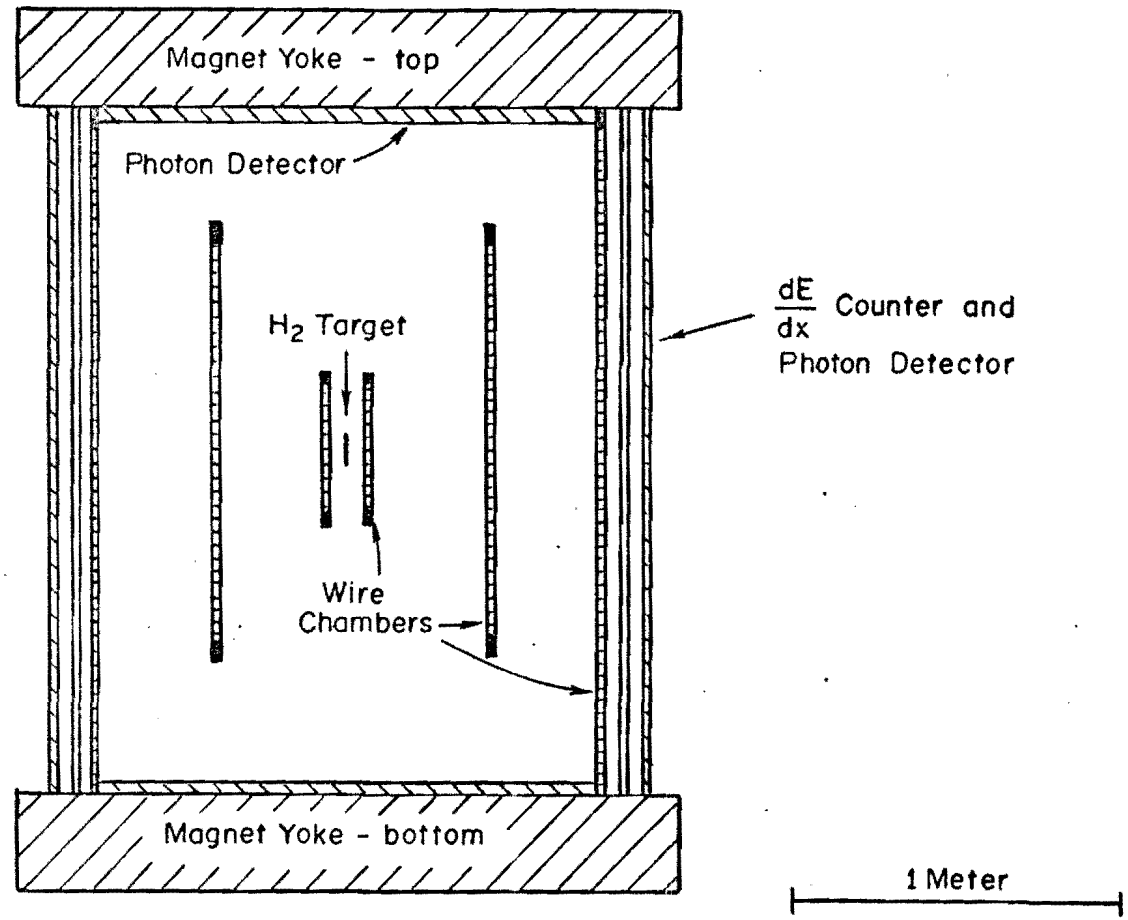

FIG. 14b END VIEW OF RECOIL DETECTION SYSTEM

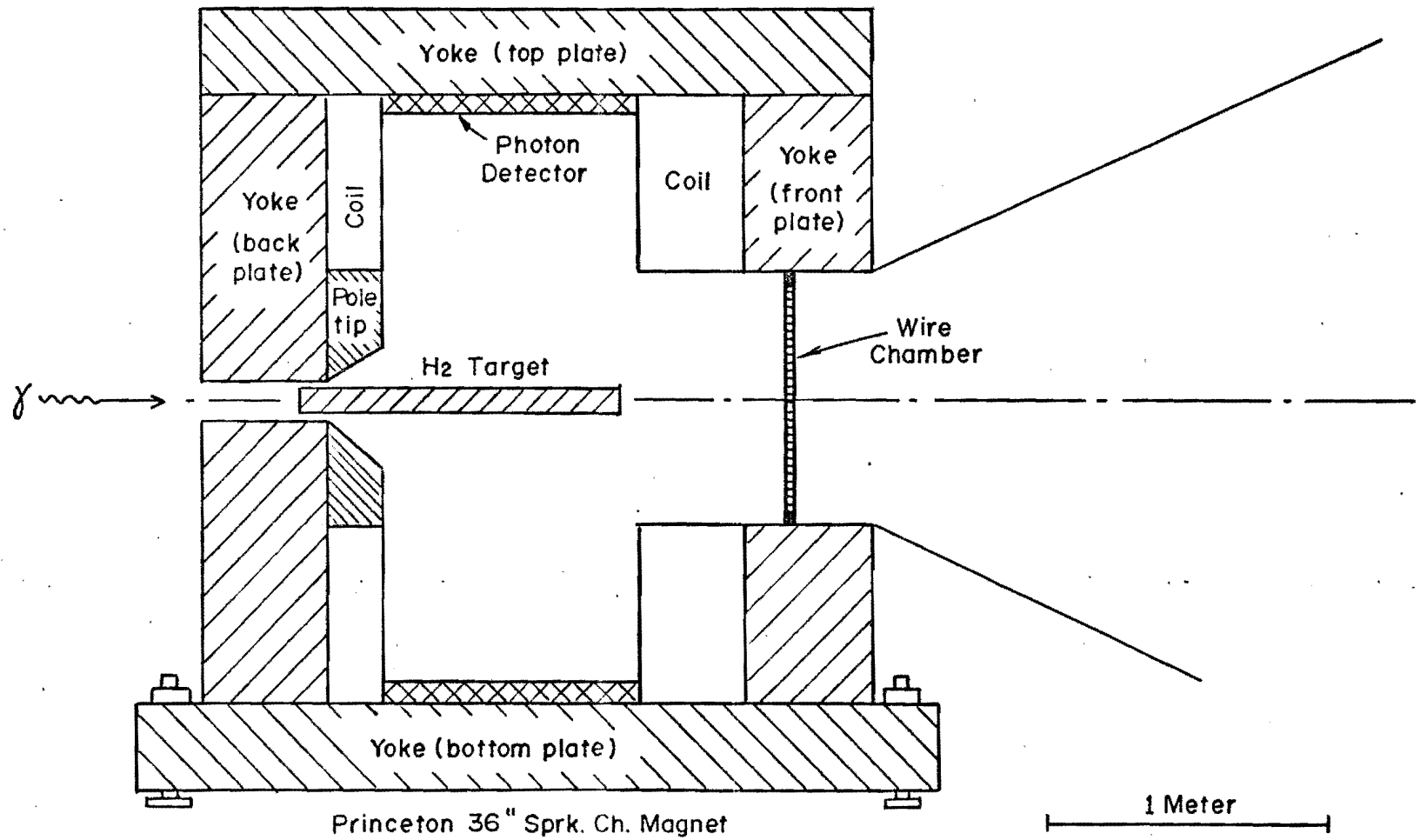

FIG. 14c SIDE VIEW OF RECOIL DETECTION SYSTEM (at mid-plane)

C. Particle Identification

One of the functions of this recoil system is the identification of the recoiling particle. In vector meson production and Compton scattering a background that must be eliminated comes from a recoiling N* of positive charge which then decays either to $\pi^0 p$ or to $\pi^+ n$. In order to identify these events it is necessary to be able to distinguish between pions and protons and to detect photons from decaying neutral pions. To detect the photons simple large area shower counters will cover as much solid angle as possible. They will be placed (i) on the ceiling and floors of the magnet, (ii) behind the momentum analyzers inside the magnet and the forward recoil detector outside, and (iii) on the pole faces. Some of these are noted in Fig 14. The shower counters will consist of lead either sandwiched with lucite or followed by very low resolution (5 cm) wire proportional chambers. Behind the momentum analyzing chambers inside the magnet thick scintillator counters will measure the rate of energy loss (dE/dx). With the knowledge of the momentum of the particle, the pulse height information from these counters (which is essentially a measure of the particle velocity), will allow a good discrimination between pions and protons. This technique has been used with success in the momentum range (200 - 800 MeV/c) in the photon beams at DESY.

D. Acceptance and Resolution

A Monte Carlo technique has been used to estimate the acceptance and resolution in momentum and angle of the proposed system. The results are summarized in Table 7. The resolutions are shown for a variety of different momenta and angles. The Monte Carlo program, which was checked extensively by hand, calculates the trajectory of a particle produced in the target, taking into account energy loss in the target and multiple scattering in the target, chambers and gas. The intersections with the chamber planes were jittered by a Gaussian with half width 1 mm, corresponding to the chamber resolution, and then the events were reconstructed. For the purpose of this calculation a flat average field of 6 kg was assumed.

Table 2: Acceptance and Resolution of Recoil Detector

P MeV	θ	Acceptance	$\delta\theta$ mrad (±)	$\delta p/p$ % (±)
250	45°	.13	16	11
	60°	.36	14	12
	75°	.41	13	11
	90°	.43	15	9.8
500	45°	.15	4.4	3.5
	60°	.30	4.9	3.6
	75°	.39	4.8	4.3
	90°	.42	4.8	5.0
750	45°	.15	2.9	5.0
	60°	.30	3.6	5.9
	75°	.39	3.9	7.3
	90°	.42	4.3	7.7
1000	45°	.17	2.6	9.3
	60°	.29	3.2	8.0
	75°	.42	3.8	9.8
	90°	.39	3.5	9.6

Notes: Monte Carlo statistical errors in resolutions and acceptance ~6%

Acceptance includes losses of Protons in 2 cm x 10 cm x 115 cm H_2 target.

CHAPTER FOUR

The Experiments

Introduction

A dominant philosophy behind this proposal is the idea that with a comprehensive apparatus a significant number of experiments can be run simultaneously, probing photon physics in many directions at new energies in an efficient use of beam time. In this chapter we will describe each of the experiments in turn, telling how they share the apparatus, what demands each makes on the apparatus, and what results we expect.

We plan to run the experiment in two steps:

The first run will be a general survey of all the reactions at the designed photon intensity of 4×10^5 per pulse for 400 hours.

All the counting rates in the experimental discussions that follow are based on 4×10^5 photons/pulse (from 10^{13} primary protons only).

For a second run of 300 hours, we plan to increase the sensitivity by a factor of ten in the searches for heavy vector mesons (down to a coupling of the order of $10^{-3} g^2_{\gamma V}$) and leptons. In this run the trigger will not accept any other reactions. The photon intensity will be increased by 10 by increasing both the tagging target thickness from .01 to .10 radiation lengths and the incident proton intensity. The more numerous zero degree electrons pairs will now be stopped in a lead plug 7 cm x 10 cm x 50 cm located 450 cm downstream from the target. We will trigger only on final states with two or more particles at angles greater than 6 mrad.

For simplicity in this chapter we group the experiments on the photoproduction of vector mesons into three sections:

Experiment B. Two body decays

Experiment C. Three body decays

Experiment D. Multi-body decays

Expt. A. $\gamma + p \rightarrow \pi^{\pm} + X$

The significance and the expected form of the cross section of

$$\gamma + p \rightarrow \pi^{\pm} + X$$

was discussed earlier. Here we outline some important experimental facts regarding this experiment.

I. Rates and Acceptance:

The total γp cross-section is $\approx 120\,\mu b$. Of this, $20\,\mu b$ comes from photoproduction of ρ, ω and ϕ. Therefore the total cross-section for the reaction $\gamma + p \rightarrow \pi^{+}(K^{+}) +$ anything, will be $\approx 100\,\mu b$.

The total event rate will be 200 per pulse.. These events will be distributed in the various regions:-

i) Forward Detector

The forward detector has an acceptance of 40 mr x 120 mr (for the purposes of momentum analysis). Therefore all particles above 2 GeV with production angles less than 40 mr are accepted. Particles produced between 40 mr and 120 mr are partially accepted.

Transform into C.M. system and consider a pion with momentum $P_{\pi} = (P_{\perp}, P_{z\,cm})$ or equivalently, with transverse momentum $P_{\perp}$, and Feynman parameter $x = \frac{P_{z\,cm}}{E}$, where $E \approx \sqrt{s}/2 \approx$ energy of photon (or proton) in the C.M. system. Then the acceptance of the forward detector in terms of $P_{\perp}$, x is given by the following table:

$P_{\perp}$ (GeV)	$\theta \leqslant$ 40 mr		$\theta \leqslant$ 120 mr	
	Pzcm (GeV)	x	Pzcm (GeV)	x
0.2	$\gtrsim$ 0.3	$\gtrsim$ 0.03	$\gtrsim$ -0.1	$\gtrsim$ -.01
0.4	$\gtrsim$ 0.39	$\gtrsim$ 0.04	$\gtrsim$ -0.1	$\gtrsim$ -0.01
1.0	$\gtrsim$ 1.0	$\gtrsim$ 0.10	$\gtrsim$ -0.1	$\gtrsim$ -.01

We conclude that for $100 \lesssim K \lesssim 200$ GeV, the forward detector is effective for almost all of the forward hemisphere (C.M.), i.e. for $P_z \gtrsim 0$ or $x \geq 0$.

ii) The Recoil Detector

The recoil detector also covers a certain range of pions. The detector is effective for pions produced approximately in the range $35^\circ < \theta < 135^\circ$. The protons can be distinguished from the pions by knowing the momentum of the particle and the energy it deposits in the dE/dx counters. The acceptance of the $\pi^\pm$ for $60^\circ < \theta < 120^\circ$ are:

$P_\perp$ (GeV)	$\theta \geq 60^\circ$		$\theta \leq 120^\circ$	
	Pz cm (GeV)	x	Pz cm (GeV)	x
0.2	≤ -1.55	≤ -0.16	≥ -4.0	$\geq -.41$
0.4	≤ -2.7	≤ -2.8	≥ -7.4	$\geq -.76$
1.0	≤ -6.2	$\leq -.64$	All $P_{z_{cm}}$	≥ -1.0

Fig. 15 summarizes the region detected by the present set up. It is clear that the set up covers a large region of interest, enabling us to perform tests of various models with the minimum of systematic errors.

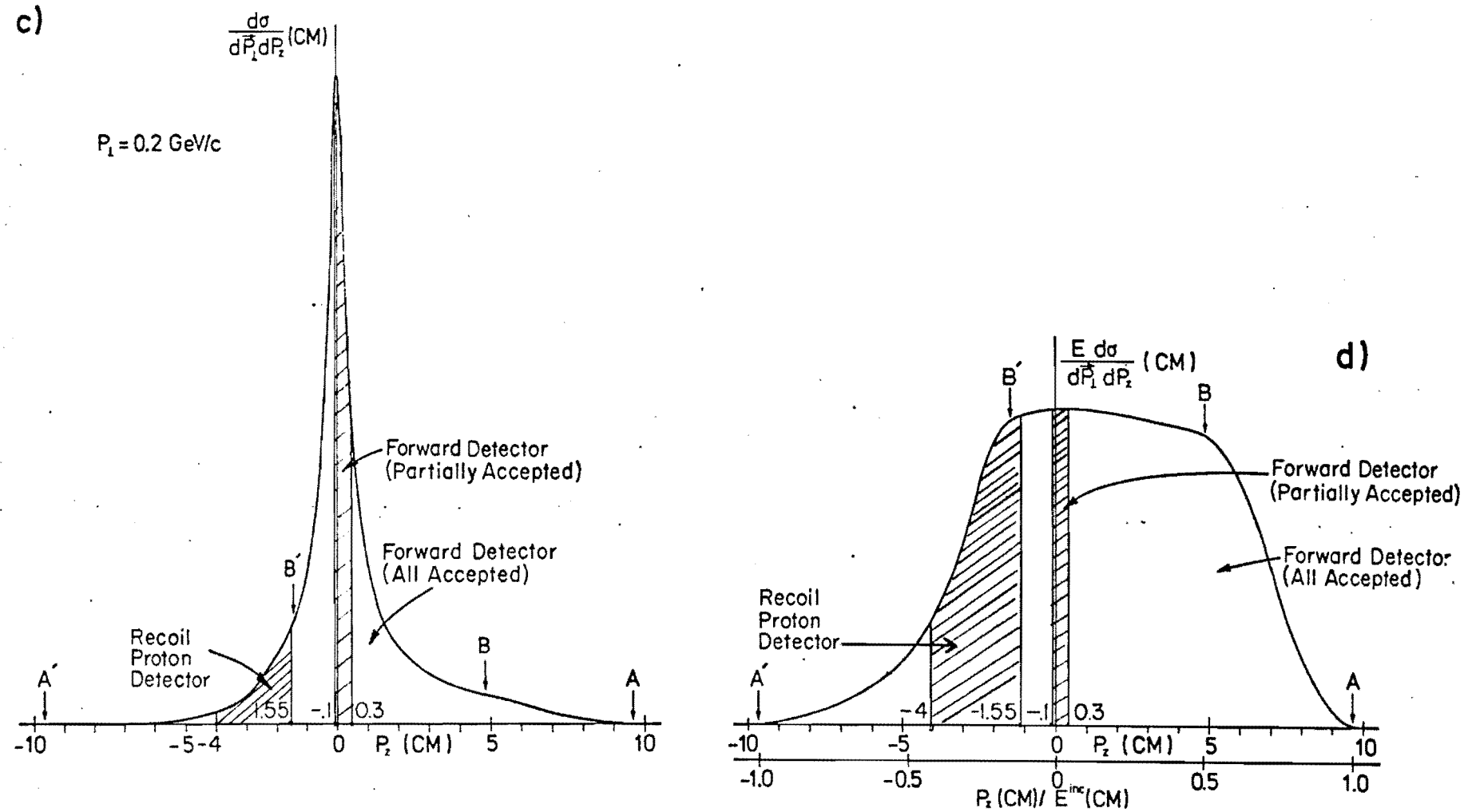
c)
$\frac{d\sigma}{d\vec{P}_\perp dP_z}$ (CM)
$P_\perp$ = 0.2 GeV/c
Forward Detector
(Partially Accepted)
Forward Detector
(All Accepted)
Recoil
Proton
Detector
A′
B′
B
A
-1.55
-.1
0.3
-10
-5
-4
0
P_z (CM)
5
10
d)
$\frac{E\, d\sigma}{d\vec{P}_\perp dP_z}$ (CM)
Forward Detector
(Partially Accepted)
Forward Detector
(All Accepted)
Recoil
Proton
Detector
-4
-1.55
-1
0.3
-1.0
-0.5
0.5
1.0
P_z (CM)/ E^{inc}(CM)

FIG. 15

II. Resolution

The resolution of the transverse momentum and the longitudinal momentum for various pion production angles and $P_\perp$ = 0.2 GeV are listed in the following table.

θ_π (mr)	100	50	10	1.0
p_π (GeV)	2	4	20	200
$\pm\,\Delta p_\perp$ (MeV)	0.5	0.9	0.9	9
$\pm\,\Delta p_\parallel$ (MeV)	3	12	40	4000
$\pm\,\delta\sigma_\pi/\sigma_\pi$ %	0.3	0.5	0.4	4.0

Assuming the differential cross-section of $\gamma p \to \pi^\pm$ + anything (at 200 GeV) to be the same analytical form as P + P $\longrightarrow$ $\pi^\pm$ + anything[3,8] (at 30 GeV/c):

$$\sigma_\pi = \frac{d^3\sigma}{d^2p_\perp\, dp_\parallel} = \frac{1}{E_\pi}\, e^{-2.44\,(p_\perp + p_\perp^2/m_p)} \cdot G(\text{const})$$

we find the uncertainty in σ_π due to measurement error in E_π and $p_\perp$ is

$$-\frac{d\sigma_\pi}{\sigma_\pi} = \left(2.44 + \frac{2p_\perp}{m_p}\right)\delta p_\perp + \frac{\delta E_\pi}{E_\pi}$$

The percentage errors for various production angles are also listed in the above table. We observe that the resolution is more than sufficient for this experiment.

III. Background

It is difficult to have a reliable estimate of the background theoretically. For one-pion distribution, on the basis of fireballs and Bremsstrahlung, the background is not expected to have a rapid dependence of the form E^{-1}. Thus the distribution, with background taken into account, is

$$\frac{1}{E_\pi} f(p_\perp) + F(p_\perp) \qquad (9)$$

where F is approximately independent of $p_\parallel$ but depends on $p_\perp$ and is inversely proportional to the incident energy. If, for a given $p_\perp$, the entire distribution in $p_\parallel$ is measured, then we can fit the result with this form and, if a reasonable fit is obtained, obtain both f and F.

In the absence of such a measurement, we can only give a rough estimate as follows:

$$\frac{1}{E_\pi} f(p_\perp) \gg F(p_\perp)$$

if

$$E_\pi \ll \frac{m_\pi}{m_\rho} E$$

Thus roughly

$$\frac{1}{E_\pi} f(p_\perp) = F(p_\perp)$$

when

$$E_\pi = \frac{m_\pi}{m_\rho} E$$

With this estimate, the background to signal ratio (for $p_\parallel = 0$) is

$$\frac{\sqrt{p_\perp^2 + m_\pi^2}}{E\, m_\pi/m_\rho}$$

For $P_\perp$ = 140 MeV/c and E = 10 GeV, we get ~13 % (maximum) background.

From the above considerations, we can give the following examples of tests of the theory.

a. Shape of the curve: One fits the measured distribution with (9), and determine $f(p_\perp)$ and $F(p_\perp)$. If an anomalously large background is needed to fit the data, i.e., if

$$\frac{F(p_\perp) E_\pi}{f(p_\perp)} \gg 10\,\%$$

at $P_\parallel = 0$, $p_\perp \leqslant 140$ MeV/c and E = 10 GeV, then test 1 fails.

b. Equality of π^+ and π^- distributions: According to theory, the function $f(p_\perp)$ is the same, while the function $F(p_\perp)$ may be different for the one-particle distributions of π^+ and π^-. The equality of f_{π^+} and f_{π^-} is further subject to the experimental limitation for isolating π's from K's which may be 5% - 10%. Accordingly, we expect

$$\left| \frac{f_{\pi^+} - f_{\pi^-}}{f_{\pi^+}} \right| \leq 10\,\%$$

at $p_\parallel = 0$, $p_\perp \leq 140$ MeV/c and E = 10 GeV. If the left side of the above equation is considerably greater than 10%, then test 2 fails.

IV. Demands on the apparatus:

For the 1st run, Čerenkov Counters (Appendix III) will be used to identify $\pi^\pm$. Later on two Čerenkov Counters may be needed to measure the $K^\pm$ production.

The region not measured by the 1st run can be covered by moving the apparatus to be centered off 0° direction.

Two Body decays of Vector Mesons

Expt. B. $\gamma + p \rightarrow p + V^{\circ}$, $V^{\circ} \rightarrow \pi^+\pi^-$ or K^+K^-

In this section we discuss the essential experimental considerations with regard to studying the production, (the s and t dependence) and the decay angular distribution (in C.M. System) of $\rho \rightarrow \pi\pi$, $\phi \rightarrow KK$ mesons, and the search for new 0^+, 1^-, 2^+, 3^- particles decaying into these modes.

I. Kinematical Considerations:

The decay angular distribution for diffractively produced vector mesons, in the V° rest frame is $\frac{3}{8\pi}\sin^2\theta^*$ (with respect to V° direction).

The momentum and angular distributions in the laboratory frame are shown in Fig. 4 of the chapter describing the forward detector. From these we conclude that for $M < 5$ GeV, $E_\gamma = 150$ GeV, most of the events will be in the forward cone of $< 5^{\circ}$. For illustrative purposes, we discuss two typical samples.

(i) For ρ production, with 100 GeV $< E_\gamma <$ 200 GeV, the proton comes out at angles between 65° and 85°. The momentum transfer is $0 < |t| < 2.0 (\mathrm{GeV}/c)^2$. The pions are all forward ($3.6_{\mathrm{mrad}} < \theta_\pi < 36_{\mathrm{mrad}}$ with $10 < P_\pi <$ 100 GeV).

(ii) For ϕ production, because of the low Q value for the $\phi \rightarrow KK$ decay, the $K^{\pm}$ come out much more forward ($1.25\,\mathrm{mrad} < \theta_K < 12.5\,\mathrm{mr}$ for $10 < P_K < 100\,\mathrm{GeV}$). Because of the diffractive nature of production the effective t range will be $< 1 (\mathrm{GeV}/c)^2$

II. Acceptance, resolution and Counting rate:

We have written a Monte Carlo program which makes the following assumptions;

(1) beam intensity 4×10^5/pulse with 1/k dependence.

(2) production cross section $\frac{d\sigma}{dt} = 120 e^{-8t}$ for ρ

and

$\frac{d\sigma}{dt} = 3.4 e^{-4.7t}$ for ϕ

with $\phi \to K^+K^- / \phi \to \text{all} = 45.5\%$

$\frac{d\sigma}{dt} = 1.0 e^{-8t}$ for new V^0

(All in units of $\mu b/GeV^2$)

(3) A decay C.M. distribution $\frac{3}{8\pi} \sin^2\theta^*$

(4) Breit-Wigner form $\frac{2 M_v \Gamma_v}{\pi} \frac{M}{(M^2 - M_v^2)^2 + M_v^2 \Gamma_v^2}$

(5) Absorption and multiple scattering

(6) Geometry of forward and recoil detector

Based on the result of Monte Carlo calculations we list the acceptances, the resolutions, and the counting rate for various reactions in the forward detector. (The recoil proton detector has an average efficiency of ~ 0.4 and a mass resolution of $\delta M_x \simeq 100$ MeV at $M_v = 5$ BeV. (This will be discussed in detail in the Section on Multi particle decays.)

Acceptances for detecting V° decays

M_{V°	M_1 or M_2 Total	$M_1 + M_2$ Small Angle
$\rho \to \pi\pi$	~ 100%	~ 100%
$\phi \to KK$	~ 100%	~ 100%
$V^\circ(3\,GeV) \to \pi\pi$	89.4%	24.8%
$V^\circ(3\,GeV) \to KK$	95.5%	24.8%
$V^\circ(5\,GeV) \to \pi\pi$	60%	2.04%
$V^\circ(5\,GeV) \to KK$	64.5%	2.67%

Rates/hour:

M_{V°	M_1 or M_2 Total	$M_1 + M_2$ Small Angle
$\rho \to \pi\pi$	34900	34900
$\phi \to KK$	788	788
$V^\circ(3\,GeV) \to \pi\pi$	259	72
$V^\circ(3\,GeV) \to KK$	276	72
$V^\circ(5\,GeV) \to \pi\pi$	174	6
$V^\circ(5\,GeV) \to KK$	181	8

(If the recoil proton is also detected, the yields in the above table should be multiplied by ~0.4)

Since for high mass vector mesons, the production cross section of 1 $\mu b/(GeV/c)^2$ has been assumed, the above table implies that our detector is sensitive for detecting vector mesons up to 5 GeV with a sensitivity of V°-γ coupling constant $g^2_{V\gamma} \leq \frac{1}{100} g^2_{\rho\gamma}$.

Resolution: The following tables list some typical results from the Monte Carlo calculations:

For ρ and ϕ ($p = p_\pi$ or p_K, $\theta = \theta_\pi$ or θ_K, δM in MeV

$E_\gamma = 2p$	$\pm\,\delta\theta$ (mr)	$\pm\,\delta p/p^2$ (%)	$\pm\,\delta M(\rho)$	$\pm\,\delta M(\phi)$
20	0.083	0.023	1.8	0.45
60	0.051	0.013	3.1	0.75
100	0.039	0.011	4.1	1.0
200	0.036	0.011	8.0	2.0

For V^0

E_γ (GeV)	M_V (GeV/c²)	LARGE ANGLE M_1 or M_2 $\pm\,\delta M$ (MeV)	SMALL ANGLE $M_1 + M_2$ $\pm\,\delta M$ (MeV)
100	3.0	81	—
100	5.0	135	—
200	3.0	-	22
200	5.0	-	36.

Because of the resolution of the wire chambers and the lever arm, the mass resolution is much better than that of most of the present data. We can therefore study $\omega\rho$ interference effects.[13]

The special problem of looking at k pairs is that one has to separate the kaons from the much higher flux of pion pairs. It is possible to use threshold Čerenkov counters in our system for photon energies up to 150 GeV, but beyond that, separation is not possible. If we assume that all pairs of particles are kaons, and make a 20 MeV mass cut around the ϕ, and further assume that the ρ shape is given by a pure Breit-Wigner, then the signal to noise ratio of $\phi \to 2K / \rho \to 2\pi$ is 2:1. This comes about because one is far away from the peak of the ρ and the mass cut is narrow. For a smaller mass cut, or if we use a mass dependent width for the ρ, this ratio will increase.

III. Background:

Presently available data on photoproduction of the ρ meson indicate that background of the type:

$$\gamma + p \rightarrow N^* + \rho$$
$$\hookrightarrow p + \pi^0$$

is about 15%

The N* type background will be rejected in two independent ways:

(1) By detecting the π^0 and p

(2) By Kinematic constraints: There are four constraints from conservation of energy and three momenta: three of these are useful in rejecting N* events:

(1) Coplanarity

(2) Conservation of momentum in the transverse direction of the production plane

(3) Conservation of energy

To understand the rejection ratio of the Kinematic constraints above, we have performed a Monte Carlo study in which 1000 $\gamma p \rightarrow N^* \rho$ events were generated. None were found to satisfy $\gamma p \rightarrow p \rho^0$.

For ϕ production, the DESY bubble chamber data shows that the reaction $\gamma p \rightarrow p + \phi + \pi^+ + \pi^-$ is about 50% of the elastic cross sections. This background will be rejected for three reasons:

(a) At high energy, the relative yields of these inelastic events to the elastic events will be smaller.

(b) Detecting the additional pions will reject the inelastic events.

(c) Coplanarity

Expt. C Three body decays $\gamma + p \rightarrow p + \omega^* \hookrightarrow \pi^+\pi^-\pi^0 \hookrightarrow \gamma + \gamma$

The photo produced ω^* stands for any meson with quantum numbers $I\,(J^P)G = 0\,(1^-)(-1)$. Because of G parity conservation, these particles can only decay into an odd number of pions through strong interactions, i.e.

$$\omega^* \longrightarrow 3\pi,\ 5\pi,\ 7\pi \ldots\ldots$$

In the following discussion, we will concentrate on the 3π decay mode.

I. Kinematics

Let $\vec{K}_+$, $\vec{K}_-$ be the momenta of the charged pions in the ω^* rest frame and $\vec{\varepsilon}$ be the polarization vector of the ω^* in the S channel helicity frame. The decay matrix of a photoproduced vector meson into $\pi^+ + \pi^- + \pi^0$ is $M \prec \vec{K}_+ \times \vec{K}_-, \vec{\varepsilon}$ (assuming helicity is conserved in the S channel helicity frame) the decay probability is

$$\sum_{\varepsilon} |M|^2 = |\vec{K}_+ \times \vec{K}_-|^2 \sin^2\theta^*$$

where θ^* is the angle between $\vec{\varepsilon}$ and the normal to the decay plane, i.e. $\vec{K}_+ \times \vec{K}_-$. The decay matrix implies that the pions from ω^* decay prefer to be far away from each other in the phase space.

With incident photon energy $150 < K < 200$ GeV, the distribution of pion momentum w.r. to the production angle for various ω^* mass is illustrated in the following table

	M = 0.783 GeV/c^2 (ω)				M = 1.018 GeV/c^2 (ϕ)			
θ(mr)	3	5	7	9	3	7	10	20
* Range of P_π (GeV/c)	8 → 142	8 → 105	7 → 60	7 → 45	6 → 150	6 → 90	6 → 53	7 → 12

	$M = 3.0$ GeV/c^2				$M = 5.0$ GeV/c^2				
θ (mr)	12.5	25	50	75	25	50	75	100	125
* Range in P_π (GeV/c^2)	10 → 130	10 → 175	6 → 22	5 → 10	15 → 100	15 → 55	10 → 32	6 → 22	3 → 15

* More than 95% of the events are in the quoted ranges)

II. Acceptance, resolution, and counting rate:

We use a Monte Carlo program to study the acceptance, the resolution and the yields. The Monte Carlo procedure is as follows:

(i) Generate incident photon (100 - 200 GeV), assuming 4×10^5/pulse

(ii) Calculate recoil proton and ω^* momenta weighted with Ae^{8t}

(iii) ω^* decays into 3π weighted by the calculated decay probability.

(iv) Transform the pion momenta into the lab. system, let the π^0 decay into two gammas and check whether all the particles are accepted by the forward detector.

(v) Apply measurement uncertainties listed in the Forward detector to the particle trajectories and reconstruct ω^* mass.

The percentage of the 3π events accepted by detector (a) and/or (b), the mass resolution and the counting rate are listed in the Table:

M	Acceptance (M1)	Acceptance (M2)	Events	ΔM	Comment
783 (ω)	100%	99%	3720/hour	15 MeV	$A = 13\mu b/(GeV/c)^2$
1018.8 (ϕ)	---	76%	202/hour	16 MeV	$A = 5\mu b/(GeV/c)^2$
1018.8 (ϕ)	100%	---	264/hour	30 MeV	
3000 ω*	74%	---	206/hour	80 MeV	$A = 1\mu b/(GeV/c)^2$ production cross section
5000 ω*	39%	---	106/hour	160 MeV	
6000 ω*	24%	---	62/hour	210 MeV	
10000 ω*	8%	---	13/hour	300 MeV	

After 300 hours of running the forward detector will accumulate 5000 events of 10 GeV ω* with coupling constant $g^2_{\gamma\omega^*} = \frac{1}{15} g^2_{\gamma\omega}$

Fig. 16, 17 & 18 show the Monte Carlo results for ϕ, ω and ω* (3 GeV/c^2) as seen by our apparatus.

We notice that the mass resolution is better for low mass particles. Since with the missing mass technique (see below) the missing mass resolutions is better for high mass particles, these two methods complement each other.

Typical t acceptance is $|t_{min}| < |t| < 1$ GeV/c^2. If recoil is also detected the rate ($m < 7$ GeV) in the table should be multiplied by approximately 0.4. Above about 7 Gev the efficiency for recoil detection is very low.

III. Background

At low energy, the OPE contribution to the ω production has been the single major background to the diffractively produced ω. OPE here includes two non-diffractive processes, $\gamma p \to \omega p$ and $\gamma p \to N^* \omega$

Since the OPE contribution falls off rapidly as energy increases, we expect it will be negligible ($\ll 5\%$ of the diffractive part) at K $\sim$ 100 GeV.

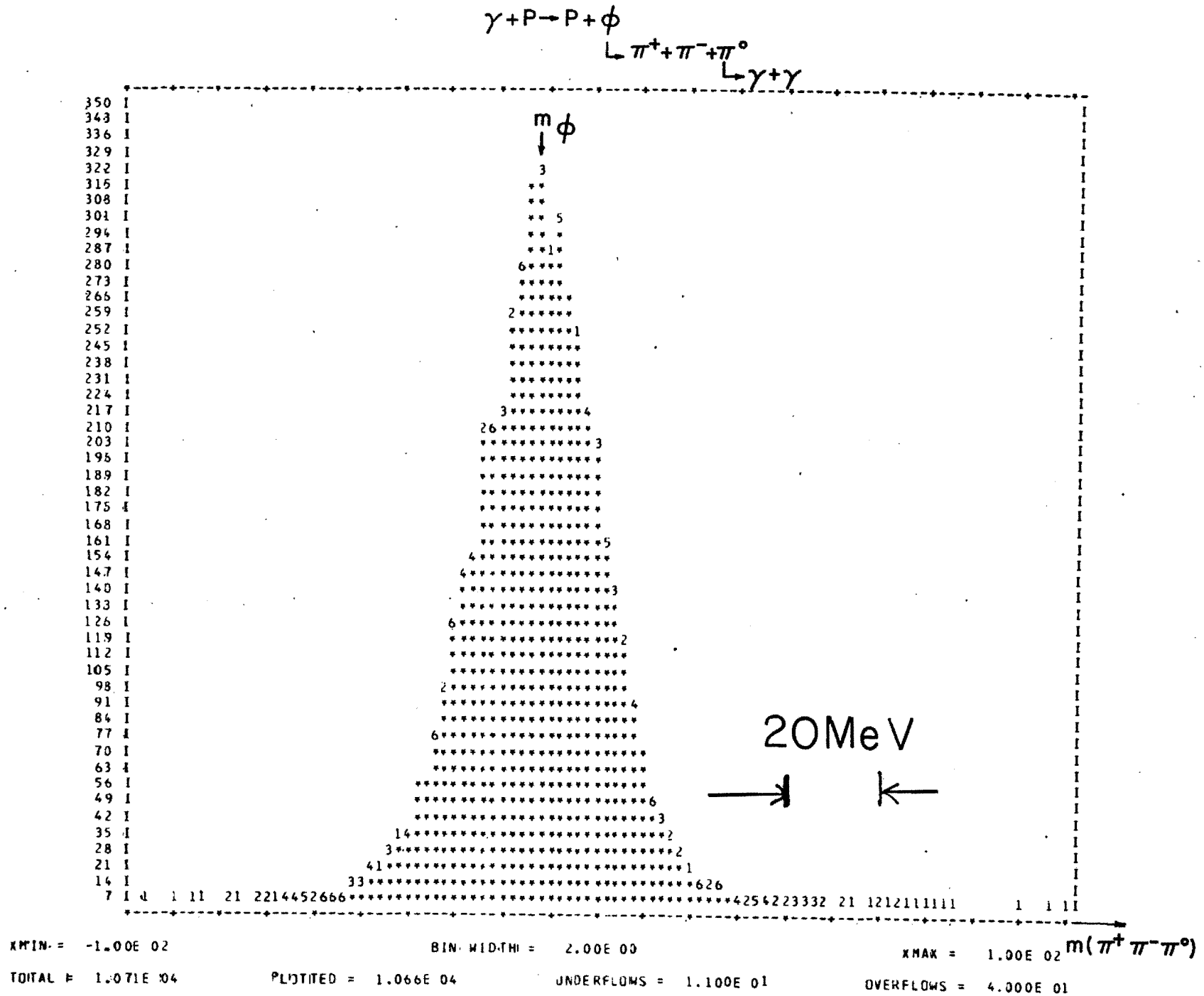
γ+P→P+φ
π⁺+π⁻+π°
γ+γ
m φ
20MeV
m(π⁺ π⁻ π°)
XMIN = -1.00E 02
BIN WIDTH = 2.00E 00
XMAX = 1.00E 02
TOTAL = 1.071E 04
PLOTTED = 1.066E 04
UNDERFLOWS = 1.100E 01
OVERFLOWS = 4.000E 01

FIG. 16

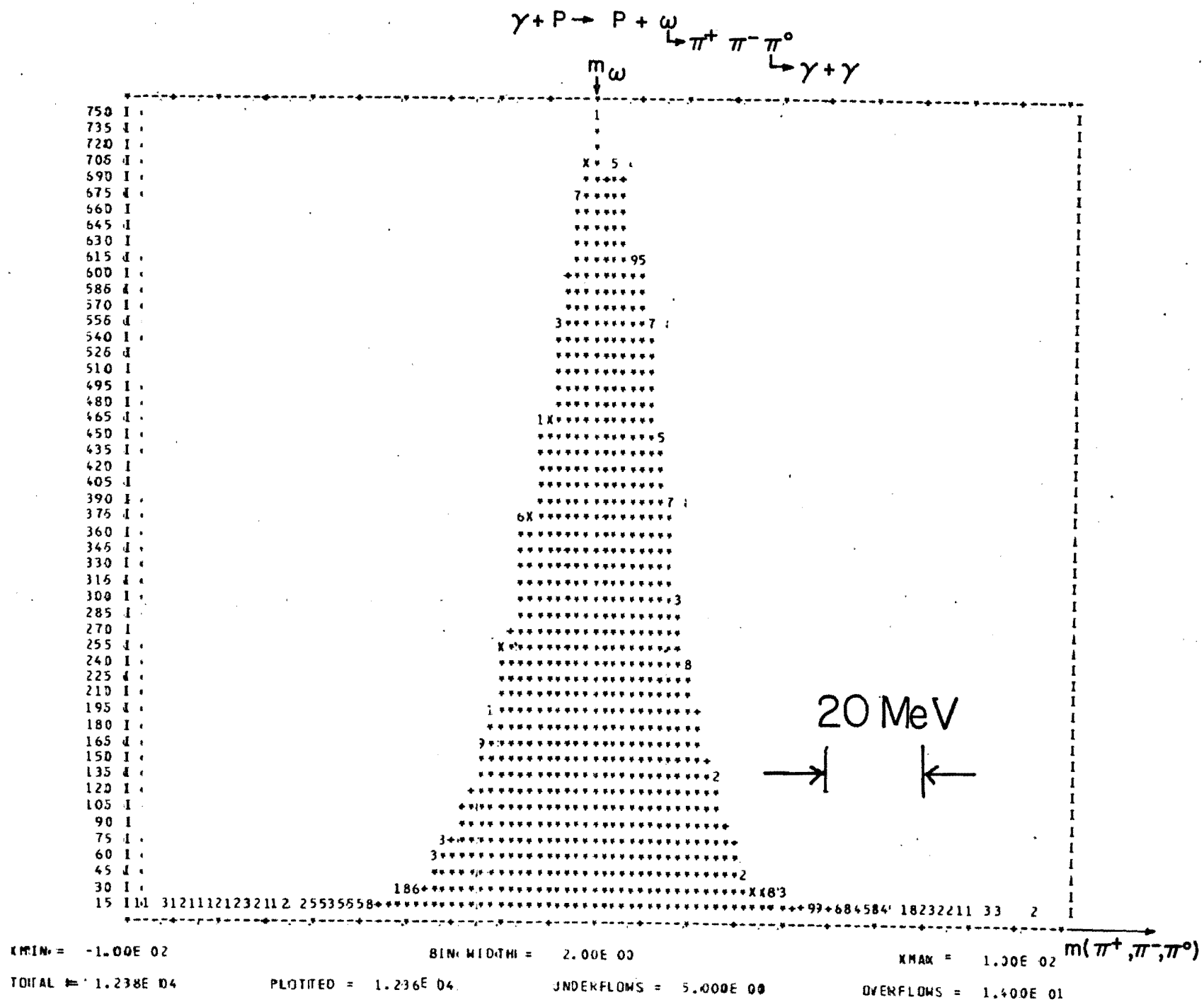
γ + P → P + ω
↳ π⁺ π⁻ π°
↳ γ + γ
m ω
20 MeV
m(π⁺, π⁻, π°)
XMIN = -1.00E 02
BIN WIDTH = 2.00E 00
XMAX = 1.00E 02
TOTAL = 1.238E 04
PLOTTED = 1.236E 04
UNDERFLOWS = 5.000E 00
OVERFLOWS = 1.400E 01

FIG. 17

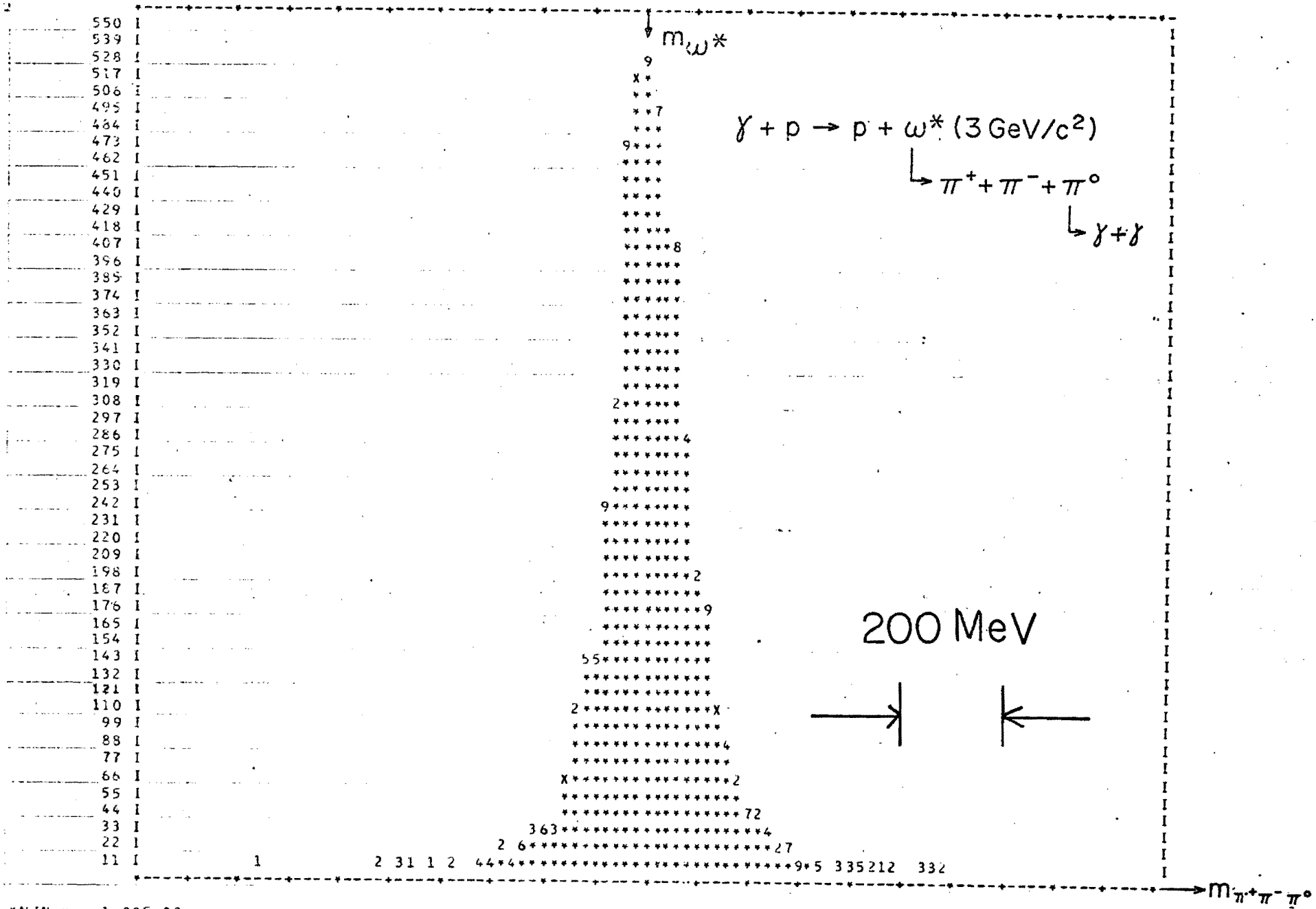

XMIN = -1.00E 03 BIN WIDTH = 2.00E 01 XMAX = 1.00E 03

TOTAL = 7.243E 03 PLOTTED = 7.227E 03 UNDERFLOWS = 0.0 OVERFLOWS = 1.530E 01

FIG. 18

Fig.19 shows the spectrum $\gamma p \to 3\pi p$, measured by the DESY Bubble Chamber Group. A t $3.5 < K < 5.8$ GeV the background is $<10\%$. The DESY measurement shows that the non resonant background decreases with K. One expects the non resonant background to go to zero at $K \sim 100$ GeV.

To reject the inelastic but diffractive reaction

$$\gamma p \to N^*(1470) + \omega$$
$$\hookrightarrow p\pi^0$$

which may not be small at high energies, we combine the forward $\pi^0\pi^-\pi^+$ measurement with the information on the recoil detector. About 0% of elastic events will have the recoil proton detected. Because of conservation of energy and momentum, there are four constraints for these events. Two of them are particularly useful, i.e. conservation of momentum in the two directions perpendicular to the beam direction. For an event like $\gamma p \to N^*\omega$ several hundred MeV/c of momentum will be carried away by the missing π^0. Monte Carlo studies show that from 1000 $\gamma p \to N^*\omega$ generated, none were identified as $\gamma p \to \omega p$ events. Independently, the counters in the recoil detector reject the N* events.

As previously discussed, for ϕ production, the main background $\gamma p \to p + \phi + \pi\pi$ can be rejected by Kinematics and by detecting the π's

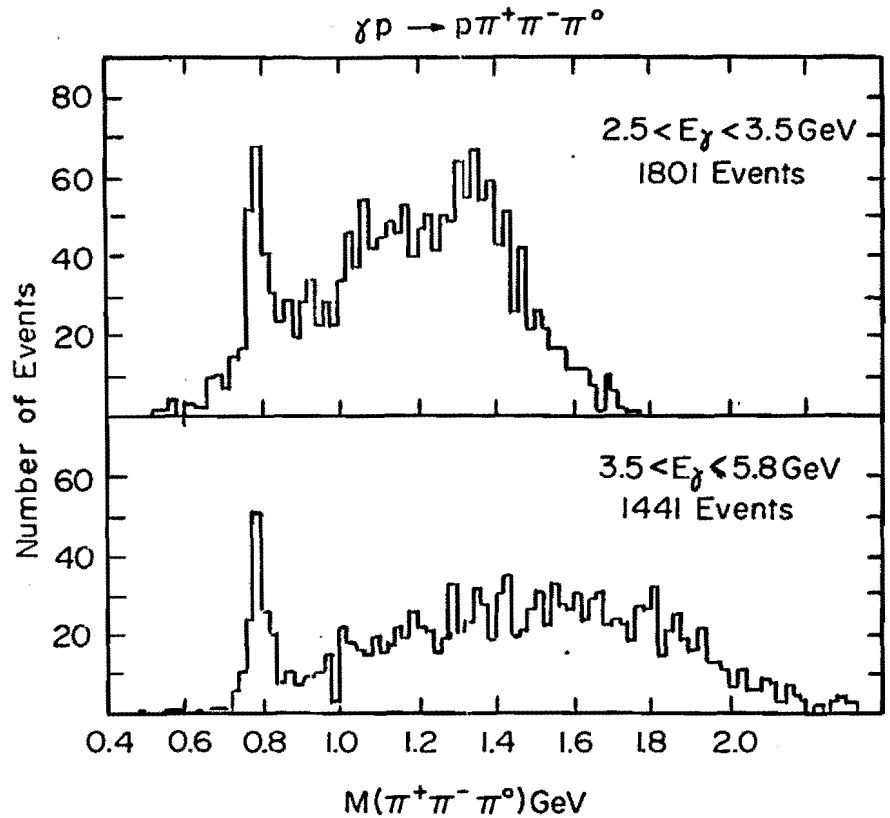

EFFECTIVE-MASS DISTRIBUTIONS $M(\pi^+\pi^-\pi^0)$ FOR ALL EVENTS COMPATIBLE WITH HYPOTHESIS $\gamma p \rightarrow p\pi^+\pi^-\pi^0$

FIG. 19

Expt. D. Multiparticle Decays of Vector Mesons

The missing mass, m_x, in the process $\gamma p \rightarrow X p$ is calculated from the measurements of the tagged photon momentum and angles, and of the recoil proton

$$m_x^2 = (K + m_p - E_p)^2 - (\vec{K} - \vec{p}_p)^2$$

The data will consist of three types:

a. Events with a complete measurement of decay products and, in many cases, the proton. For example $V^0 \rightarrow \omega^0 \pi \rightarrow \pi^+\pi^-\pi^+\pi^-$. For this class of data we will be able to analyze the decay distributions and obtain information on the properties of the new resonances.

b. Events for which the number and charge of decay products is known but kinematic information is not known for all decay particles. The recoil proton is measured, so that the missing mass will be determined. This type of event will be separated into categories distinguishing different multiplicities and particles. Missing mass spectra for each category can be plotted so that the dominant decay channels will be known. In this way, a resonance with a small production cross section in one channel will not be lost in the continuum of the other channels, as happens in standard missing mass searches which do not have channel separation.

c. Events with high particle multiplicities. Only the missing mass can be measured.

I. Acceptance, Rates and Resolution

Listed in the following Table are the missing mass resolutions and rates calculated by the Monte Carlo program described earlier.

Note that as the missing mass increases, the absolute mass resolution actually improves if the momentum resolution and other parameters remain the same. This may be understood by noting that

$$\delta m_x^2 = f(p_p, \theta_p, \ldots \delta p_p)$$

where f does not depend on m_x. Thus

$$\delta m_x = \frac{1}{2m_x} f(\ldots)$$

The table also shows the efficiency for acceptance, and includes the losses due to both energy loss in the target and due to angular acceptance of the recoil system. Integrating over this acceptance, and assuming a diffraction production distribution

$$\frac{d\sigma}{dt} = A e^{bt}$$

we have estimated the rates shown in the Table.

These tables indicate how sensitive this experiment will be to new vector mesons. After 200 hours of running time at 150 GeV we should collect about 16,000 events of a 5 GeV resonance with a cross section of the order of 1% of that of the ρ meson.

k GeV	m_x GeV	$-t$ $(GeV/c)^2$	θ_p Degrees	P_p MeV	Recoil[1] Acceptance Efficiency	δM_x[2] MeV	Expected[2] Rate/hour $\frac{d\sigma}{dt} = e^{8t}$ $\mu b/(GeV/c)^2$
100	2	.1	77	321	.43	156	
		.3	71	571	.39	367	113
		.5	68	756	.38	582	
	5	.1	56	321	.25	87	
		.3	60	571	.32	48	62
		.5	59	756	.27	124	
	7	.15	35	395	.02	127	
		.3	45	571	.15	78	10
		.5	47	756	.19	50	
150	2	.1	78	321	.41	237	
		.3	72	571	.37	481	107
		.5	68	756	.33	1031	
	5	.1	65	321	.31	97	
		.3	65	571	.36	105	80
		.5	62	756	.30	227	
	7	.1	47	321	.20	142	
		.3	55	571	.24	60	45
		.5	55	756	.30	82	
200	2	.1	79	321	.44	331	
		.3	73	571	.39	826	115
		.5	68	756	.38	1414	
	5	.1	69	321	.35	116	
		.3	67	571	.37	179	92
		.5	64	756	.31	447	
	7	.1	57	321	.29	123	
		.3	60	571	.28	67	69
		.5	59	756	.33	197	

N.B. (1) includes probability of proton leaving target. Monte Carlo statistical error in acceptance is $\sim \pm .03$.
(2) Monte Carlo statistical error is 6%.

(3) Target length used = 1.15m

The search for high mass resonances requires that the forward detector have as wide an acceptance as possible combined with good momentum resolution. The angle covered by the decay particles increases with increasing mass. The pions from ρ decay have opening angles typically of the order of 10 mrad at 150 GeV. A 10 GeV vector meson decaying to two pions has a minimum opening angle of 133 mrad. This compares to $\pm$ 33 mrad, which is the angle covered by the furthest chambers following M2 in the forward detection system. Pions from such high mass decays will often enter the chambers following M1, which extend to $\pm$ 120 mrad. Thus, chamber plane 3 is required for the high mass search. For higher masses and multiplicities, the required solid angle will be even larger. Detecting tracks from such events without a momentum determination is one of the functions of the special chamber plane immediately following the recoil magnet.

The requirement of good missing mass resolution provides the most severe requirements on the measurement resolution of the recoil system.

II. Extension of the Missing Mass Range

The upper limit on missing mass with the apparatus we described in the last section is about 8 GeV. With the chambers located as shown in Fig. 14 of the recoil detector section, the angular range from 25° to 35° is undetected. This shadow is a result of the compromise (low power) field setting used in the recoil magnet. In order to maintain the momentum resolution at a low field it was necessary to position the outer

chambers 75 cm away from the target. If these chambers are moved to 50 cm and the middle chambers are moved in correspondingly, this shadow region will be accepted. We intend to cover this region in a short run by turning the power in the forward detector magnets to a very low field and increasing the recoil magnet field to compensate for the shorter lever arm. In this way, without drawing more power, we will be able to extend the mass range to about 10 GeV. The forward detectors will determine the multiplicity and charge of decay particles and perform a rough momentum measurement.

Expt. E ϕ-ω Regeneration

As discussed earlier, the ρ yields on hydrogen give 34,900 events/hour. There will thus be plenty of events from the reactions

$$\gamma A \rightarrow A + V^{0}(\rho, \omega, \phi)$$

The photoproduction of vector mesons is coherent on nuclei and the rate increases as $A^{1.8}$. We can therefore expect an event rate of ~ 1000/hour for ω, ϕ (simultaneously) on nuclei.

To find out if $\phi\omega$ regeneration does occur, we note the following facts from present data:

(1) For ρ production $\sigma_{\rho} \propto A^{1.8}$

(2) $\sigma_{\omega N} \simeq \sigma_{\rho N} \simeq 28\,mb$ (The ω-N and ρ-N cross sections are almost equal)

(3) $\sigma_{\phi N} \ll \sigma_{\rho N}$; $\sigma_{\phi N} \approx 10\,mb$.

We further expect that at 200 GeV, all reactions are purely imaginary. In the model of Ross-Stodolsky one has

$$\phi = \cos\theta_N \phi^{0} + \sin\theta_N \omega^{0}$$
$$\omega = -\sin\theta_N \phi^{0} + \cos\theta_N \omega^{0}$$

The free parameters are θ_N, $\sigma_{\omega^0 N}$, $\sigma_{\phi^0 N}$

We propose to make systematic measurements of $\frac{d\sigma}{dt}(\rho, \omega, \phi)$ on H, Be, C; Al, Ti, Cu, Ag, Cd, In. Ta, W, Au, Pb, U (all with 99% purity).

Following (1), (2), (3) we observe that:

(1) if $\theta_N = 0$, no regeneration, then $\left(\frac{d\sigma_\omega}{dt}\right)_{t=0} \sim A^{1.8}$ in exactly the same way as $\frac{d\sigma_\rho}{dt}$. Any difference in A dependence between $\frac{d\sigma_\omega}{dt}(A)$ and $\frac{d\sigma_\rho}{dt}(A)$ implies $\theta_N \neq 0$.

(2) the measurement of $\frac{d\sigma_\phi}{dt}(A)$ together with $\frac{d\sigma_\omega}{dt}(A)$ will determine the value of θ_N.

The table below lists the yields (assuming $\phi_N = 0$) for thin (High A) targets. The yields were calculated from available data, extrapolated to 150 GeV.

TARGET	H	C	Cu	Pb
A	1	12	63.54	207.2
ρ gm/cm^2	0.07	1.55	8.96	11.35
thickness(cm)	115	3	0.1	0.05
$\phi \to$ all /hr	1465.5	1165.8	280.5	208.
$\phi \to 3\pi$ /hr	264	210	50.5	37.4
$\omega \to$ all /hr	3811	3031	729	541
$\omega \to 3\pi$ /hr	3430	2728	656	487

Thus for a 100 hour run on 14 elements, we can do a 1 - 2% accuracy experiment.

II. Backgrounds: On high Z nuclei, the e^+e^- yields increase as Z^2. On Pb the measured e^+e^- cross section is 4×10^4 mb, the ω cross section being 0.7 mb. The $e^+e^-/3\pi$ is 6×10^4.

There are three ways to reject this background:

(1) the trigger rejection is 10^{-3} to 10^{-4}

(2) off line, we can reconstruct 3π events.

(3) we can also desensitize the central part of the forward proportional chambers.

Expt. F Search for Heavy Leptons

I. Kinematics and triggering.

Following the discussion in the physics section, we note that

(1) the production of L^+L^- will be in the forward cone very close to 0° and has a yield $\propto Z^2 G_E^2(q^2)$;

(2) if $M_L < 1$ BeV, the decay of $L \to \pi\nu_h$ dominates the $L \to \ell\nu\nu$ mode.

(3) if $M_L > 1$ BeV, then the $L \to \ell\nu\nu$ mode dominates over the $L \to \pi\nu$ mode. if $M_L > 5$ BeV, most of the decay will be in the $\ell\nu\nu$ mode.

Following from (1), (2) and (3), we conclude that an effective search for heavy leptons must have a detector which satisfies the following conditions:

(1) two and only two charged particles come out;

(2) the total energy of the charged particles is $< E_\gamma$;

(3) many elements must be used to test the $Z^2 G_E^2(q^2)$ dependence;

(4) we must be able to distinguish the π from the K and the μ from the e ;

(5) a close to 4π detector is necessary to reject events of the type $\gamma + Z \to 2\mu + 2e + Z$ or $\gamma + A \to K^+K^- + A'$ or $A' + \pi^+ + \pi^-$.

II. Counting Rate.

Using the total L^+L^- production cross section

$$\sigma(E_\gamma) = \alpha Z^2 r_h^2 \left(\frac{28}{9} \ln \frac{2E_\gamma}{m_h} - \frac{218}{27}\right)$$

The rates for h^+h^- pair production in different decay channels for 300 hours of running time at 4×10^5 photons/burst on 1 meter of hydrogen are listed in the following table.

Rates/300 hours for Various Decay Channels of h^+h^-

m_h (GeV)	0.6	1.0	1.5	3.0
$\pi\pi$	1430	204	32	0.6
πe	550	212	69	5.4
$\pi\mu$	550	212	69	5.4
e e	50	51	39	12.2
$\mu\mu$	50	51	39	12.2
μe	110	102	78	24.0
Total	2740	832	326	59.8

If the leptons with strangeness $S = +1$ are coupled to photons with the same strength as ordinary leptons the calculated rates for the K^+K^- decay for various values of M_h are (per 300 hours) :

M_h (GeV)	0.5	1.0	1.5	3.0
rates/300hr	1400	670	250	40

In order to increase the sensitivity for detecting h^+h^-, after the 300 hours of low intensity running, we plan to run another 300 hours at ten times higher intensity.

III. Background:

The most serious background is the decay in flight of $\pi^\pm$

$$\pi^\pm \text{ (in flight)} \rightarrow \mu^\pm + \nu$$

Therefore a $\pi^\pm$ pair produced may end up looking like $\pi\mu$ or $\mu\mu$. A large amount of energy will be missing, carried away by the neutrino in π decay. However the other decay channels, K^+K^-, $\pi^+\pi^-$, πe , μe , and e^+e^- should be free from serious contamination.

Expt. G. Compton scattering

I. Acceptance and Rates

In order to estimate the counting rate for elastic Compton scattering we use the SLAC data:

$$\frac{d\sigma}{dt} = 0.8\, e^{8t}\ \mu b/(GeV/c)^2$$

The acceptances as a function of t, calculated by the Monte Carlo program is shown in fig. 20. The acceptance, together with the above cross-section yields (assuming $4 \times 10^5\ \gamma$/ burst) 64 elastic Compton events per hour.

After 300 hours of running, 20,000 events should be accumulated. Fig. 21 shows a Monte Carlo simulation of how the data should look as a function of t after 200 hours. The plot was generated assuming a $0.8\ e^{8t}$ distribution. A best fit to this simulated data is shown in the figure. This fit indicates that the measurement error in the diffraction slope will be about $0.35(GeV/c)^2$, and the error in A will be about 6%.

II. Background and Resolution

Because of the smallness of the cross section, the crux of the Compton scattering experiment is the elimination of background from inelastic processes like

$$\gamma p \rightarrow \gamma N^{*+} \hookrightarrow \begin{cases} \pi^+ n \\ \pi^0 p \end{cases} \qquad (10)$$

and

$$\gamma p \rightarrow p\,\omega \hookrightarrow \pi^0 \gamma \hookrightarrow \gamma\gamma \qquad (11)$$

The full measurement of all particles in the initial and final states will allow us four constraints to remove this kind of background and obtain a clean sample of elastic Compton data. In addition events due to Reaction (10) will be identified and rejected by the detector. Shower counters surrounding the recoil system will detect photons from π^0 decay, and the dE/dx counters

will distinguish π^+ from protons.

The four kinematic constraints are:

1 and 2: Three independent measurements of the momentum transfer, t.

3. Coplanarity, $\phi_\gamma = \phi_{p+} \pi$

4: Energy conservation, $k + m_p = k' + E_p$

We will discuss each of these in turn.

The momentum transfer will be measured in three independent ways. From the measurement of the proton recoil angle, θ_p, we have

$$t_\theta \simeq -\left(\frac{2m_p}{\tan\theta\,(1+m_p/k)}\right)^2$$

The measurement of the proton momentum gives the kinetic energy T and

$$t_p = -2m_pT$$

Finally, from the scattered photon angle measurement we have

$$t_\gamma \approx -(k\theta_\gamma)^2$$

The expected resolution from each of these measurements of t has been calculated using the Monte Carlo techniques described earlier, and checked by hand. The results as a function of t for incident photon energy of 150 GeV are shown in Fig. 22a The resolution in t_θ gets worse at lower $|t|$ because of the increased multiple scattering. Thus δ_{t_θ} is best for $|t| \gtrsim 0.2$ (GeV/c)^2. On the other hand the proton momentum measurement improves at low $|t|$, so that t_p is best in that region. For very small $|t|$, however, the effect of energy loss in the target must be corrected for, and this correction brings in the uncertainty in the vertex location. Thus at very small $|t|$, the resolution in t_p becomes somewhat worse. The scattered photon angle relative to the incident angle, θ_γ, is determined over a 80 m lever arm from measurement

of the tagging vertex, the target vertex, and the final detection of the photon. The beam spot is 1 cm wide by 8 cm high. This provides information on the horizontal location of the vertex to $\pm .5$ cm. By tracing the proton trajectory back to the target a similar resolution in the vertical direction will be obtained. This, combined with the tagging vertex resolution of ± 0.5 cm, determines the incident photon angle to about ± 0.2 mrad. This error dominates $\delta\theta_\gamma$. (At energies of 150 GeV, the shower produced by a photon interacting in lead is very limited. We expect a spatial resolution of ± 3 mm to ± 5 mm).

The three measurements of momentum transfer provide two constraints: $t_p = t_\gamma = t_\theta$. According to the Monte Carlo calculations ϕ_p can be measured to $\delta\phi_p \lesssim 1^\circ$ for $|t| \gtrsim 0.1 (\mathrm{GeV}/c)^2$. The accuracy of ϕ_γ is 6° at $t = -.1$ $(\mathrm{GeV}/c)^2$ and is inversely proportional to θ_γ. This dependence dominates the resolution of the coplanarity check as shown in Fig.22b, The coplanarity constraint is particularly useful when there are one or more undetected particles such as in $\gamma p \to \gamma p n \bar{n}$.

The fourth constraint, energy conservation, depends on how well the scattered photon energy is measured. The thick lead glass counters behind the final plane of chambers determine the energy to $\pm 5\%$ or better. This constraint will be used to exclude processes which have a forward going photon in conjunction with undetected particles. The key fact behind this constraint is that the scattered photon in elastic Compton scattering has an energy no more than 0.5 GeV lower than the incident photon as long as $|t|$ is less than 0.75 $(\mathrm{GeV}/c)^2$.

In order to get a feeling for how successfully these kinematic constraints will reject background events a Monte Carlo program was used to generate events with the N* decaying into both available channels. ($\gamma p \to \gamma N^{*+}$). Out of 1700 events none were able to fake elastic events.

The above rejection is achieved by using Kinematic constraints alone. In addition we have rejection from the hardware identification of π^0 and photons by the recoil system. This should increase the rejection by a factor of 10.

The total rejection against the N* background will therefore be better than 10,000→20,000 to 1.

The other possible source of significant background are events coming from $\gamma p \to \omega^0 p$ with the ω decaying to $\pi^0\gamma \to 3\gamma$. There are three photons in the final state and the possibility that two of these are missed by the detection system would allow an event to fake elastic Compton. The photoproduction cross section can be estimated, and from such an estimate and a calculation of the chances of missing 2 out of 3 photons we conclude that without kinematical constraints, this and similar backgrounds will not be more than a few per cent of elastic Compton. The kinematic constraints will push this type of background to a very low level.

The reaction $\gamma p \to \pi^0 p$ gives a background similar to ω production. However, the rate should be no higher than a few per cent of Compton at these energies because of the rapid fall off of the photoproduction cross section with energy. In addition the ability to detect both photons from π^0 decay and the kinematic constraints will keep this type of contamination at an insignificant level.

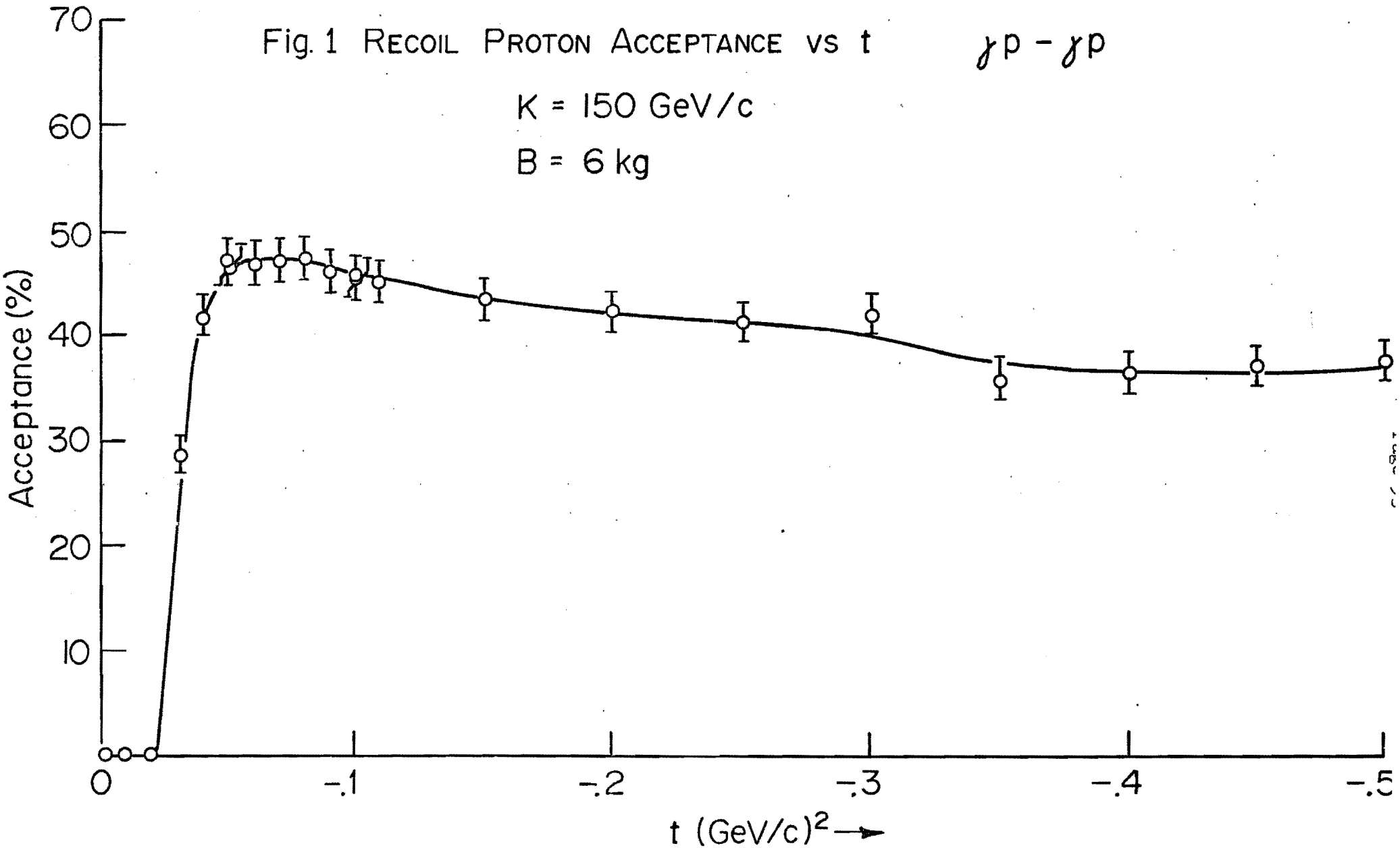
Fig. 1 RECOIL PROTON ACCEPTANCE VS t
γp - γp
K = 150 GeV/c
B = 6 kg
Acceptance (%)
70
60
50
40
30
20
10
0
-.1
-.2
-.3
-.4
-.5
t (GeV/c)²

FIG. 20

Fig. 21

EXPECTED COMPTON SCATTERING RESULTS AFTER 200 HOURS RUNNING

$K_{max} = 150$ GeV

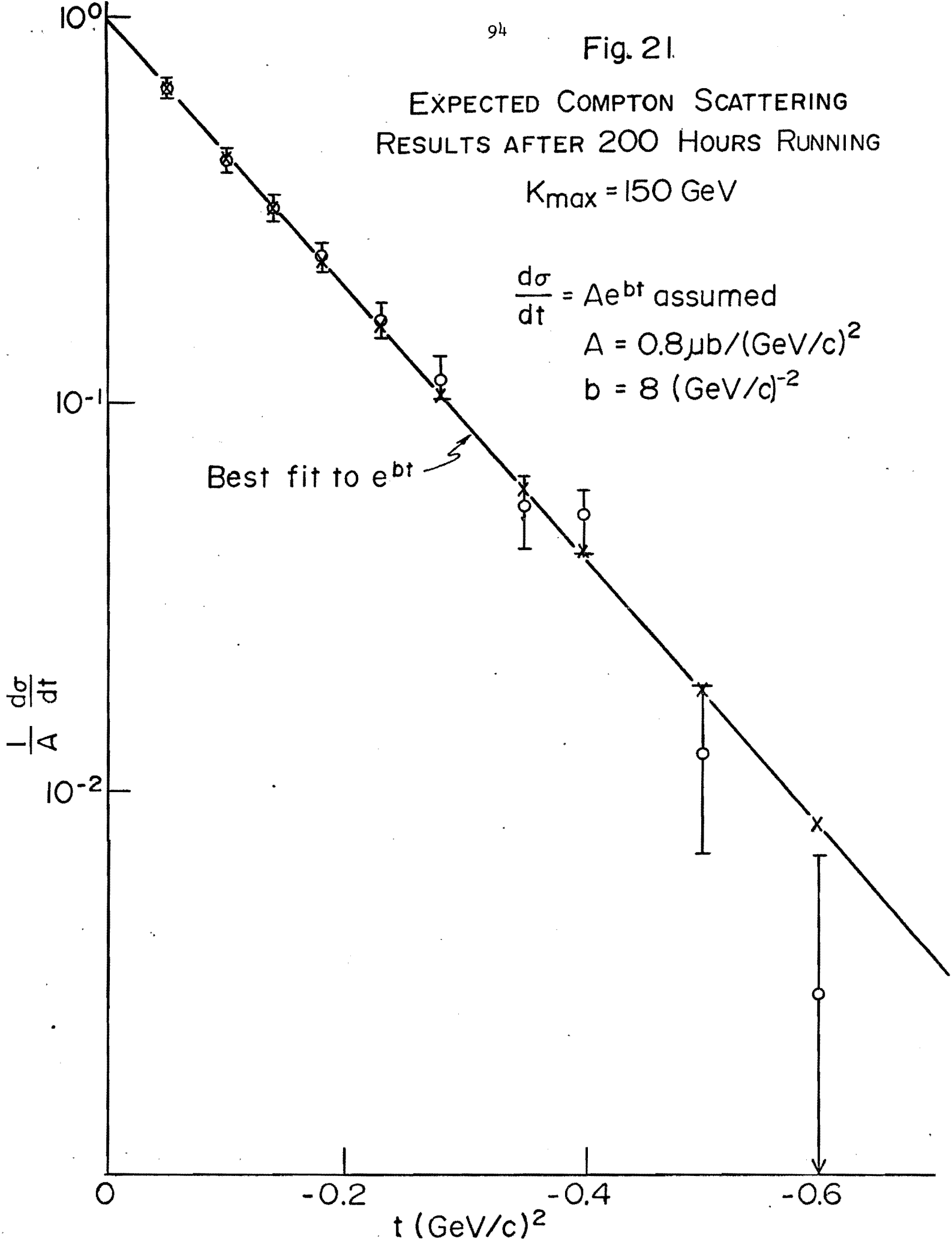

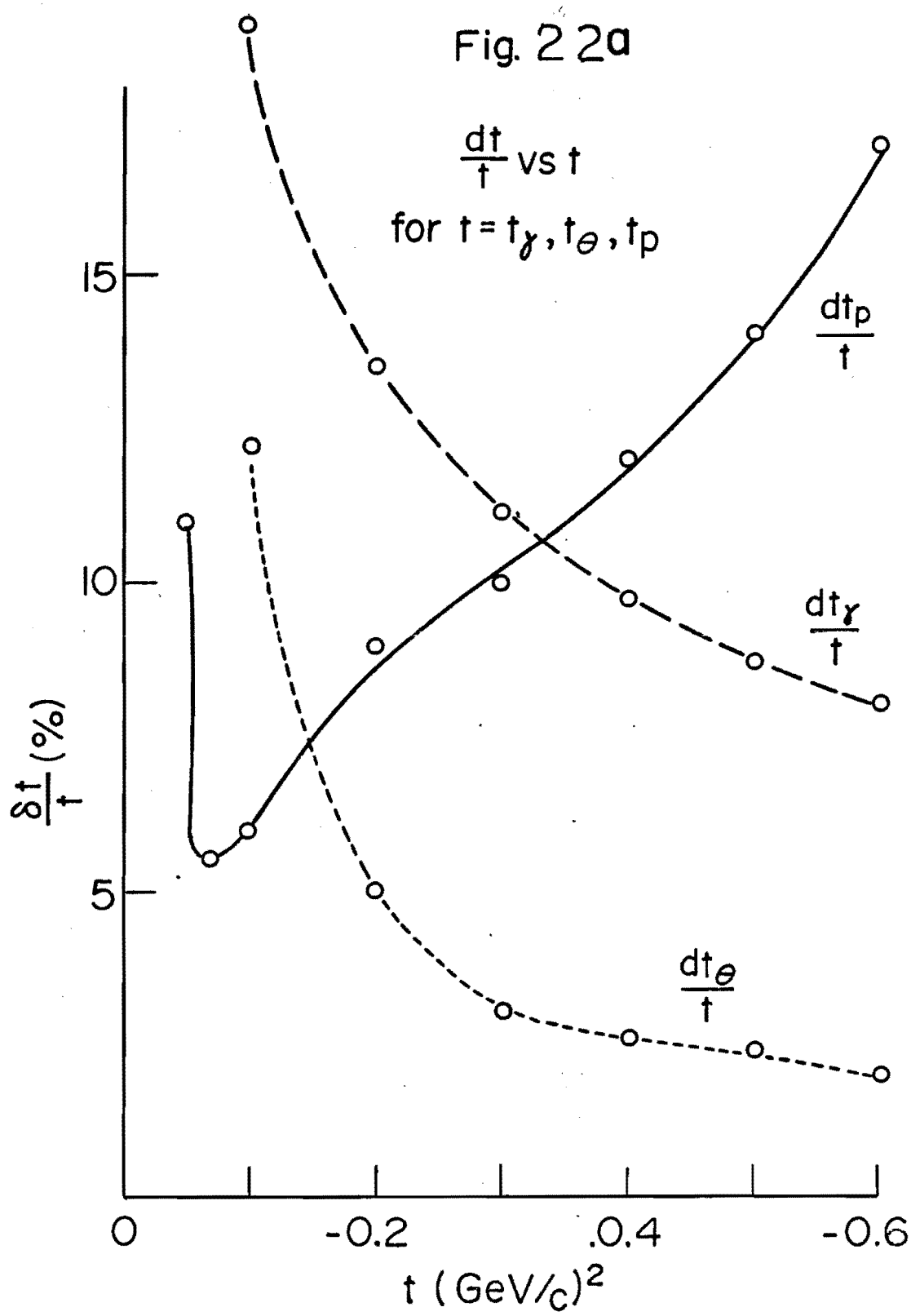
Fig. 22a
dt/t vs t
for t = tγ, tθ, tp
15
10
5
δt/t (%)
dtp/t
dtγ/t
dtθ/t
0
-0.2
.0.4
-0.6
t (GeV/c)²

Fig. 2 2b

COPLANARITY UNCERTAINTY

$\delta\phi_{coplanarity}$ vs t

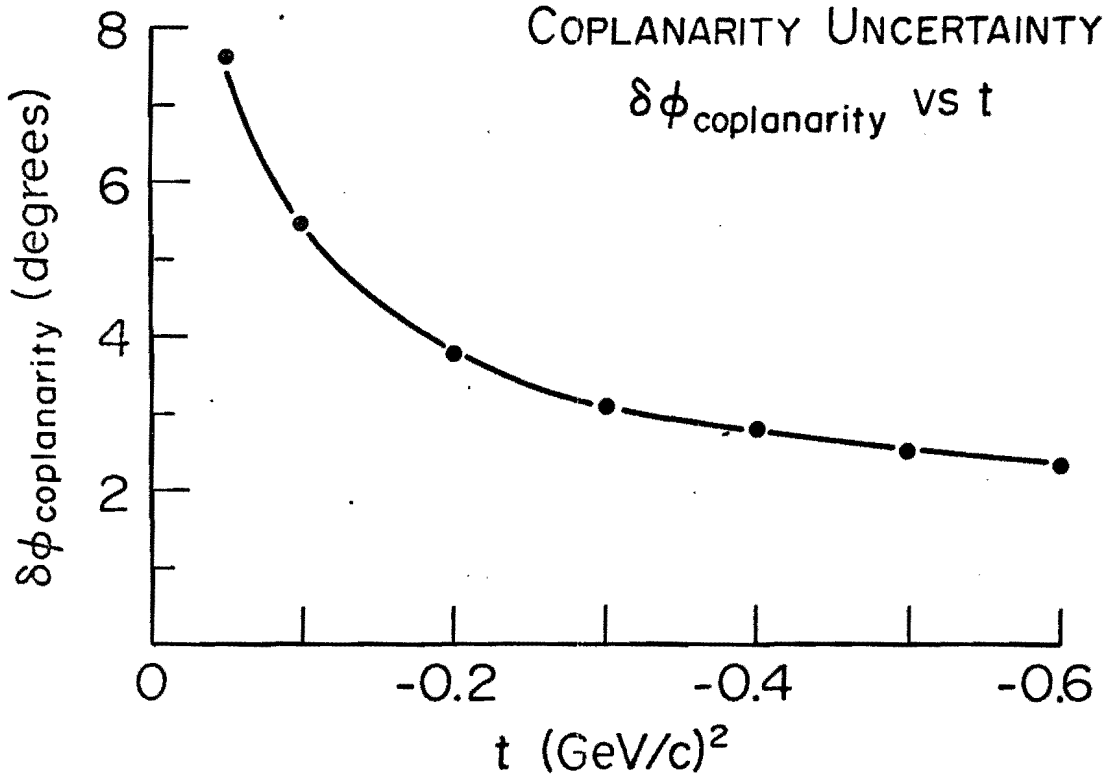

Expt. H

Total Cross Section

$\gamma p \rightarrow$ all hadrons

I. We will be able to measure the total cross section in the following manner. A hadronic event is defined when:

(i) a tagging signal occurs

(ii) there is no e^+e^- pair signal observed,

(iii) there is no noninteracting photon along the beam line, with energy equal to the tagged photon energy, detected in SH_2 and counter B.

(i) (ii) (iii) is the classical attenuation method for measuring σ_t .

With the above measurements alone, an accurate determination of σ_t cannot be obtained. Corrections due to false tag signals (either due to beam halo scattered on the wall of the magnet, or due to soft e^- produced in the tagging target, or due to π^- induced events) are likely to be quite large.

However, in our experiment, we will have additional information from track counting in the wire chambers. Since the proposed system covers a very large solid angle in the C.M. system, we will catch at least one particle in our apparatus for all hadronic events. Furthermore, since the average number of particles produced at these high energies is quite large, the chance of detecting none of them due to inefficiency of the chambers and counters is very small. There are only two classes of events which may not be detected, both of which have a very small cross section. One is forward neutral particle production, e.g. $\gamma p \rightarrow p \pi^0$, which has a negligible

cross section at high energy. Another class of events, which may be accidentally vetoed by the trigger system, is when a high energy photon is produced at the same angle as a high energy charged particle. When combined together, the two of them would simulate a forward high energy electron and get rejected. About 5% of the ω decay events belong to this category. Since ω production is about 1% of the total cross section, the induced error is negligible.

With almost all the hadronic events detected, we can add up all the observed hadronic events and normalize them to the number of tagged photons recorded.

The calculated rate of total hadronic events as a function of incident photon energy is listed in Table below. We see that the rate is high enough up to energies of 290 GeV.

Rates of Total Hadronic Events per 10^{13} Incident Protons at 500 GeV/c

Incident e^- Energy E_e (GeV)	200 GeV		300 GeV	
Photon Energy Range E_γ(GeV)	100-145	145-190	200-245	245-290
Total Hadronic Events Rate (Events/hour)	1.8×10^6	1.3×10^6	7.6×10^4	6.3×10^4

II. Experimental Checks

The overall normalization, including the efficiency of the tagging system and the entire detecting system, can be determined by comparing the

measured rates and spectrum of the e^+e^- pair production with the QED calculation. The spectrum of the e^+e^- pairs serves as a most reliable overall calibration of the system, (as has been used at DESY for several years).

An independent measurement of the total cross section will be made for 30 hours by switching off magnets M1 and M2. This has the advantage of not distrubing the electromagnetic e^+e^- pairs, thus proving a completely different measurement of σ_t. As before, all hadron events will still be measured.

As discussed on page 83, we will increase the field in the recoil magnet which will allow us to extend the missing mass range.

OPERATIONS SCHEDULE

We have planned the following sequence of operations:

1. Beam construction — 9 months

2. Beam studies aimed at understanding and improving the beam. Parts of the experimental apparatus will appear on the floor during this period. — 3 months

3. Debugging of apparatus. (Mainly parasitic operation, distributed suitably in time.) — 200 hours

4. First an experimental survey run with 4×10^5 photons/ pulse, $\delta k_\gamma = \pm 0.5\%$, a 1% radiation length tagging radiator and 10^{13} protons/ pulse incident on the production target. — 300 hours on Hydrogen; 100 hours on Complex nuclei

   After this run, we will increase the intensity by a factor of ten as discussed before. This can be achieved by a) increasing the electron intensity by a factor of 2-3 and/or b) increasing the tagging radiator to 0.1 radiation lengths. The purpose of this increase in intensity is to improve the sensitivity of the search for heavy leptons and vector mesons by a factor of 10.

   Increasing the tagging radiator thickness will worsen the photon energy resolution. However, Monte Carlo studies show that up to an energy resolution of 2.5%, the missing mass resolution up to 7 GeV is essentially unchanged. This is because the multiple scattering in the chambers and the sagitta measuring errors for the recoil proton still dominate the missing mass resolution.

5. High intensity run. Triggering only on large angle (~ 6 mrad) pairs to increase sensitivity of search for heavy vector mesons and leptons. — 300 hours

ACKNOWLEDGEMENTS

It is a pleasure to acknowledge many useful discussions with A. Mashke, L. Read, J. Sculli and T. Yamanouchi from NAL, F. Low from M.I.T., L. Bertocchi from Trieste. Thanks are also due to C. Heusch of Santa Cruz for discussions on shower counters.

APPENDIX I

COST CONSIDERATIONS:

The following estimates, quoted in U.S. 1971 dollars, are very preliminary:

1.	Liquid hydrogen target (NAL)	$ ——
* 2.	Recoil detector:	
	Magnet (Moving & Modification)	10k
	Proportional Wire Planes	70k
	Scintillator Counters	30k
	Shower Detector	5k
3.	Forward detector:	
	Magnet M1 (Moving & Modification)	10k
	Magnet M2	300k
	Proportional Wire Planes	70k
	Shower Counters	75k
	Scintillation Counters	35k
4.	Electronic logic	100k
5.	On line data facility	40k
6.	Tagging system	
	Magnets (Moving & Modification)	10k
	Proportional Wire Planes	5k
	Scintillation Counters	5k
	Shower Counters (Modification)	5k
	TOTAL	$ 770k

The experiments will be funded by the resources of the high energy groups appearing on the proposal.

* The cost of the Alternative Recoil Detector, described in Appendix II is estimated at $ 85k as follows:

Proportional Wire Planes	($60k)
Scintillator Counters	($20k)
Shower detector	($ 5k)

Hence, the overall total cost of the system would change to $740k.

APPENDIX II

Alternative Recoil Detector

The recoil detector described in the main body of the proposal utilizes a longitudinal magnetic field in a large magnet to measure the momenta of recoil protons and pions at large angles with respect to the beam. We have designed an alternative non-magnetic system which utilizes the range technique to measure the kinetic energy of the recoiling proton. This technique has two serious drawbacks: (i) We shall not be able to measure the momenta of the pions for production angles $\gtrsim 10^{\circ}$, thus curtailing a part of our study of semi-inclusive reactions. (ii) The recoil proton momentum ranges from 200 MeV/c to 800 MeV/c. Nuclear absorption corrections, even though they are completely calculable in principle, represent an almost 40% loss in our recoil detection efficiency at the upper end of the proton momentum spectrum.

The design criteria for the angle measurement, the charged pion separation, π^{0} rejection and solid angle accepted are similar to those of the magnetic detector. The kinetic energy resolution demanded was 9% -- with this resolution, the fractional angular error and the momentum error make approximately equal contribution to the missing mass resolution at missing mass of 4.5 GeV/c^2 produced by 150 GeV incident photons. Fig. 23 and 24 show the apparatus:

a) Angle measurement: PWC 1 to PWC 2 are proportional wire chamber planes which measure θ_p. PWC 1 is as close as conveniently possible to the target to locate the vertex in hydrogen. A weak longitudinal magnetic field

(a few hundred gauss-cm) may be necessary at the downstream end in case the soft recoil electron background becomes a problem.

b) Charged pion separation: PWC 1 and PWC 2 are immediately followed by a $\frac{dE}{dx}$ counter. Pulse height information and range observed will allow us to reject, off line, recoils accompanied by pions.

c) Range: the $\frac{dE}{dx}$ counters are followed by a range "telescope" in which absorbers alternate with PWC's with very coarse resolution ($\pm$ 5 cm), achieved by tying together, through resistors, twenty-five wires in our standard 2 mm wire separation planes. With 12 absorbers in the telescope, the desired kinetic energy resolution of 9% is achieved. Range straggling due to gaussian fluctuations in ionization loss has been computed and amounts to at most 1.3%

d) π^0 Rejection: The range telescope is followed by 3 radiation lengths of lead and a course resolution proportional plane. The material in the range telescope already represents 2 radiation lengths, so that we shall have a very high efficiency to detect π^0's. "Freak" events, in which the $\frac{dE}{dx}$ counter gives a proton signal and the range telescope indicates an anomalously long range due to π^0 conversion in the absorbers, will be rejected in off-line analysis.

The ϕ acceptance of the system is $\sim$ 3 radians. The θ acceptance depends on the reaction under study. For a 4.5 GeV/c^2 missing mass, and 150 GeV incident photons, the system has an efficiency of $\cong$ 50%.

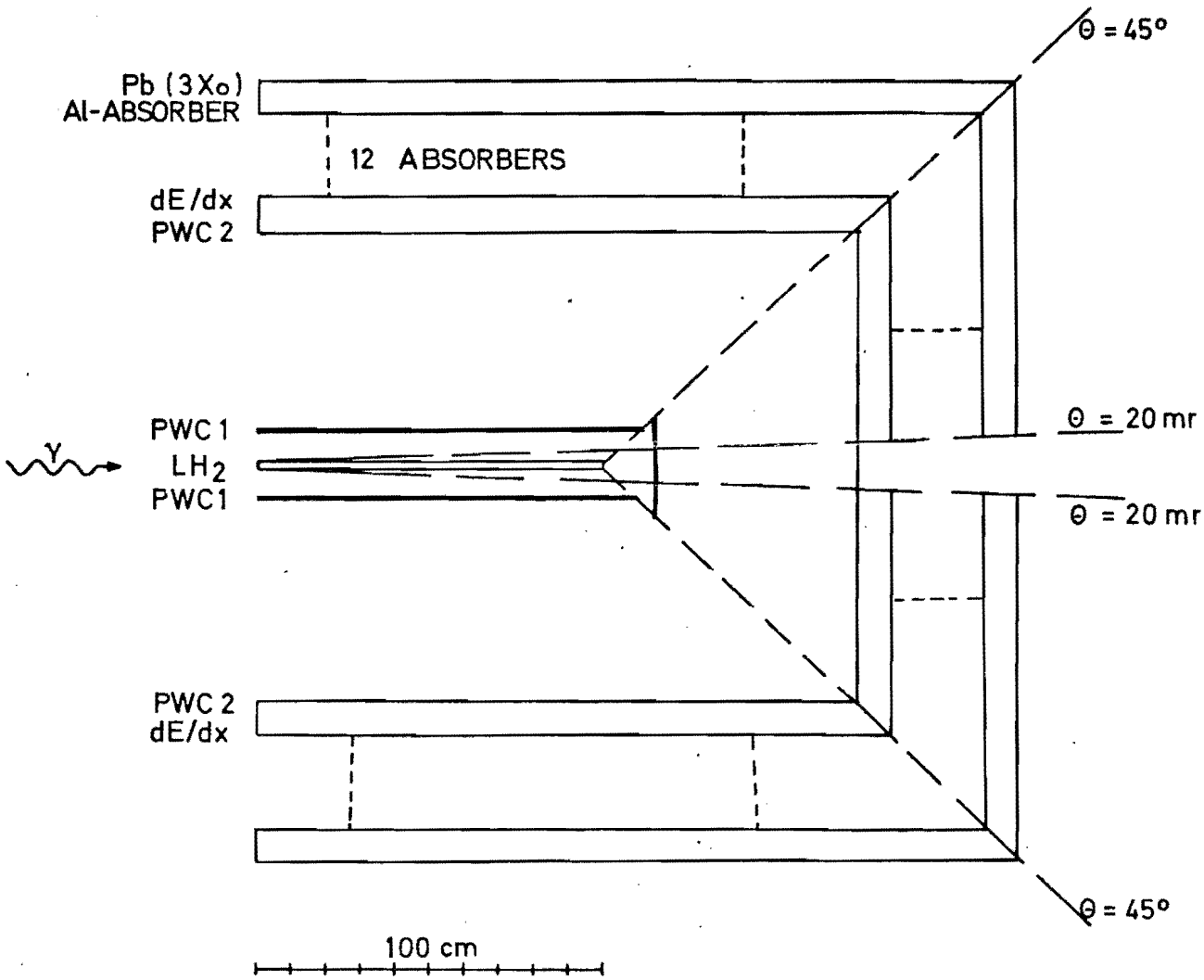

RECOIL DETECTOR
(RANGE TECHNIQUE)

FIG. 23

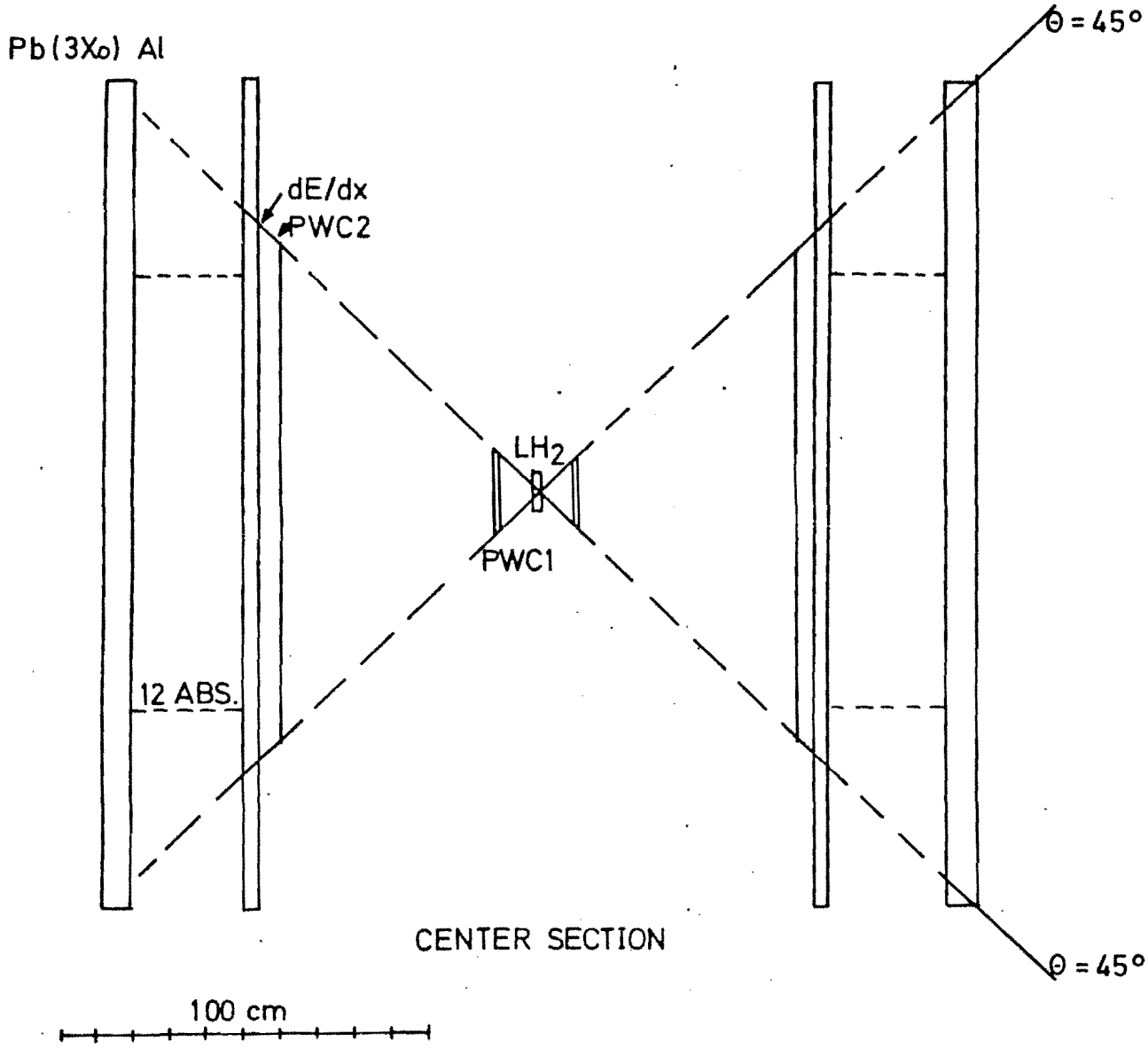

RECOIL DETECTOR
(RANGE TECHNIQUE)

FIG. 24

APPENDIX III

THRESHOLD ČERENKOV COUNTERS

In order to study photoproduction of particles up to 200 BeV/c, it is most important that we not only measure their angle and momenta, but also identify them. This is particularly true in reactions like

$\gamma + p \rightarrow \pi^+ +$ anything

$\gamma + p \rightarrow K^+ +$ anything where we want to compare the distributions of the π and K flux.

In reactions like $\gamma + A \rightarrow A + \phi$, there are two decay modes of ϕ which we can use. The $\phi \rightarrow K^+K^-$ mode had a branching ratio which is four times larger than the $\phi \rightarrow \pi^+\pi^-\pi^0$ mode.

In a search for new vector mesons and heavy leptons (KK mode), it is also important to be able to distinguish the π's from K's.

We have looked into the possibility of using threshold Čerenkov counters in our forward detector to distinguish π, K and protons.

Space Available for Č Counter in the Forward Detector:

In the present plans for the forward detector there are two long free sections:

1) between plane (3) & M2 there is 7.5 meters
2) between M2 & the final detector there is 15 meters.

There are good reasons for not using the first space. Between

the two magnets the amount of material should be minimized, since e^+e^- pairs produced in this region will not be vetoed in our present triggering system. Pairs produced after M2 cause no problem of this kind.

Number of Photoelectrons Produced in Č Counters:

The state of the art in Č counters is such that provided one is extremely careful to collect all the Čerenkov light, uses UV transmitting windows & UV reflecting surfaces, and uses very carefully selected phototubes, it is possible to obtain $150\theta^2$ photoelectrons per cm of particle path. (θ is the angle of production of Čerenkov light in radians) (See for example Yovanovitch et al.[24]

Using this number ($N = 150\theta^2$) we have computed how many photoelectrons we could obtain in a 7.5 m and a 15 m Cerenkov counter. The results are shown in Fig. 25a and 25b.

In Fig. 25a we have assumed that the pressure is set so that at threshold, $\beta = 0.999956$ for 100 GeV protons. The curves are for light emitted by one and two particles having momenta P_1 & P_2, with $P_1 + P_2 = 150$ GeV.

In Fig. 25b similar plots are given for $\pi\pi$ & KK. This time the assumption is that threshold is $\beta = 0.999988$, corresponding to 100 GeV K's.

From these curves we can conclude the following:

1) A 15 m Č counter can be used to separate efficiently (> 5 photoelectrons) π's & K's in the momentum range 45 - 105 GeV.
Thus a 15 m C counter in space 2 would help in identifying ϕ's up to K ~170 GeV.

2) If we were interested in separating protons from kaons in the same momentum range, a 7.5 m Č counter placed in space 1 could do the job.

It turns out that even if we use both space 1 & 2 for a π/K separating Č counter (total path length 22.5 meters), we cannot increase substantially the momentum range where separation can be achieved. The number of photoelectrons for π's drops rapidly as the threshold for K's is increased.
e.g. if K threshold is increased to 120 GeV the number of photoelectrons for drops by ~30%.

Construction of Č Counters:

Fig. 26 illustrates the variation of the momentum at threshold of π's, P's and K's.

It can be seen that the P/K separating Č counter would have to operate at near atmospheric pressure while the π/K separating counter would be at ~0.35 atmospheres of helium.

The 7.5 m counter would have to cover an area 150 x 50 cm^2, while the 15 m one (in space 2) would cover an area 150 x 50 cm^2 at the front and 250 x 100 cm^2 at the back. In both cases one would probably make the counters out of cylinders, but use concave mirrors only where necessary. The structure could be similar to that described by Denisov et al.[25,26]

The following points would have to be watched:

1) phototubes cannot operate in a He environment and therefore quartz windows are necessary.

2) the reflectivity of UV from aluminized glass is 80%; on the other hand it is considerably lower from aluminum foil. It would probably be necessary to place concave mirrors inside the $\check{C}$ counter. This would be alright for the counter after M2 but would not be acceptable for the one between M1 & M2.

Conclusion:

It seems feasible, for the first round of experiments with our spectrometer, to build a 15 m C counter in the region between M2 and the final detector plane. It should be capable of separating π's & K's in the momentum range 45 - 105 GeV.

SOLID CURVES CORRESPOND TO TOTAL NUMBER OF PHOTOELECTRONS PRODUCED BY P_1 AND P_2

$P_1 + P_2 = 150$ GeV i.e. $K_\gamma = 150$ GeV

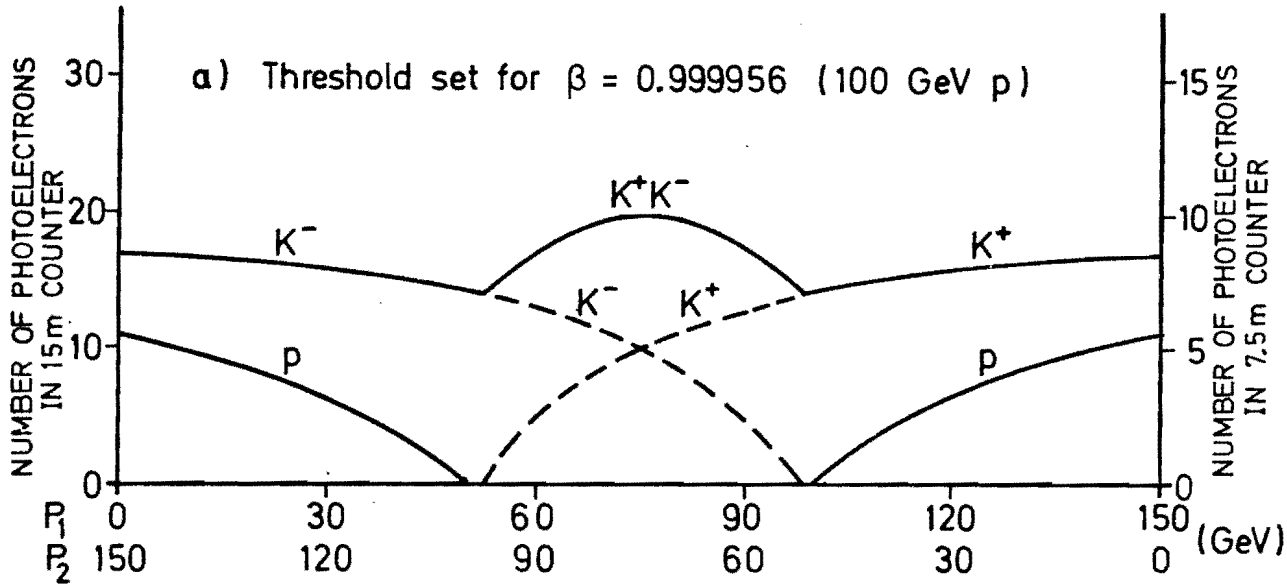

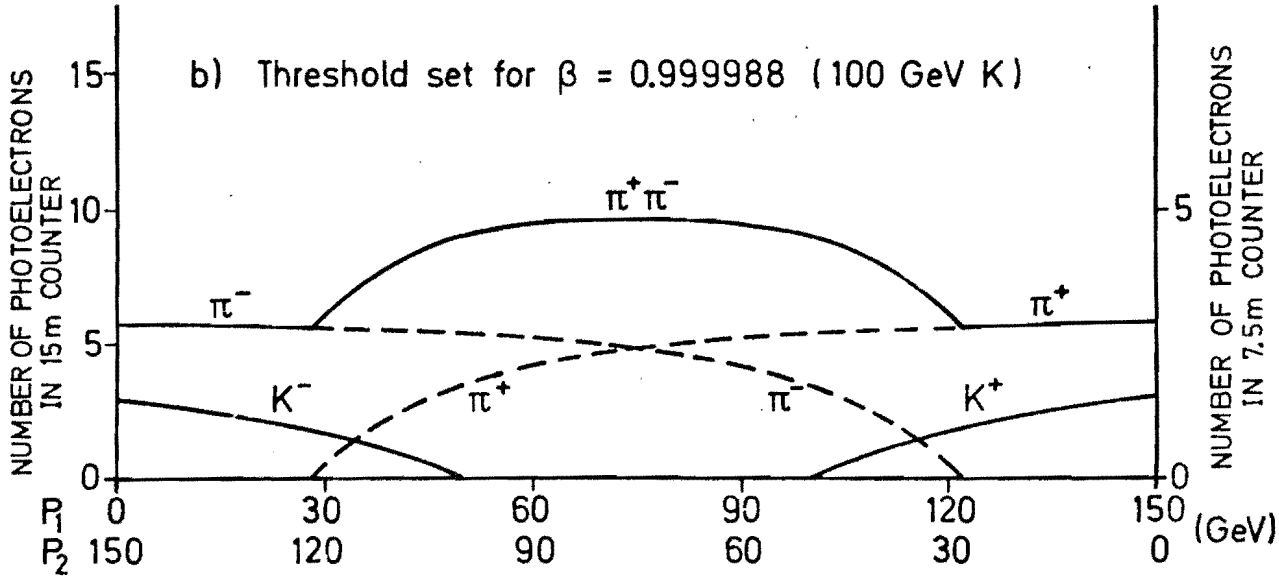

NUMBER OF PHOTOELECTRONS THAT CAN BE OBTAINED IN 7.5m & 15m COUNTERS

FIG. 25

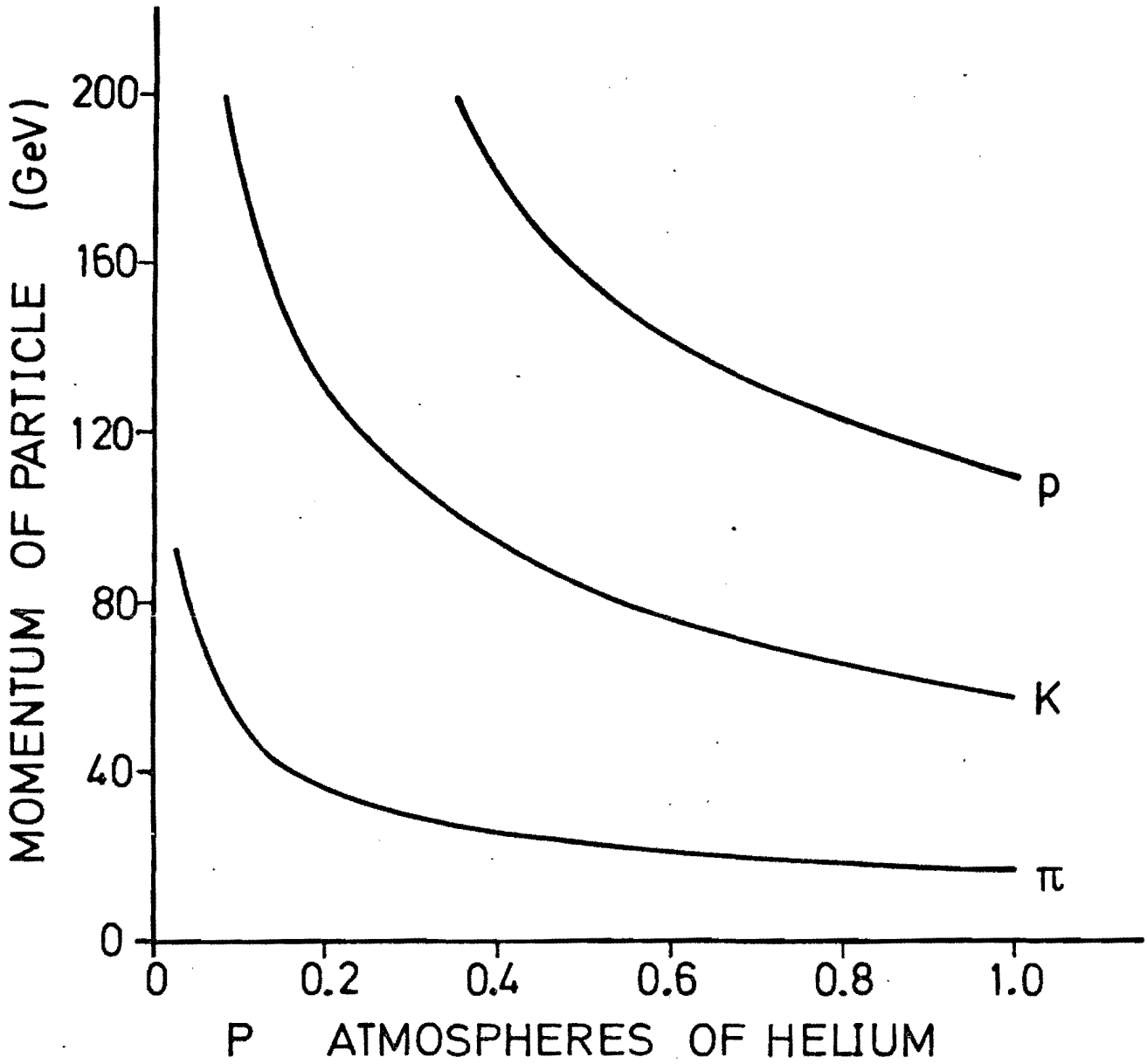

PRESSURE OF HELIUM AT THRESHOLD FOR CERENKOV RADIATION

FIG. 26

APPENDIX IV

In this appendix we discuss some aspects of the data aquisition and data handling for the experiments described in the text, together with some notes on the resolving time and construction of the proportional chambers.

Data aquisition rates and data handling:

We first estimate the record length associated with a typical event. We consider a 15,000 wire system, and assume an average of 5 charged tracks per plane though the forward detector planes(almost certainly an overestimate for the back planes), and an average of one track per plane in the recoil detector planes. For each track cluster (a cluster being defined as 1,2 (and possibly) 3 adjacent wires which have a signal output), we will write the address and the cluster size into a 16 bit word. This encoding will be done at the chamber. (A 1000 wire chamber requires 10 bits for the address, and 2 bits for the cluster size, with the remaining bits identifying the chamber plane).

With the above assumptions a typical event record will consist of:

~ 70 words for encoding track clusters
~ 8 words for encoding scintillation counter information
~ 12 words for ADC information
~ 12 words for TAC information
~ 8 words for other monitoring and bookkeeping purposes
~ 110 words = 220 8 bit bytes

To accommodate events having more than this 'average' number of tracks , it would seem that a record length 150 words is reasonable. This is a quite modest record length for the information content, and is achieved largely by the compact encoding of the chamber information.

At a writing density of 800 bytes per inch on magnetic tape, each event event will occupy 3/8". For the runs with the least selective triggering, therefore, we will use 75 inches of tape per beam burst, assuming 200 events per burst. Taking into account the duty cycle of the machine, this means that we use 25" of magnetic tape per second. Thus a 2400 ' tape will last about 20 minutes at these high rates. Our word aquisition rate will also be high, and the data will have to be read out from core storage onto temporary (disk) or permanent (magnetic tape) storage on a continuous basis. For the more selective triggers these figures will be much lower.

We hope to use a standard NAL user's computer package (PDP 11,with teletype, fast 9 track magnetic tape deck, and 611 storage scope)together with another PDP11 incorporating disk and magnetic tape peripherals. (The PDP 11's could be completely interactive). Two PDP 11's are required (together with at least two high quality magnetic tape units and other peripherals) if we are to have adequate data storage and useful display programs for on-line monitoring of the equipment and for crude checks on the data.

Resolving time of proportional chambers:

The complete trigger for most events consists of the following parts:

a) a signal from one of the triggering hodoscopes and one lead glass counter in the tagging arm. (The upstream momentum hodoscope is recorded, but is not part of the trigger).

b) no output from three sets of veto conditions against e^+e^- pairs

c) In parallel with (b) above, some positive trigger requirements from the various shower counters, and /or from C_i and D_i, or from the recoil proton arm.

Because of the long distances separating these counters, it is important to rationalize the trigger system so as to minimize the overall delay between t = o (when an interesting event is tagged), and the time when above trigger conditions signal an interesting event. This time is very relevant to the output electronics design of the proportional chambers. Each wire in the system is independent and continuously sensitive, and a signal becomes available from each activated wire in a time ~50 nanoseconds after the particle traversed the chamber. This time is much too short compared with the delays introduced by the decision making process outlined above, and some means of 'freezing' the information at the chamber outputs is required. This can be achieved by means of multiple delay lines (which have the advantage that the intrinsic resolving time of the chambers can be preserved, but are expensive and messy), or by generating a pulse at each amplifier output of sufficient length that the data is preserved for the necessary length of time. (We will probably use both methods). In the case of the wire chambers in the tagging arm, we will use delay cables to make them contemporary with the chambers in the hydrogen target area. The chambers in this area have the maximum waiting time, corresponding to the time taken for the particles to get to the end of the forward detector, and the time taken to get a signal back at the hydrogen target region. Together with the time delays in the electronic logic, this amounts to ~450 nanosec. Thus, for some chambers, the effective resolving time will be ~ 0.5μsec, much the same as for conventional spark chambers.

In the event that we are troubled by a high rate of e^+e^- pairs from low energy (untagged) photon interactions in the hydrogen target, there are a number of ways in which we can cut down on this resolving time. It is convenient to distinguish between two basic types of random background according to whether it occurs before or after a good event (within the resolving time, say 500nsec). In the case where the random occurs before a good event, we can automatically reset the chambers if a tag signal does not arrive within a narrow gate (~± 5nsec) delayed to correspond to the particle flight time between the tagging system and the hydrogen

target. This would reduce the effective resolving time by a factor 50. For the second type of contamination, we can if necessary, delay the signals from the chamber immediately downstream of the hydrogen target by up to 500 n sec, and require a coincidence between the wires and the tagging signal to $\pm$ 25 n sec. By doing this, we would reduce this contamination by a factor of 10.

Proportional Chamber construction:

Although some of the areas to be covered by proportional chambers are quite large (up to 360 cm x 110 cm), we will be able to standardize on smaller, overlapping modules, and we do not envisage having to make chambers larger than about 150 cm x 150 cm. Even at these sizes, the thin tungsten wires will require some additional support, and we will use vinyl threads for this purpose. The high voltage planes will be made of Be-Cu wires strung in a direction orthogonal to the signal wires, with a thin mylar gas seal on the outside. With this construction, multiple scattering (which is particularly important in the recoil detector) will be kept to the minimum practical limit.

References

1. a. G. Cocconi, Phys. Rev. 111, 1699 (1958).

   b. K. Niu, Nuovo Cimento 10, 994 (1958).

   c. P. Coik, T. Coghen, J. Gierula, R. Holynski, A. Jurak, M. Miesowicz, T. Saniewska, and J. Pernegr, Nuovo Cimento 10, 741 (1958).

   d. M.L. Good and W.D. Walker, Phys. Rev. 120, 1857 (1960).

   e. B. Peters, Proc. International Conference on Cosmic Rays, Jaipur 1963.

   f. Y. Pal and B. Peters, Nat. Fys. Medd. Dan. Vid Selsk 33, No. 15 (1964).

   g. R.K. Adair, Phys. Rev. 172, 1370 (1968).

2. a. C. Goebel, Application of Mandelstam Representation to Peripheral Collision, International Conference on Theoretical Aspects of Very High Energy Phenomena, ed. by J.S. Bell et al (1961), (CERN 61-22)., p. 353.

   b. D. Amati, A. Stanghellini, and S. Fubini, Nuovo Cimento 26, 896 (1962).

   c. L. Bertocchi, E. Predazzi, A. Stanghellini, and M. Tonin, Nuovo Cimento 27, 913 (1963).

   d. O. Czyżewski and A. Krzywicki, Nuovo Cimento 30, 603 (1963).

   e. K.G. Wilson, Acta Physica Austriaca 17, 37 (1964).

   f. F. Zachariasen and G. Zweig, Phys. Rev. 160, 1322 (1967).

   g. G.F. Chew, M.L. Goldberger, and F.E. Low, Physical Review Letters 22, 208 (1969).

3. a. T. Regge, Nuovo Cimento 14, 951 (1959).

   b. T.W.B. Kibble, Phys. Rev. 131, 2282 (1963).

   c. V.N. Gribov, I. Ya. Pomeranchuk, and K.A. Ter-Martorosyan, Phys. Rev. 139B, 184 (1965).

   d. J.C. Polkinghorne, Nuovo Cimento 36, 857 (1965).

   e. F. Zachariasen and G. Zweig, Phys. Rev. 160, 1326 (1967).

   f. N.F. Bali, G.F. Chew, and A. Pignotti, Phys. Rev. 163, 1572 (1967).

3. g. Chan Hong-Mo, J. Łoskiewicz, and W.W. M. Allison, Nuovo Cimento 57A, 93 (1968).

h. C.E. DeTar and D.R. Snider, Phys. Rev. Letters 25, 410 (1970).

i. A.H. Mueller, Phys. Rev. D2, 2963 (1970).

j. Chan Hong-Mo, C.S. Hsue, C. Quigg, and J.M. Wang, Phys. Rev. Letters 26, 672 (1971).

4. a. T.T. Wu and C.N. Yang, Phys. Rev. 137B, 708 (1965).

b. N. Byers and C.N. Yang, Phys. Rev. 142, 976 (1966).

c. T.T. Chou and C.N. Yang, Some Remarks Concerning High Energy Scattering, in High Energy Physics and Nuclear Structure, ed. by G. Alexander (North-Holland Publishing Co., 1967), p. 348.

d. T.T. Chou and C.N. Yang, Phys. Rev. 170, 1591 (1968).

e. T.T. Chou and C.N. Yang, Phys. Rev. Letters 20, 1213 (1968).

f. T.T. Chou and C.N. Yang, Phys. Rev. 175, 1832 (1968).

g. C.N. Yang, Hypothesis of Limiting Fragmentation, in High Energy Collisions, ed. by C.N. Yang et al. (Gordon and Breach Publishers, Inc., 1969), p. 509.

h. J. Benecke, T.T. Chou, C.N. Yang, and E. Yen, Phys. Rev. 188, 2159 (1969).

i. T.T. Chou and C.N. Yang, Phys. Rev. Letters 25, 1072 (1970).

j. C.N. Yang, High Energy Hadron Hadron Collisions, 15th International Conference on High Energy Physics at Kiev (1970).

5. a. R.P. Feynman, The Behavior of Hadron Collision at Extreme Energies, in High Energy Collisions ed. by C.N. Yang et al., (Gordon and Breach Publishers, Inc., 1969), p. 237.

b. R.P. Feynman, Phys. Rev. Letters 23, 1415 (1969).

6. a. H. Cheng and T.T. Wu, Phys. Rev. Letters 22, 666 (1969).

b. H. Cheng and T.T. Wu, Phys. Rev. 182, 1852, 1868, 1873, and 1899 (1969).

c. H. Cheng and T.T. Wu, Phys. Rev. Letters 23, 670 (1969).

d. H. Cheng and T.T. Wu, Theory of High Energy Diffraction Scattering, in High Energy Collisions, ed. by C.N. Yang et al., (Gordon and Breach Publishers, Inc., 1969), p. 329.

e. H. Cheng and T.T. Wu, Phys. Rev. Letters 23, 1311 (1969).

f. H. Cheng and T.T. Wu, Phys. Rev. D1, 456, 459, and 467 (1970).

g. H. Cheng and T.T. Wu, Phys. Rev. Letters 24, 1456 (1970).

h. H. Cheng and T.T. Wu, Impact Picture - Theory of High Energy Scattering, 15th International Conference on High Energy Physics at Kiev (1970).

i. H. Cheng and T.T. Wu, Physics Letters 34B, 647 (1971).

7. H. Cheng and T.T. Wu, Diffractive Inelastic Processes at Extremely High Energies, DESY Report 71/36 (1971).

8. a. S. D. Drell, Proceedings of Int. Conf. on Expectations for Particle Reactions at the new accelerators; at Madison (Wisconsin).

b. A. C. Melissinos, T. Yamanouchi, C. G. Favio, S. J. Lindenbaum and L. C. L. Yuan, Phys. Rev. 128 (1962) 2373.

c. E. W. Anderson, E. J. Bleser, G. B. Collins, T. Fujii, J. Manes, F. Turkot, R. A. Carrigan, Jr., R. M. Edelstein, W. C. Hien, T. J. McMahon and I. Nadelhaft, Phys. Rev. Letters 19 (1967) 198.

d. D. B. Smith, R. J. Sprafka and J. A. Anderson, Phys. Rev. Letters 23 (1969) 1064

e. Yu. B. Bushnin, S. P. Denisov, S. V. Donskov, A. F. Dunaitsev, Yu. P. Gorin, V. A. Kachanov, Yu. S. Khodirev, V. I. Kotov, V. M. Kityin, A. I. Petrukhin, Yu. F. Prokoshkin, E. A. Razuvaev, R. S. Shuvalov, D. A. Stoyanova, J. V. Allaby, F. Binon, A. N. Diddens, P. Duteil, G. Giacomelli, R. Meunier, J. P. Peigneux, K. Schlupmann, M. Spighel, C. A. Stahlbrandt, J. P. Stroot and A. M. Wetherell, Phys. Letters 29B (1969) 48.

f. N. A. Abolins, G. A. Smith, Z. Ming Ma, E. Gellert and A. B. Wicklund, Phys. Rev. Letters 25 (1970) 126.

g. W. E. Ellis, R. R. Kinsey, T. W. Morris, R. S. Panvini and F. Turkot, Phys. Letters 32B (1970) 641.

h. L. W. Jones, A. E. Bussian, G. D. de Meester, B. W. Loo, F. E. Mills, D. D. Reeder, K. N. Erickson and B. Cork, Phys. Rev. Letters 25 (1970) 1679, and references therein.

i. J. V. Allaby, F. Binon, A. N. Diddens, P. Duteil, A. Klovning, R. Meunier, J. P. Peigneux, E. J. Sacharidis, K. Schlupmann, M. Spighel, J. P. Stroot, A. M. Thorndike and A. M. Wetherell, CERN 70-12 (1970).

j. C. W. Akerlof, D. G. Crabb, J. L. Day, P. Johnson, P. Kalbach, A. D. Krisch, M. T. Lin, M. L. Marshak, J. K. Randolph, P. Schmuser, A. L. Read, K. W. Edwards, J. G. Asbury, G. J. Marmer and L. G. Ratner, Phys. Rev. D3 (1971) 645.

9. a. G. Veneziano, Nuovo Cimento 57A, 190 (1968).

b. J. A. Shapiro, Phys. Rev. 179, 1345 (1969).

10. a. J. J. Sakurai Ann. Phys. (N.Y.) 11, 1 (1960).

b. M. Gell-Mann, Phys. Rev. 125, 1067 (1962).

c. N. M. Kroll, T. D. Lee and B. Zumino, Phys. Rev. 157, 1376 (1968).

11. a. H. Joos, Proc. Int. Conf. on Ele. Particles (Heidelberg) 1967.

b. S. C. C. Ting, Proc. of Int. Conf. on High Energy Phys. (Vienna) (1968)

c. H. Joos, Phys. Lett 24B, 103 (1967)

d. J. J. Sakurai, Univ. of Chicago Preprint EFI (1968) 59.

e. A. Silverman, Proc. Int. Symp. Electron/Photon Phys. (Daresbury) (1969)

f. J. S. Trefil Phys. Letts. 24B 106 (1967)

12. a. N. Hicks, A. Eisner, G. Feldman, L. Litt, W. Lockeretz, F. M. Pipkin, J. K. Randolph and K. C. Stahfield, Phys. Letters 29B, 602 (1969).

b. G. McClellan, N. Mistry, P. Mostek, H. Ogren, A. Osborne, A. Silverman, J. Swartz, R. Talman and G. Diambrini-Palazzi, Phys. Rev. Letters 23, 718 (1969).

c. F. Bulos, W. Busza, R. Giese, E. E. Kluge, R. R. Larsen, D. W. G. S. Leith, B. Richter, S. H. Williams, B. Kehoe, M. Beniston and A. Stetz, Phys. Rev. Letters 26, 149 (1971).

d. H. Alvensleben, U. J. Becker, W. K. Bertram, M. Chen, K. J. Cohen, R. T. Edwards, T. M. Knasel, R. Marshall, D. J. Quinn, M. Rohde, G. H. Sanders, H. Schubel and S. C. C. Ting, Phys. Rev. Letters 26, 273 (1971).

e. S. Hayes, R. Imlay, P. M. Joseph and P. C. Stein, Phys. Rev. Letters 24, 1369 (1970).

f. A. Benvenuti, D. Cline, R. Rutz, D. D. Reeder, and V. R. Scherer (Wisconsin preprint) 1971

13. a. W. G. Jones, D. Kreinick, R. Anderson, G. Gustavson, J. Johnson, D. Ritson, F. Murphy, M. Gettner and R. Weinstein, Phys. Rev. Letters 21, 586 (1968).

b. F. Bulos, N. Busza, R. Giese, R. R. Larsen, D. W. G. S. Leith, B. Richter, V. Perez-Mendez, A. Stetz, S. H. Williams, M. Beniston and J. Rettberg, Phys. Rev. Letters 22, 490 (1969).

c. G. McClellan, N. Mistry, P. Mostek, H. Ogren, A. Silverman, J. Swartz, R. Talman, K. Gottfried and A. I. Lebedev, Phys. Rev. Letters 22, 374-382, (1969).

d. H. Alvensleben, U. Becker, W. K. Bertram, M. Chen, K. J. Cohen, T. M. Knasel, R. Marshall, D. J. Quinn, R. Rohde, G. H. Sanders, H. Schubel and S. C. C. Ting, Nucl. Phys. B18, 333 (1970).

e. H. Alvensleben, U. Becker, M. Chen, K. J. Cohen, T. M. Knasel, R. Marshall, D. J. Quinn, M. Rohde, G. H. Sanders, H. Schubel and S. C. C. Ting, Phys. Rev. Letters 25, 1377 (1970).

f. P. J. Biggs, D. W. Braben, R. W. Clifft, E. Gabathuler and R. E. Rand, Daresbury Preprint (1970).

g. J. Ballam et al. (SLAC-Tufts-Berkeley Collaboration) Phys. Rev. Letters 24, 1364 (1970).

h. P. L. Braccini, C. Bradasehia, R. Castaldi, L. Foa, K. Lubelsmeyer and D. Schmitz, Nucl. Phys. B24, 173, (1970).

i. Y. Eisenberg et al. (Weizmann-SLAC-Tel. Aviv Collaboration) Phys. Letters 34B, 439 (1971).

j. H. J. Behrend, C. K. Lee, F. Lobkowicz, E. H. Thorndike, A. A. Wehmann and M. E. Nordberg, Jr., Phys. Rev. Letters 26, 151 (1971) and 27, 65 (1971).

k. G. McClellan, N. Mistry, P. Mostek, H. Ogren, A. Osborne, J. Swartz, R. Talman and G. Diambrini-Palazzi, Phys. Rev. Letters 26, 1593 (1970).

14. J. V. Allaby, A. N. Diddens, R. W. Robinson, A. Klovning, J. Litt, L. S. Rochester, K. Schleupman, A. M. Wetherell, U. Amaldi, R. Biancastelli, C. Bosio, and G. Matthiae, Phys. Letters 34B, 431 (1971).

15. M. Ross and L. Stodolsky, Phys. Rev. Letters 17, 563 (1966).
L. Bertocchi (Private communication).

16. K. S. Kolbig and B. Margolis, Nucl. Phys. B6 85 (1968)

17. a. F. E. Low, Phys. Rev. Letters 14, 238 (1965).
b. S. J. Brodky (Private Communication).

18. R. Jost, J. M. Luttinger and M. Slotnik, Phys. Rev. 80, 189 (1950)

19. J. J. Sakurai: Preprint (1971)

20. a. M. Deutsch. E. Loh, G. Marini, P. M. Patel, R. Stiening and K. Tsipis, Proc. Int. Conf. on electron/photon physics (1967).
b. M. Deutsch and D. F. Jacobs, Bull. Am. Phys. Soc. 15, 608 (1970).
c. R. L. Anderson, D. Gustavson, J. Johnson, I. Overman, D. Ritson, B. H. Wiik, R. Talman, J. K. Walker and D. Worcester, Phys. Rev. Letters 25, 1218 (1970).
d. G.Buschhorn, L. Criegee, L. Dubal, G. Franke, C. Geweninger, P. Heide, R. Kotthaus, G. Poelz, U. Timm, K. Wegener, H. Werner, M. Wond and W. Zimmerman, Phys. Letters 33B, 241 (1970).
e. A.M. Boyarski, D. H. Coward, S. Ecklund, B. Richter, D. Sherden, R. Siemann and C. Sinclair, Phys. Rev. Letters 26, 1600 (1971).

21. a. M. Gell-Mann, M. L. Goldberger and W. Thirring, Phys. Rev. 95, 1612 (1964)

22. a. S. L. Adler and R. F. Dashen, Current Algebras, p. 330 (Benjamin 1968)

b. M. Damashek and F. J. Gilman, Phys. Rev. D1, 1319 (1970).

23. a. H. Joos, DESY Preprint 1967.

b. L. Stodolsky, Phys. Rev. Letters 18, 135 (1967).

c. S. J. Brodsky and J. Pemplin, Phys. Rev. 182, 1794 (1969).

d. M. Nauenberg, Phys. Rev. Letters 22, 556 (1969).

e. K. Gottfried and D. R. Yennie, Phys. Rev. 182, 1595 (1969).

f. B. Margolis and C. L. Tang, Nucl, Phys. B10, 329 (1969).

g. A B B H H M Collaboration, Phys. Letters 27B, 474 (1968).

h. SLAC-Tufts-Berkeley Collaboration, Phys. Rev. Letters 21, 1544 (1968) and 23, 498 (1969).

i. D. O. Caldwell, V. B. Elings, W. P. Hesse, G. E. Jahn, R. J. Morrison, F. V. Murphy and D. E. Yount, Phys. Rev. Letters 23, 1256 (1969).

j. D. H. Meyer, B. Naroska, J. H. Weber, M. Wong, V. Heyhen, E. Mandelkow and D. Notz, Phys. Letters 33B, 189 (1970).

k. T. A. Armstrong, W. R. Hogg, G. M. Lewis, A. W. Robertson, G. R. Brookes, A. S. Clough, J. H. Freeland, W. Galbraith, A. F. King, W. R. Rawlinson, N. R. S. Tait, J. C. Thomson, D. W. L. Tolfree, Phys. Letters 34B, 535 (1971).

24. "A threshold Gas Cerenkov counter for a 200 GeV/c beam"
D. D. Yovanovitch et al., ANL/HEP 7104

25. "A high resolution threshold Cerenkov counter"
S. P. Denisov et al., Nucl. Instr. & Meth. 85 , 101 (1970)

26. "Threshold Cerenkov counters at NAL"
S. Pruss, NAL Summer Study, p. 212 (1970)